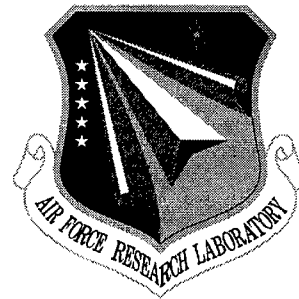


AFRL-IF-RS-TR-1999-104
Final Technical Report
May 1999



TRAFFIC FLOW VISUALIZATION AND CONTROL

ITT Systems

Robert Larson, Jack Zhuang, and Jim Novak

APPROVED FOR PUBLIC RELEASE; DISTRIBUTION UNLIMITED.

AIR FORCE RESEARCH LABORATORY
INFORMATION DIRECTORATE
ROME RESEARCH SITE
ROME, NEW YORK

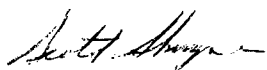
DTIC QUALITY INSPECTED 4

19990707 059

This report has been reviewed by the Air Force Research Laboratory, Information Directorate, Public Affairs Office (IFOIPA) and is releasable to the National Technical Information Service (NTIS). At NTIS it will be releasable to the general public, including foreign nations.

AFRL-IF-RS-TR-1999-104 has been reviewed and is approved for publication.

APPROVED:



SCOTT S. SHYNE
Project Engineer

FOR THE DIRECTOR:



WARREN H. DEBANY, Jr., Technical Advisor
Information Grid Division
Information Directorate

If your address has changed or if you wish to be removed from the Air Force Research Laboratory Rome Research Site mailing list, or if the addressee is no longer employed by your organization, please notify AFRL/IFGA, 525 Brooks Rd, Rome, NY 13441-4505. This will assist us in maintaining a current mailing list.

Do not return copies of this report unless contractual obligations or notices on a specific document require that it be returned.

REPORT DOCUMENTATION PAGE			Form Approved OMB No. 0704-0188	
<small>Public reporting burden for this collection of information is estimated to average 1 hour per response, including the time for reviewing instructions, searching existing data sources, gathering and maintaining the data needed, and completing and reviewing the collection of information. Send comments regarding this burden estimate or any other aspect of this collection of information, including suggestions for reducing this burden, to Washington Headquarters Services, Directorate for Information Operations and Reports, 1215 Jefferson Davis Highway, Suite 1204, Arlington, VA 22202-4302, and to the Office of Management and Budget, Paperwork Reduction Project (0704-0188), Washington, DC 20503.</small>				
1. AGENCY USE ONLY (Leave blank)		2. REPORT DATE May 99		3. REPORT TYPE AND DATES COVERED Final Nov 94 - Nov 98
4. TITLE AND SUBTITLE TRAFFIC FLOW VISUALIZATION AND CONTROL			5. FUNDING NUMBERS C - F30602-94-C-0279 PE - N/A PR - R507 TA - 01 WU - 01	
6. AUTHOR(S) Robert Larson, Jack Zhuang, and Jim Novak				
7. PERFORMING ORGANIZATION NAME(S) AND ADDRESS(ES) ITT Systems 4410 E. Fountain Blvd. PO Box 15012 Colorado Springs, CO 80935-5012			8. PERFORMING ORGANIZATION REPORT NUMBER	
9. SPONSORING/MONITORING AGENCY NAME(S) AND ADDRESS(ES) AFRL/IFGA 525 Brooks Rd. Rome, NY 13441-4505			10. SPONSORING/MONITORING AGENCY REPORT NUMBER AFRL-IF-RS-TR-1999-104	
11. SUPPLEMENTARY NOTES AFRL Project Engineer: Scott Shyne, IFGA, 315-330-4819				
12a. DISTRIBUTION AVAILABILITY STATEMENT Approved for public release; distribution unlimited.			12b. DISTRIBUTION CODE	
13. ABSTRACT (Maximum 200 words) The TFVC system was developed in collaboration with the New York State Department of Transportation, the Federal Highway Administration, and the US Air Force Research Laboratory. It is a video-camera-based, wide-area, traffic surveillance and detection system that provides real-time traffic information to traffic management center operators. The TFVC system uses a unique method of video sensing which automatically detects traffic patterns present in a captured traffic scene. This approach begins with a video image which is obtained from the output of an off-the-shelf video camera. Image processing algorithms verify traffic lanes and begin to extract traffic data, in real-time, from the live video. Vehicle count, flow speed, headway, queue length and occupancy are some of the information that can be collected. The processed traffic data is then sent to a control center for further analysis and used by traffic operators attempting to analyze traffic on the highway.				
14. SUBJECT TERMS Traffic Analysis, Distributed Sensor Network, Image Processing			15. NUMBER OF PAGES 106	
			16. PRICE CODE	
17. SECURITY CLASSIFICATION OF REPORT UNCLASSIFIED	18. SECURITY CLASSIFICATION OF THIS PAGE UNCLASSIFIED	19. SECURITY CLASSIFICATION OF ABSTRACT UNCLASSIFIED	20. LIMITATION OF ABSTRACT UL	

TABLE OF CONTENTS

	<u>Page</u>
Table of Contents	i
List of Figures	ii
List of Tables	iii
1.0 TFVC System Overview and Design	1
2.0 System Description	3
2.1 Sensor	3
2.2 Graphical User Interface	5
2.3 Database Server	6
2.4 Network	6
3.0 Summary of Technical Work Accomplished	7
3.1 Hardware Subsystems	7
3.2 Software Developed	7
3.3 Incident Detection Algorithms	7
3.4 Innovations in Artificial Intelligence Traffic Control	8
3.5 Reference Documentation	8
3.6 Environmental Screening Test Plan	8
4.0 Information Gained/Lessons Learned	12
4.1 Approach	12
4.2 Integration	12
4.3 Fielding	12
4.4 Iris Control	12
4.5 Software Methods	12
4.6 Network	12
4.7 Software Maintenance and Upgrade Issues	16
4.8 Fiber Optics Development	17
4.9 Overall Cost/Performance Tradeoffs of Networking Approaches	17
5.0 Flow Speed Calculation	18
5.1 Introduction	18
5.2 Collapsed Waveform Algorithm	19
5.3 Correlation Algorithm for Flow Speed Computation	21
5.4 Real Application	44
5.5 Conclusions	49
6.0 Camera Perspective	51
6.1 Introduction	51
6.2 Relation Between Camera Perspective and Flow Speed Computation	51
6.3 Conclusions	95

LIST OF FIGURES

	<u>Page</u>
FIGURE 1 System Description	3
FIGURE 2 RSS Environmental Testing	10
FIGURE 3 Cable System Block Diagram	15
FIGURE 4 2-D Image of a Traffic Lane	19
FIGURE 5 1-D Collapsed Waveform $g(P_y)$ of a Traffic Lane	21
FIGURE 6 Redraw of 1-D Collabpsed Waveform $g(P)$ of a Traffic Lane	22
FIGURE 7 1-D Collapsed Waveform $G(P) = g(P - dP)$ of a Traffic Lane	23
FIGURE 8 (a) – (d) Example Waveforms and Correlation Functions of One Vehicle	26-27
FIGURE 9 The Shifted 1-D Waveform with Varied Calibration Factor	29
FIGURE 10 Example Waveforms and Correlation Functions of Two Vehicles with Varied Calibration Factors	43-44
FIGURE 11 Schematic Drawing of the Camera Perspective	52

LIST OF TABLES

	<u>Page</u>
Table 1 TFVC Site Locations	2
Table 2 ESS Testing	9

1.0 TFVC System Overview and Design

The Traffic Flow Visualization and Control (TFVC) system is a video-camera-based, wide-area, traffic surveillance and detection system that provides real-time traffic information to traffic management center operators. TFVC is a distributed system consisting of: (1) a network of video cameras with collocated image processors, (2) centralized command, control and display located in a traffic management center that are used to manage the system and its data, and (3) a communications subsystem that links the remote sensors to the central computer.

TFVC video data processors use advanced image processing techniques to calculate traffic flow parameters in real-time and forward the data to the central computer. Distributed image processing is used to minimize communications requirements and to maximize the content of data transmitted to the traffic management center.

The TFVC system was developed to work with a spectrum of communications media including RF cable modems, ISDN and POTs (plain old telephone) phone lines, and wireless Ethernet. TFVC could also be readily adapted to work with fiber optics networks. The bandwidth of the communications network dictates the frequency at which data is forwarded to the central computer.

The TFVC central computer monitors commands and controls system resources. It provides a graphical user interface (GUI) for displaying traffic parameters, video images and system status, and it manages and archives system data.

Features and capabilities of the TFVC system include the following:

- High-speed processing of video images to compute traffic volume, density, and speed.
- Visual monitoring of traffic via pan-zoom-tilt control.
- Automatic incident detection and operator notification.
- Automatic return to presets with lane verification algorithms.
- Archival of historical reduced traffic data in a SQL accessible database.
- Presence of vehicles in lanes and shoulders.
- Occupancy and headway (derived from traffic data).

The TFVC system was developed in collaboration with the New York State Department of Transportation, the Federal Highway Administration, and the US Air Force's Rome Laboratory. In June of 1995 Kaman Sciences deployed a research system along the Long Island Expressway (LIE) in New York that consisted of five video sensors and local processors, and a central computer located in the LIE's INFORM Center. (Note: in December 1997 Kaman Sciences

Corporation became a part of ITT Industries (ITT Systems), and in November 1997 Rome Laboratory became the Air Force Research Laboratory, Information Directorate.) This system demonstrated system feasibility, tested system capabilities and interfaces, and collected data to refine system design, construction, and operation. In October of 1997, Kaman Sciences began deploying a full-scale system of 19 sensors along the LIE, listed below.

Site	Direction	Location	Link
K6	West	North Ocean Avenue - 63 (NW immediately past bridge)	Wireless
K5	East	Blue Point Road (SE .3 mile)	Wireless
K4	West	Waverly Avenue (NW immediately past bridge)	Wireless
K3	East	Nicolls Road - 62 (SW of intersection)	Wireless
K2	West	Holbrook Road (NE of intersection)	Wireless
K1	East	Patchogue-Holbrook Road - 61 (NW immediately past bridge)	Wireless
36	East	Hawkins Avenue - 60 (SW - after 2nd bridge - pole in center)	RF modem
35	West	Terry Road - after Ocean - 59 (NW of intersection)	POTS
34	West	Veterans Memorial Hwy - 57 (NW immediately after underpass)	POTS
33	West	Wheeler Road-Joshuas Path - 56 (NW of intersection)	RF modem
32	West	Washington Avenue - after 55 (NW immediately past bridge)	POTS
26	East	Crooked Hill Road - after 53 bear left (SE of intersection)	RF modem
25	West	Commack Road - 52 (NW of intersection)	RF modem
37	West	West bound Rest Stop - between 52/53 (NW end of Rest Area)	RF modem
24	West	Deerpark Avenue - 51 (NE .2 mile; close lane for bucket truck)	RF modem
23	West	Bagatelle Road - before 50 (NW .2 mile)	RF modem
21	East	Route 110 - 49 (above LIE on south median)	RF modem
20	West	Plainview - Washington Road (NE of intersection)	RF modem

TABLE 1 TFVC Site Locations

The TFVC system uses a unique method of video sensing which automatically detects traffic patterns present in a captured traffic scene. This approach begins with a video image which is obtained from the output of an off the shelf camera. The camera retains its original traffic monitoring capabilities because, after initial setup, automatic pan, tilt, and zoom hardware return the camera to preset sensing locations. Image processing algorithms developed by ITT automatically verify traffic lanes; the image within those lanes is processed to retain only pertinent traffic information. As individual frames from the video camera are analyzed, the main processor extracts the traffic data. For example, overall traffic flow speed is obtained directly from the processed traffic image for each direction, individual lanes and for both directions simultaneously. The processed traffic data are then sent to a control center for further analysis. The archived traffic data can be easily accessed by any SQL compliant database (a simple Microsoft Access application program was developed to allow a quick check of the data). In addition, the TFVC GUI can analyze and display on its console historical data retrieved from the archived traffic database. Government purpose license rights are in effect for specific portions of the TFVC system. For more information contact ITT Systems (bob.larson@ssc.de.ittind.com) or the Air Force Research Laboratory.

2.0 System Description

The following figure shows the major TFVC system components: Sensor, Graphical User Interface -- GUI, Database Server, and Network. Each will now be described. Technical specifications and details are included in the TFVC Hardware Systems Manual.

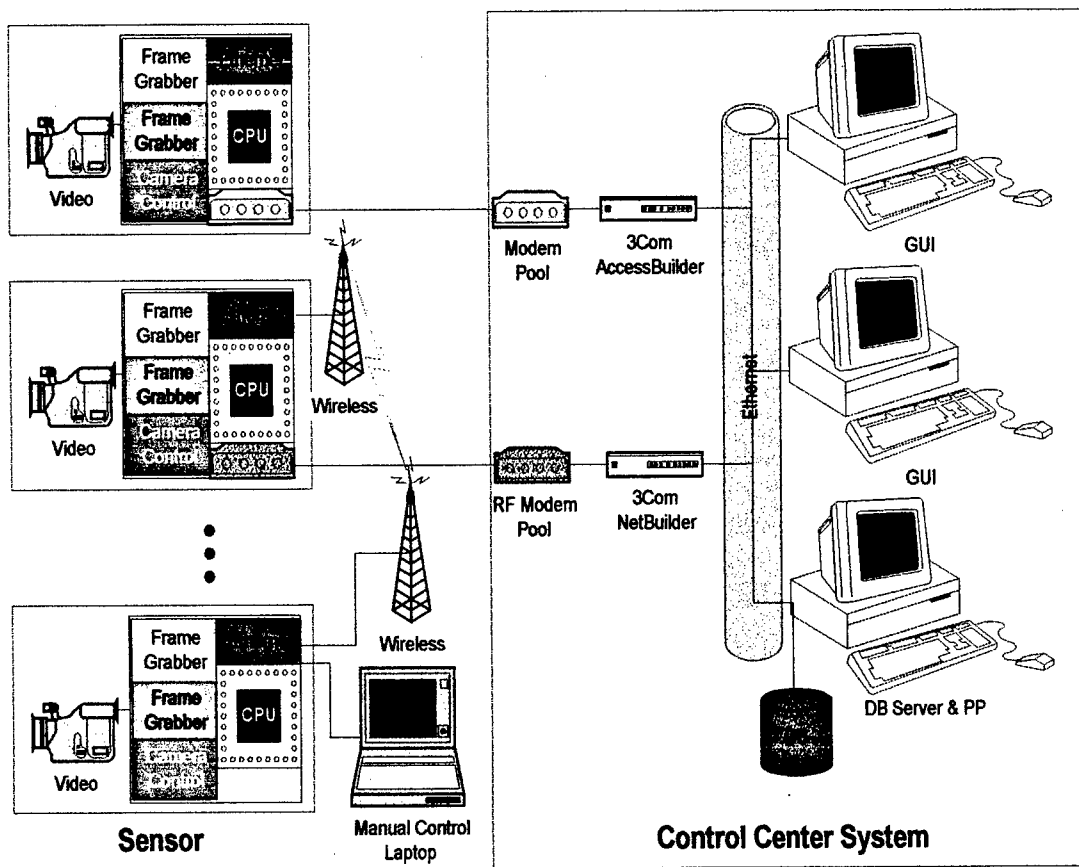


FIGURE 1 System Description

2.1 SENSOR

2.1.1 Functional Characteristics. The remote video sensor is responsible for acquiring and processing scene images, computing traffic parameters, and forwarding data to central computers. The specific functions are described in the following sections.

2.1.2 The TFVC Sensor is capable of simultaneously processing information from up to four (4) separate video sources including Video Cameras, CCTV video image sensors and video tape players. The video sources may be, but are not required to be, synchronized or line locked. The video is digitized and analyzed at a rate of 60 fields per second. Each of the 4 video cameras may be used for surveillance when installed with an optional Pan/Tilt/Zoom system. This is accomplished through the use of a video-multiplexing switch in the camera control board.

Because the switch must share resources between cameras, some performance degradation is seen for greater numbers of cameras used.

The SENSOR is able to detect and provide traffic parameters in a minimum of seven regions within each of the video cameras Field Of View (FOV).

The SENSOR is able to capture and transmit to the Control Center System (CCS) or traffic controller a black & white or color video snapshot of the video camera field of view. The update rate for the snapshot depends upon the bandwidth of the network and varies between 2 to 3 frames per second to 2 to 3 seconds per frame. With an adequate communication infrastructure, motion video could be transmitted.

The SENSOR is able to report to the CCS hardware status and system temperature for diagnostic purposes.

The SENSOR is designed to use TCP/IP as a communication protocol for interface to various communication architectures. These include Plain Old Telephone Service (POTS), Integrated Services Digital Network ISDN, wireless Ethernet, RF cable modem, and fiber.

When installed with the optional Pan Tilt Zoom unit the SENSOR is able to control pan, and tilt functions; no external control is required. All TFVC configurations are capable of controlling the zoom, focus and iris mechanism of each video camera.

2.1.3 Video Camera. TFVC is capable of using the output of off the shelf cameras that comply with the standards defined in the following sections. The SENSOR requires a video camera that supplies RS170A NTSC video. The video camera must have a remotely controllable lens with manual zoom, focus and iris control operating from +/- 8 volts DC. If the system requires complete surveillance capability each video camera site will have a pan and tilt assembly capable of an accuracy and repeatability of 0.1 degrees. Each pan and tilt assembly is capable of storing 32 mechanical presets, including pan, tilt, zoom, and focus settings and must support a differential RS-422 communication link. The video camera enclosure is capable of withstanding typical roadside environments with automatic heating, defrosting and cooling. The video camera enclosure contains a wiper for adverse weather conditions. Some performance degradation is seen when the wiper is used. In addition, adverse weather causing swaying in the sensor's pole can result in some degradation.

2.1.4 Traffic Regions. TFVC is capable of generating traffic parameters for the seven different regions shown and defined in the sections that follow. The SENSOR calculates Flow Speed, Density, and Volume for these lanes: The high occupancy vehicle (HOV) region, lane 1, lane 2, lane 3, the left shoulder lane, the right shoulder lane, and the far lane (defined as a collection of all lanes in the roadway at a point that begins beyond the 6 main lanes). Occupancy and headway parameters are readily derived from this data. Presence of vehicles in the left or right shoulder handled can be determined.

2.1.5 Traffic Parameters. The traffic parameters obtained by the TFVC system are Flow Speed (miles per hour), Density (vehicles per mile), and Volume (vehicles per hour). The

definition and accuracy of each parameter is given in the following sections. Occupancy and headway parameters are readily derived from this data.

2.1.6 Incident Detection. The SENSOR monitors all lanes within the field of view and is capable of detecting incidents. Congestion is detected using threshold-based algorithms developed by ITT traffic engineers and scientists. The threshold-based algorithm is discussed in section 3.3.1 and section 5.0.

2.1.7 Environmental and Mechanical Requirements. The SENSOR operates reliably in the adverse environment found in the typical roadway traffic cabinet. The SENSOR is capable of operating from -32 to 60 degrees C outside ambient. The SENSOR consumes less than 800 watts when connected to 120 volts 60 Hertz AC source. **Mechanical Requirements.** The SENSOR is 19-inch rack mountable. Nominal outside dimensions not including connectors is 9.5" x 17" x 13.5" (H x W x D). The SENSOR weighs 35 pounds not including external connectors.

2.1.8 Interface

- AC power connections are made to an IEC 320 power line inlet.
- Interconnection to the Video Camera is made through a dual 13 point barrier strip capable of supporting 16 AWG wire and a single BNC connector for video.
- Interconnection to the Serial communication port is made to a male 9 pin D connector.
- Interconnection to the Ethernet communication port is made to a female RJ-45 connector.
- Interconnection to POTS communication port is made to a female RJ-45 connector.
- Interconnection to ISDN communication port is made to a female RJ-45 connector.
- Fiber optic interface is made with standard fiber optic connectors and network adapters.
- Wireless interface. Connection to TFVC sensors is via 10BaseT RJ-45 crossover cables or using standard 10BaseT cables with a small mini hub, which utilizes standard RJ-45 connections.

2.2 Graphical User Interface – GUI

2.2.1 The GUI simultaneously processes all traffic parameters from all of the Remote Video Sensors. It displays the results of all traffic parameters in a graphical representation. It displays black & white or color video transmitted from the SENSOR at update rates that depend on the network bandwidth. The GUI alerts operators of any out of bound SENSOR status and temperature. It is capable of alerting operator of any incident detected. It is capable of pan, tilt, zoom, focus, and iris control of the video cameras attached to the SENSOR. The GUI uses multiple communication protocols for interface to various communication architectures. TCP/IP is used to communicate with the sensors. Other common networking protocols such as TCP/IP, IPX/SPX, and NetBEUI can be used to interface to the GUI on a LAN. The GUI is able to remotely setup and configure a SENSOR. The GUI software can be run on any workstation running Microsoft Windows NT 3.51.

2.3 Database Server - DB

2.3.1 The Database Server polls all traffic and Health / Status parameters from all of the Remote Video Sensors. It logs all data into the SQL database using Microsoft SQL Server version 6.0. The DB is able to display the results of a database SQL query.

2.4 Network

2.4.1 The SENSOR provides a convenient interface to all wireless Ethernet, RF coaxial cable, fiber, and phone (both ISDN and POTS) communication links described in this specification.

2.4.2 Types

- RF Cable Modems. The TFVC SENSOR can interface to RF cable modems operating over existing coaxial cable.
- Plain Old Telephone System (POTS). The SENSOR is capable of transmitting data over POTS link at a rate of 28.8 Kilobits per Second (KBPS). All lines provide for surge suppression. The link uses adaptive speed leveling for poor line conditions, error control to maintain data integrity, and data compression for increased data throughput.
- Integrated Systems Digital Network (ISDN). The SENSOR is capable of transmitting data over two 64 KBPS bearer channels and one data channel. This protocol is commonly known as a Bearer Rate Interface (BRI). The effective throughput rate is 96 KBPS full duplex. All lines provide for surge suppression.
- Wireless Ethernet. The SENSOR is capable of transmitting data over a 2 Megabits per Second (MBPS) wireless Ethernet link. The Wireless Ethernet media runs at 2.4 Ghz spread spectrum. The wireless bridges operate in the 2.4 GHz range using a spread spectrum technique that increases security and boosting data integrity. The Wireless Ethernet option requires that line-of-

sight be maintained between antennas at adjacent sites without obstruction.

- Fiber. The TFVC sensor is readily adaptable to fiber optic networks. The high bandwidth of fiber will greatly enhance the performance of the system, especially the video frame rate update.

3.0 Summary of Technical Work Accomplished

3.1 Hardware Subsystems

3.1.1 An innovative modular sensor subsystem was developed that locally housed the image processing and control equipment for TFVC. The design for this used cost effective, off-the-shelf hardware. The TFVC sensor realizes a distributed architecture design that maximizes the networking resources employed. This subsystem includes a camera controlled by an adaptive auto iris for contrast control. A customized Pan/Tilt/Zoom mechanism was developed to accurately return the camera to a predetermined view. The processor uses a single Intel Pentium chip and common frame grabber boards; this design can be leveraged for increased performance as this hardware state of the art advances.

3.1.2 The network subsystem reflects flexibility and adaptability for creative use in a wide variety of situations. RF cable modems can be used with TFVC when cable backbones are present in the existing infrastructure. Plain old telephone systems (POTs) and a wireless Ethernet option bound the bandwidth possibilities developed on the project. A discussion of ISDN and fiberoptic implementations are included in this report.

3.2 Software Developed

3.2.1 Software developed for the sensor subsystem represents some of the most creative work done. Efficient flow speed algorithms developed, coded, and tested under the TFVC project allowed for accurate calculations of traffic parameters using the cost effective hardware design. (This work is summarized in appendix A.) Incident detection methods were developed to automatically notify the operator of a potential problem, based on the flow speed parameters over time. Communications and TCP/IP sockets solutions were also developed. Software for compressing JPEG image data for transmission over network media was also developed.

3.2.2 GUI application software to facilitate control of the TFVC system as well as display of system data and parameters was written in an object-oriented manner using Microsoft Visual C++ and Microsoft Foundation Classes. The application made it easy to view the status of the entire system and also image data from selected sensor sites.

3.2.3 The database application was developed to archive system data for later analysis. This program interfaces to an MS SQL Server database for easy access by any SQL compliant method. The application also polls each of the sensors regularly, automatically retrieving the data from the sensors. It also allows the user to easily query the database of traffic data.

3.3 Incident Detection Algorithms

3.3.1 The initial incident detection philosophy during the development of the TFVC system was to combine as many traditional traffic parameters as necessary with efficient and accurate artificial neural networks (ANNs) to provide reliable (low false alarm rate) incident detection. Other methods that were also explored included threshold-based algorithms and horizontal movement detection by checking regions. This was done from single sensor and multiple sensor data sources. Ultimately, a wide area solution was sought as opposed to a point case (grain of sand) solution. Threshold based algorithms examined flow speed, volume, and density over a period of time and compared them with operator selected values. Ultimately the threshold-based approach was implemented in the TFVC MC code.

3.4 Innovations in Artificial Intelligence Traffic Control

3.4.1 ANN approaches to incident detection used the current and two previous values for flow speed, density, and volume as well as time of day and day of week to train standard multi-layer perceptron neural network backpropagation algorithms with forward and backward training. This resulted in up to 1,830 total inputs for three lanes and three parameters from time, day and date. ANN outputs examined were 1) congested conditions, 2) roadway obstruction, and 3) possible accident -- for a total of three outputs. Multi-sensor methods were also studied to combine data from more than one site.

3.5 Reference Documentation

Traffic Flow Visualization and Control System (TFVC) Preliminary Design Review Final Report CDRL A003, K95-23U(R), 24 March 1995.

Traffic Flow Visualization and Control System Design Plan CDRL A008, K95-12U(R), 28 March 1995.

Traffic Flow Visualization and Control System Safety Hazard Analysis Report CDRL A011, K95-10U(R), 13 April 1995.

3.6 Environmental Screening Test Plan

3.6.1 This section details the environmental test procedures for the TFVC Remote Sensor Subsystem (RSS). It is intended that the RSS, made up of commercially off the shelf (COTS) sub-assemblies, be dedicated for use under adverse field conditions through testing. The ITT supplied Central Control Subsystem (CCS) will not be subjected to ESS testing since the unit will be used in a favorable control room environment.

3.6.2 Referenced Documents

- MIL-STD-785, Task 301 Environmental Stress Screening (ESS)
- MIL-STD-810E Environmental Test Methods and Engineering Guidelines

A summary of ESS testing is shown in Table 2.

Burn-in for 100 hours.	Functional test prior to and after burn-in. Heart beat monitored during burn-in.
Temperature cycling 3 cycles 0 to 55 degrees C.	RTD mounted centrally within the RSS. Functions tested prior to, during and after temperature cycling.
Thermal protection, safe system shutdown verification, 1 hot cycle greater than 60 degrees C.	Verify system shuts down and auto re-boots.

TABLE 2 ESS Testing

3.6.3 Failure Criteria. Troubleshooting of a discrepancy and retest of the discrepant item will be at the direction of the program manager. As a minimum, after the discrepancy has been corrected, testing will proceed with the last successful test completed.

3.6.4 Burn-In Test. This test detects material and workmanship defects that occur early in the component life (infant mortality). The minimum burn-in time for the RSS prior to exposure to temperature cycling will be 100 hours. Burn-in will be conducted at bench level in lab environment. The RSS will not be installed in the 330 enclosure. The RSS will be instrumented and tested as stated in Functional Test A prior to starting burn-in. Heartbeat will be monitored, as a minimum, for the 100 hours of burn-in. Functional tests may be conducted anytime during the burn-in period to detect early failures rather than waiting for the 100 hour post burn-in test to detect burn-in failures. Once burn-in has been successfully completed, the unit can now be subjected to ESS Temperature Cycling.

3.6.5 Temperature Cycling Test (ESS). This test detects material and workmanship defects while demonstrating field worthiness of the COTS subassemblies selected for the use in the RSS, in addition, verification of the RSS internal environment control systems will be demonstrated. Refer to Figure 2 during the following discussion.

The RSS will be subjected to three (3) temperature cycles from 0 to 55 degrees C. A fourth high temperature cycle greater than or equal to 60 degrees C will be performed to verify the over-temperature safe system shutdown and re-boot system performance. The RSS will be placed in a suitably sized environmental chamber. (Note: The RSS will not be installed in the 330 enclosure). Once placed in the chamber, as a minimum, one (1) RTD will be affixed centrally within the RSS. This RTD response will be the controlling temperature for controlling purposes. Chamber ambient air will be observed using the chamber controller display. The RSS will be instrumented and tested as stated in the Functional Test B procedure during temperature cycling activities. Prior to starting the temperature cycle test, a functional test (Functional Test A) will be conducted at room temperature. Once successfully completed, the RSS is turned off and ready to begin the 3 temperature cycles. A temperature cycle begins with the RSS at room temperature. With the RSS turned off, the chamber ambient air is reduced to -10 degrees C. (Note: An overshoot by 5 degrees C (-15 degrees C) will accelerate the temperature transition of the RSS mass.) Once the RTD mounted in the RSS has reached -10 degrees C, the RSS is turned

on and tested in accordance with Functional Test B procedure. Once completed with the RSS remaining on the chamber ambient air is then increased to 55 degrees C. (Note: An overshoot by 5 degrees C (60 degrees C) will accelerate the transition of the RSS mass). Use caution as not to exceed the maximum internal temperature of 55 degrees C during testing. Once the RTD mounted in the RSS has reached 55 degrees C, perform the test in accordance with Functional Test C. Turn power off to the RSS and reduce the chamber to ambient air to 0 degrees C. When the chamber air passes through room temperature (23 degrees C), this completes 1 temperature cycle. Repeat the above two additional times to complete three (3) temperature cycles. At the end of the third cycle, the chamber ambient air is reduced to room temperature (23 degrees C). Once the RTD has reached room temperature, turn power on and perform the test in accordance with Functional Test A. Once the above has been successfully completed, increase the chamber ambient air to greater than 60 degrees C (65 degrees C). In accordance to Functional Test D, monitor the RSS until the unit demonstrates the safe system shutdown provision. Verify actual temperature of the RSS by the temperature controller display. Reduce chamber ambient air to 23 degrees C and verify unit recovery temperature. Turn off power to the RSS and allow to return to room temperature (23 degrees C). Perform a post ESS test in accordance with Functional Test A. This concludes the RSS Environmental Stress screening testing.

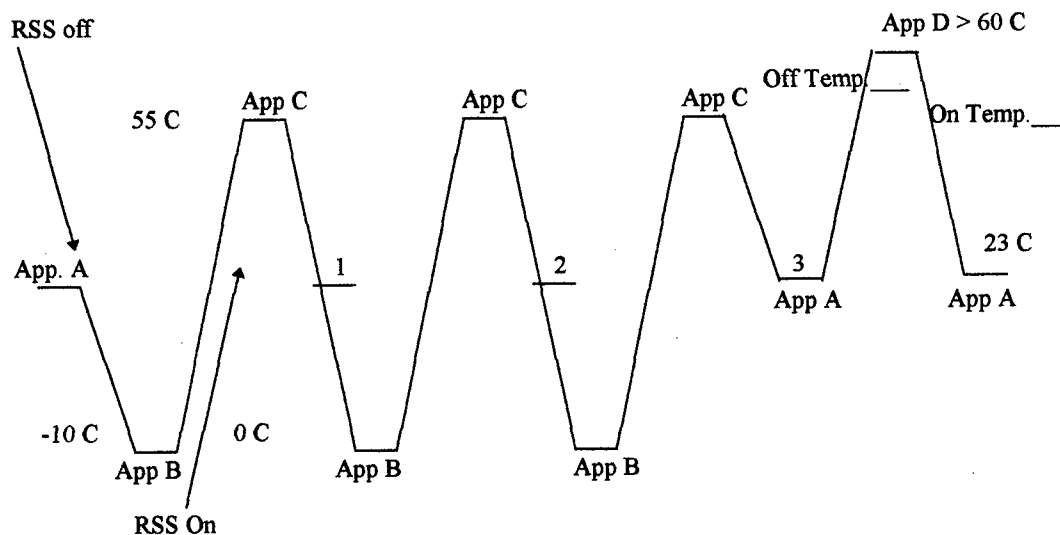


FIGURE 2 RSS Environmental Testing

3.6.6 Functional Test A

1. Connect video source to Camera 1,2,3,4 of Remote Sensor Subsystem (RSS) if not already done.
2. Connect communication link to RSS and to Central Control Subsystem (CSS) if not already done.
3. Connect video monitor to RSS video out if not already done.
4. Connect power cord to 110 volt and to RSS via AC line separator if not already done.
5. If RSS is not already on turn system on, measure and record AC current.

6. Verify power indicator and status indicator are illuminated and remain illuminated after 2 minutes.
7. From the CSS request a B/W snapshot, Color snapshot and Health from camera 1. Log health information.
8. Repeat snapshots for remaining cameras.

3.6.7 Functional Test B (with low temperature heater operation)

1. Turn AC power on.
2. Monitor AC current.
3. On first cycle current should increase by approximately .5 amps when system turns on. On remaining cycles system should come on immediately.
4. Measure and record AC current.
5. Verify power indicator and status indicator are illuminated.
6. From the CSS request a B/W snapshot, Color snapshot and Health from camera 1. Record health information.
7. Repeat snapshots for remaining cameras.

3.6.8 Functional Test C (at high temperature)

1. Measure and record AC current.
2. Verify power indicator and status indicator are illuminated.
3. From the CSS request a B/W snapshot, Color snapshot and Health from camera 1. Log health information.
4. Repeat snapshots for remaining cameras.

3.6.9 Functional Test D (at safe shutdown temperature)

1. Increase Chamber temperature until AC current drops to zero. Record the turn off chamber temperature. Caution, do not allow ambient to exceed 65 degrees C.
2. Decrease ambient temperature while monitoring AC current. Continue to reduce chamber temperature until current returns to approximately .5 amps.
3. Record the turn on chamber temperature.
4. Measure and record AC current.
5. Verify power indicator and status indicator are illuminated.
6. From the CSS request a B/W snapshot, Color snapshot and Health from camera 1. Log health information.
7. Repeat snapshots for remaining cameras.

4.0 Information gained / Lessons learned / Results

4.1 Approach. TFVC proved to be an innovative approach to a difficult problem. It provided cost-effective real-time traffic flow data and achieved promising results to a variety of tough technical problems.

4.2 Integration. System integration is a key element in the development of a system such as TFVC. Systems such as these need to be tested in a modular fashion. In particular, the network subsystem must be fully tested before the rest is deployed. Network problems comprised the great majority of fielding difficulties.

4.3 Fielding. Fielding a system such as this at an urban site requires the support of local agencies and contractors. TFVC had very good support from NYSDOT and their contractors Johnson Electric and Wiley Engineering. These costs grew over time, however, and future efforts need to take this into account and budget accordingly.

4.4 Iris Control. Iris control is a critical element in camera based surveillance systems. It is a key to providing adequate contrast for traffic flow speed algorithms to be effective. The TFVC approach to iris control was creative and innovative, but complicated. This needs to be an area of further work and development, particularly taking into account weather related effects. A more robust iris control algorithm needs to be developed and tested. Our experience teaches us that this important issue (for all video based traffic detection systems) that should be carefully addressed.

4.5 Software Methods. Object oriented software methods provide efficient ways to develop and test the software used on this project. Microsoft Visual C++ is an excellent development platform. The extended DOS environment used on the sensor worked well, but had some limitations. Using Windows NT for the sensor operating system would be the next logical step.

4.6 Network. Network issues proved to be the most difficult in the implementation of the TFVC system. The ISDN and the wireless system experiences will now be discussed in detail.

4.6.1 ISDN Implementation within the TFVC system. During the FASTRACK phase of the TFVC program the use of ISDN (Integrated Services Digital Network) as a high bandwidth communications channel was evaluated on 4 of the original 5 sites. It was also originally planned to be used as the primary communications channel for the six eastern most sites that had no access to the INFORM cable trunk. These sites were subsequently outfitted with a wireless LAN system, but the ISDN access was installed as a backup. One Primary Rate Interface (PRI) line was installed at the INFORM control center at the state building in Hauppauge N.Y. One full Basic Rate Interface (BRI) line was installed at each of the four selected sites. A full BRI is made up of 2 data channels @ 64kbps. A Gandalf network bridge with PRI interface was used as the ISDN concentrator in the INFORM control center. Combinet ISA based adapter cards were used in the sensor hardware to interface to the ISDN lines. These adapters appeared as network interface cards to the sensor operating system. The INFORM maintenance contractor performed TFVC cabinet wiring of the ISDN interface. Bell

Atlantic/NYNEX performed all the provisioning of the ISDN lines as well as the installation of the PRI line in the INFORM control center.

The PRI line required quite a lot of time to be installed by NYNEX, resulting in a delay. The GANDALF concentrator went through several software revisions before a working revision worked. This was a problem primarily with compatibility with the multi-link protocol and user authentication. In addition, local Tariffs of ISDN lines can make them *very* expensive to use. The dial-on-demand features did not work reliably. TFVC sensor software had problems monitoring or acting on ISDN connection status.

The COMBINET ISDN adapter card appeared as a network interface card to the operating system which meant no special software was needed for the network connections. This card also had a back door via a terminal program that allowed for monitoring the connection status. NYNEX provisioned the site ISDN BRI lines quickly, and they worked immediately. The PRI line, once it was installed, worked right away. When we had a connection from the GUI to the sensor, the extra bandwidth really improved the video response. This was especially helpful during Pan/Tilt operations.

Once the GANDALF concentrator was working, the ability to link the two "B" channels to get 128 kbps of raw data speed proved invaluable. Due to software and protocol overhead our actual data rates were around 100 kps. This was far better than the 28.8 kbps raw data speed of the POTS lines. ISDN lines can establish a connection on the order of hundreds of milliseconds while POTS lines take around 30 to 50 seconds.

4.6.2 Wireless Ethernet. Wireless communication products were purchased from TTI Wireless. The processor/transmitters (bridges) are designed to work up to 5 miles, or up to 30 miles with optional amplifiers. The antennas require very high clearance over the ground for this distance. The bridges that were obtained operate in the 2.4 GHz frequency range using a spread spectrum technique. The 2.4 GHz range was selected over the other 915 MHz range because of interfering competition from wireless phones and other systems within the 915 MHz range.

Alignment of the antennas using the software utility PTPDIAG as noted by the manufacturer is critical to a proper functioning system. When two antennas were required at a site they were offset by 4 to 5 feet and cross polarized for adjacent sections. This setup of antennas is explained in the Sensor hardware manual and is done to reduce signal effects of two antennas placed back to back. A wireless section consists of two bridges with two antennas beaming signals between them. These bridge pairs must also have the same Network ID (NWID). The NWID is alternated to reduce the effects of cross talk between non-adjacent antennas.

Although several sites had Poor or Acceptable Link Quality Assessment it did not seem to affect the effective bandwidth of that or neighboring sites. Sites should be tested using a sensor link from the remote GUI, or two computers one being an FTP server and the other computer requesting a large data file. Obstacles like highway signs in the line of sight greatly affect effective bandwidth even if the Link Quality Assessment is Good. The AC power plugs to the bridges and the connectors from each antenna were of a push-on type that could come easily

loose. Usually the bridge was mounted with that end down. Cable ties were used to keep these connections in place. In order to run diagnostics on a bridge node a keyboard and monitor must be carried to each site. Two bridges at adjacent sensor sites must be set in the diagnostic mode. Once the proper diagnostic mode is started the keyboard and monitor can be removed and used at an adjacent site to monitor all functions or make antenna adjustments. These diagnostic modes will continue indefinitely as long as power is not interrupted. When testing is completed both bridges must be rebooted for proper operation to automatically resume. The power plug must be removed to interrupt power. There is no need to have the keyboard and monitor attached to return the bridges to normal operation. For the most part the sites east of Hawkins were staggered from east to westbound sides of the LIE. This proved to be very effective in cutting down on obstruction problems especially along the sides of the road. The antennas used were of a lightweight aluminum in an open "bird cage" design with very low wind shear. This open design is also valuable in decreasing snow and ice buildup. We used the same pole bracket, horizontal arm, and 360-degree tilt bracket from Pelco that are used on fixed cameras.

There is a pretty steep learning curve on learning these systems and setting them up in a lab environment is a must. The test system should include two antennas *facing away from each other* to reduce high gain problems. Each bridge must be individually checked and configured, as the overall system requires. Note that for sites requiring two antennas that there are two associated cards in each bridge that must be configured.

Once the bridges are set up in the lab, the installation is straightforward. Assembling the antennas, which come in two pieces, is a simple five-minute operation that should be done on the ground at the site. Installation of the antenna(s) by electricians is a simple matter from a bucket truck. The antenna cable can be installed at the same time if desired, but was usually preinstalled by Johnson Electric (NYSDOT Electrical Contractor) to save time. The antenna should be "eyeballed" to the nearest associated antenna. The bridges are easily mounted to the equipment rails in the 330 enclosure. ITT Systems personnel usually mounted the bridge ahead of time. Once the antenna is secure simply connect the antenna cable(s), connect a 10BaseT cable to the sensor, and power on the unit. The final alignment can be done between any two fully functioning sites using the PTPDIAG utility. It usually takes just a few minutes to find the optimum direction.

These units have required no service once they were configured and installed. The units perform completely to their specifications. The total cost for the wireless hardware came to almost \$31,000. For the 6 additional sites that is \$5,166 per site. Although this is a high initial cost there are no monthly charges as in leased lines at 56K and ISDN. The cost effectiveness is quite low when compared with installing brand new coax or fiber optic cable to these sites.

4.6.3 The RF Cable Modem implementation within the TFVC system includes nine of the TFVC sites use the existing INFORM RF cable backbone infrastructure to send and receive data to the TFVC GUI and SQL server computers in the INFORM control center. The site at Hawkins Ave. (#36) also acts as a collection point for the six wireless Ethernet LAN sites east of Site #36. This was chosen over other solutions to support high data rates between the TFVC sensors and the GUI computers. Also, the equipment was purchased as capital items with no recurring charges for leased lines that would come out of an operational budget.

Cable Modem System Components:

- 1 3COM NetBuilder 2 Router with 4 HSS ports to support 9 cable modem sites.
- 9 3COM NetBuilder 221 Routers for each of the TFVC sensor sites.
- 16 RF Networks 5450 Cable Modems @ 256K data rate
- 2 RF Networks 5450 Cable Modems @ 1544K data rate
- 18 V.35 cables to go between the router and cable modem. One each per pair.
- 2 TONER TDA-112 1GHz. Broadband Drop Amplifier
- 2 TONER XGVS-16 1GHz 16 Way Splitter
- 10 BLONDER TONGUE DSV Multiplexers
- RG59U cable with F-connector

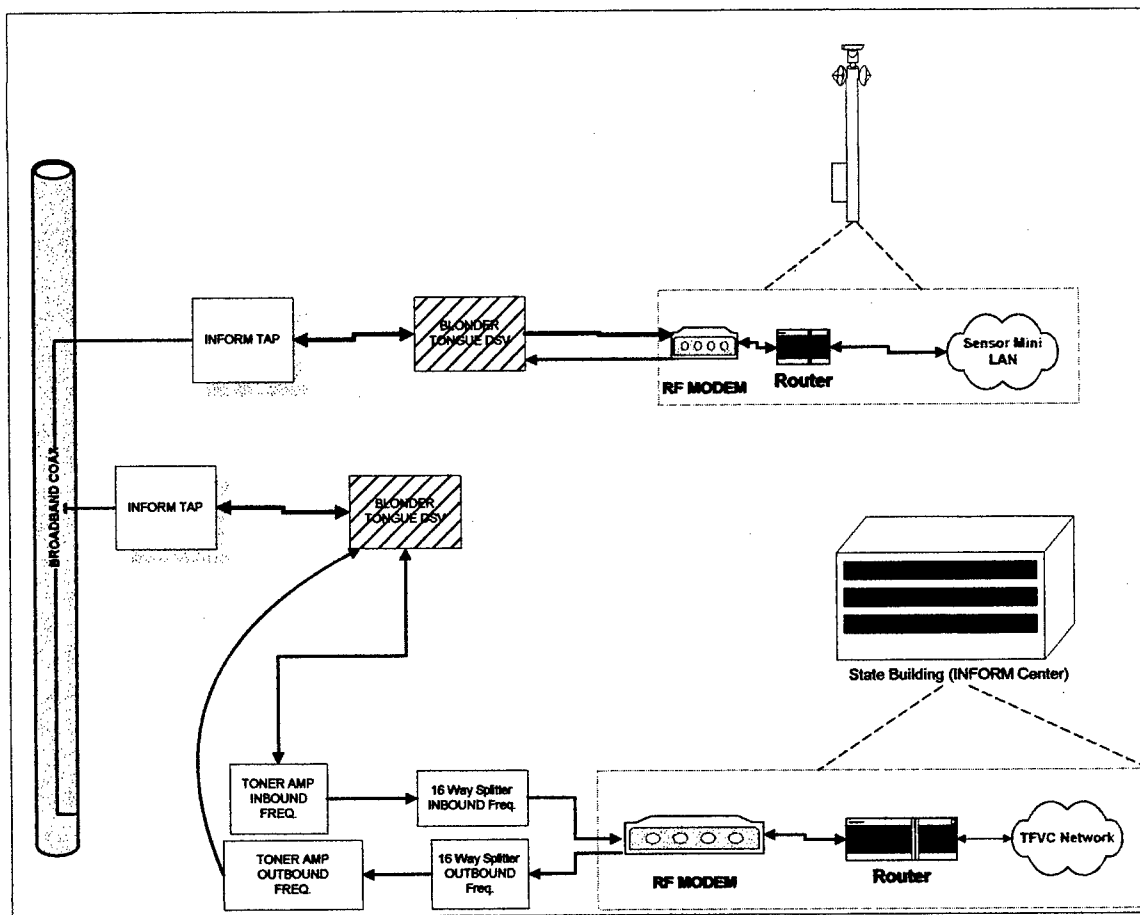


FIGURE 3 Cable System Block Diagram

There were difficulties encountered with the Cable system. The original frequency allocations for these RF cable modems only allowed for one outbound channel to be shared by all cable sites. The routers require that each site have its own channel for both inbound and outbound data. The INFORM cable did not have enough spare bandwidth available in the lower frequency band (5MHz - 30MHz). So channels were reallocated for 1 1544KB channel each way and 8 channels that could support 256K data rates each way.

Sixteen of the modems were sent back to RF Networks to have a data rate change from 1544Kbps to 256Kbps. This was attempted in the field, as the vendor (RF Networks) indicated to us that this is possible. However, specialized test equipment was required. Also, this was a new revision of their data rate kit, and installation procedures were not available. All of this resulted in considerable time delays.

The cable modems are actually designed to use a separate cable for inbound and outbound channels. Even with the inclusion of a splitter there was a lot of output power feeding back into the receiver and causing problems. We solved this with the inclusion of the DSV Multiplexer, which has very little insertion loss but a lot of isolation between the inbound and outbound frequency range. Each sensor site got one of these. Plus one was needed in the INFORM control center.

The receiver in the cable modem has a narrow AGC range. With all of the different taps, splitters, etc. on the system at each sensor site, keeping the input power within this range was difficult.

The NBII had a problem for awhile that kept it from doing its bridging function. With 3COM technical supports help, it was finally determined that the files on the FLASH boot drive was corrupted. Once this was fixed the NBII worked fine.

The RF Networks cable modems rely solely on their modulation scheme for bit error rate reduction. The NBII/NB221 routers only do error detection on the incoming packets. These two combined don't pose a problem as long as the transmission medium is relatively error free. This was not the case. The routers will drop a connection when they detect too many errors. They will try to reestablish the link but most often this would fail. Therefore operator intervention was required to bring the link back up. This happened with a very high frequency. A cable modem that utilized an error correction scheme on the bit stream would have been helpful.

The INFORM maintenance contractors started doing a major tune-up of the cable trunk during TFVC fielding. This caused a lot of variability in the signals on the cable trunk and made debugging our problems all the more difficult.

Sections of the LIE where our sensors reside were undergoing a major road upgrade. This resulted in the cable trunk or electrical power being interrupted. This also caused time delays.

When a good connection was established, the live video worked very well. We didn't really see much difference in frame rate from the 1544Kbps site vs. a 256Kbps site. This probably indicates that we are processor limited (to some extent) on the GUI and SENSOR ends.

4.7 Software Maintenance and Upgrade Issues

4.7.1 TFVC GUI systems run on top of Windows NT 3.51 as the base operating system. Microsoft has stopped support of this revision of NT. We have tested the GUI code under NT 4.0

and know of no compatibility issues. Microsoft has not finished Y2K compliance testing as of August 1998. MS Office Pro 4.3, the suite that was used with the system has numerous Y2K issues, particularly with Access 2.0.

4.7.2 TFVC SERVER systems utilize Windows NT 3.51 Advanced Server as the base operating system. Microsoft has stopped support of this revision of NT. Microsoft has not finished Y2K compliance testing as of August 1998.

4.7.3 TFVC Database Server is SQL Server 6.0 and is not scheduled to be Y2K compliance tested, but SQL server 6.5 is. We bought SQL 6.5 for TFVC but never installed it on the delivered server. We would need to test our database connectivity with SQL 6.5 to determine if there are any issues.

4.7.4 TFVC Sensor utilizes MSDOS 6.2 and Y2K compliance results have not been released yet. We believe there may be compliance issues with MSDOS 5.0. Everything else should be O.K., but we have not tested it for Y2K compliance.

4.7.5 Development Environments. In general, all of the TFVC development suites are several revisions old and would need to be updated for further development. The compilers in particular will have Y2K issues. This would include the following:

GUI and DB codes:

Microsoft Visual C++ 4.2

LeadTools V9.0

Matrox MIL-Lite

Sensor code:

Watcom C++ 10.5

PCTCP Developers kit.

Bitflow Raptor SDK

4.8 Fiber Optics Development

4.8.1 Adapting the TFVC system to be used with a fiber optic based network would be straightforward. The details of the network topology would have to be defined before an approach could be envisioned, however. Basically, TFVC consists of networked PCs -- much as any LAN or enterprise network would function. This basic design feature allows for current state-of-the-art technology and off the shelf networking solutions to be leveraged efficiently into a solution. Particular issues that are unique to the TFVC network development deal with accessibility to sites and bridging between different media. Otherwise, any standard networking approach could be implemented within the TFVC system with minimal impact on the overall architecture.

4.9 Overall Cost / Performance Tradeoffs of each Networking Approach Used

4.9.1 Based on TFVC development and fielding experience we would rank the various networking approaches that were used in terms of cost and performance as follows. The scale is from one to ten (ten being high cost and high performance).

	<u>Cost</u>	<u>Performance</u> (if working)
Telephone modem – POTS	2	2
Telephone modem – ISDN	8	5
RF cable modem	9	6
Wireless Ethernet	8	9

5.0 Flow Speed Calculation

5.1 Introduction

For traffic monitor and control, one of the most important parameters is vehicle speed. Currently, the loop sensor determines the vehicle speed by determining the vehicle length and the time it takes to pass the loop, which yields the speed. This method is not reliable due to the noise and other errors in determining the length of the vehicle. It also requires an accurate calibration for it to work properly. The main problem comes from the fact that it determines vehicle speed vehicle by vehicle, which is more susceptible to noise and other errors. Also, by monitoring only individual vehicle, we can not have a good picture of the overall traffic condition, and thus, will not be able to react fast enough to a sudden traffic condition change. In order to alleviate the noise factor and be able to monitor the overall traffic condition, we need to have a method which treats the overall traffic as a whole and determines its condition. With this type of method, most of the individual noise and other errors will be suppressed and it can see the correlation between the traffic conditions within a large region.

In this article, we will describe such a method. The method uses correlation algorithm to determine the overall traffic speed in the region of interest (ROI). We will call this algorithm Correlation for Flow Speed (CFS) algorithm. This algorithm comprises two parts: the collapsed waveform and the correlation. The collapsed waveform method collapses a 2-D image of the lane(s) into a 1-D waveform along a certain direction (Currently it is horizontal direction unless the lanes are horizontal. In that case, it will be vertical. In the later development, we will use horizontal when the lanes are less than 45° from the vertical direction and vertical when the lanes are more than 45° from vertical direction) by averaging the pixel intensities along that direction. The collapsed waveform will carry most of the important features of the 2-D image. It will demonstrate a peak (or valley, depends on the color of the vehicle) wherever there is a vehicle and the length of the vehicle. The only information that it will lose is its width and its shape. Nonetheless, this loss of information will not affect the accuracy of our flow speed computation.

In the following, we will call the camera focal plane as the image plane and the roadway system as the object plane.

5.2 Collapsed Waveform Algorithm

In this section, we will discuss the collapsed waveform algorithm. In all the formulas in this section, we will use P_x and P_y as coordinates in the image plane. Bear in

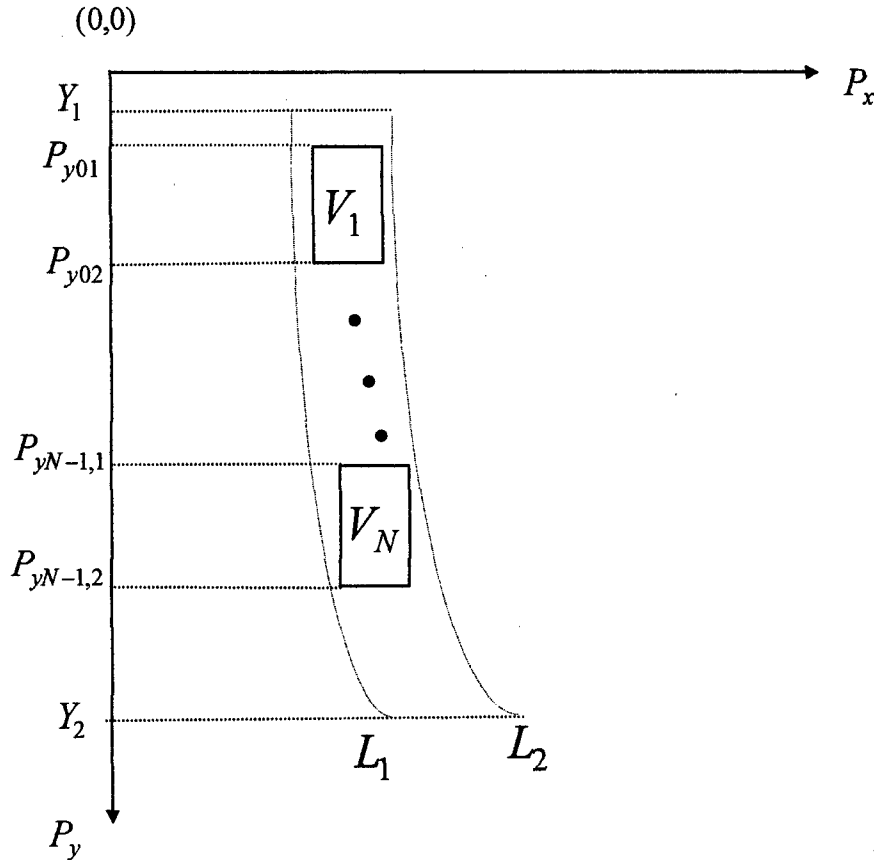


FIGURE 4 Image of a Traffic Lane

mind that P_x and P_y are discrete, that is, they only increment by integral values since we have only discrete pixel mesh.

Assume we have a 2-D traffic image with a lane (For multiple lanes, the conclusion will be the same since we collapse only one physical lane or one super-lane comprised of multiple lanes), as shown in FIGURE 4. L_1 and L_2 are the left and right curves of the lane. Assume that the equations for the two curves are order 2 parabolic functions (this is a valid assumption in that the traffic lane curves are generally less than or equal to order 2 within a small region in which we are interested. The derivation below, however, will be still valid for higher order polynomial functions):

$$L_1: \quad P_{x1}(P_y) = a_1 P_y^2 + b_1 P_y + c_1 \quad (\text{II.1a})$$

and

$$L_2: \quad P_{x2}(P_y) = a_2 P_y^2 + b_2 P_y + c_2 \quad (\text{II.1b})$$

The ROI starts from Y_1 to Y_2 . Assume that there are N vehicles, V_i , with bottom and top P_y coordinates P_{yi1} and P_{yi2} , $Y_1 \leq P_{yi1} \leq P_{yi2} \leq Y_2$, $0 \leq i < N$, in the ROI, and that the intensities for the vehicles are uniform with value 1 and the background intensity is 0. Let $f(P_x, P_y)$ be the intensity function of the 2-D image. Thus,

$$f(P_x, P_y) = \begin{cases} 1 & (P_x, P_y) \text{ on or inside a vehicle} \\ 0 & (P_x, P_y) \text{ outside a vehicle} \end{cases}$$

$$P_{x1}(P_y) \leq P_x \leq P_{x2}(P_y) \quad \text{and} \quad Y_1 \leq P_y \leq Y_2 \quad (\text{II.2})$$

We then collapse the traffic lane $f(P_x, P_y)$ into 1-D waveform $g(P_y)$ by averaging over the traffic lane horizontally (or along the x direction) to give

$$g(P_y) = \frac{1}{P_{x2}(P_y) - P_{x1}(P_y) + 1} \sum_{P_x=P_{x1}(P_y)}^{P_{x2}(P_y)} f(P_x, P_y)$$

$$\Rightarrow \quad g(P_y) = \sum_{i=0}^{N-1} [u(P_y - P_{yi1}) - u(P_y - P_{yi2})]$$

$$Y_1 \leq P_y \leq Y_2 \quad (\text{II.3})$$

where $u(P_y)$ is a step function

$$u(P_y) = \begin{cases} 1 & P_y \geq 0 \\ 0 & P_y < 0 \end{cases} \quad (\text{II.4})$$

$g(P_y)$ is as shown in FIGURE 5.

In the above, we assume, for simplicity, that the vehicles fill up the whole traffic lane to still yield average intensity 1 (Normally that is not the case. However, a vehicle generally occupies most of a lane width, so the average intensity will be slightly below 1. Thus, it is a valid assumption).

The collapsed waveform algorithm basically reduces the complexity of a 2-D image into a 1-D waveform while maintains important information. This is significant since it generate the same results with less computational power, which saves cost and time of a development cycle.

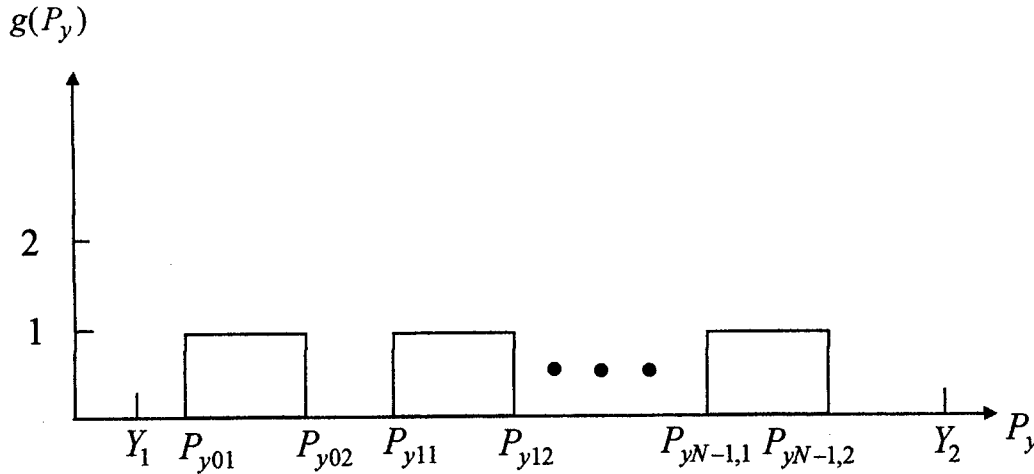


FIGURE 5 1-D Collapsed Waveform $g(P_y)$ of a Traffic Lane

Now that we have the collapsed waveform, we can process it to generate useful results such as the flow speed. In the following, we will discuss the correlation algorithm for flow speed determination.

5.3 Correlation Algorithm for Flow Speed Computation

Because we will deal with 1-D collapsed waveform in this section, we will drop the subscript y in P_y in the above collapsed waveform for simplicity. Thus, Eq.(II.3) becomes:

$$g(P) = \sum_{i=0}^{N-1} [u(P - P_{i1}) - u(P - P_{i2})]$$

$$Y_1 \leq P \leq Y_2 \quad (\text{III.1})$$

and FIGURE 5 becomes FIGURE 6.

We will use y coordinate for the object plane to distinguish the coordinates between the image plane and the object plane.

In order to demonstrate the idea of using correlation algorithm to determine flow speed, we will ignore in subsection A the camera perspective, that is, we will assume that the calibration factor for the whole y direction is the same. The effect of camera perspective on the flow speed computation using correlation algorithm will be discussed in subsection B.

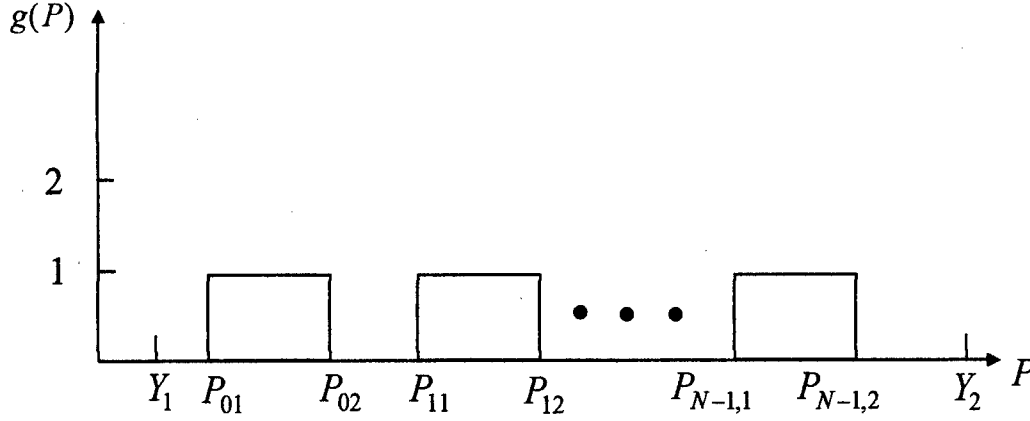


FIGURE 6 Redraw of 1-D Collapsed Waveform $g(P)$ of a Traffic Lane

A. Uniform Calibration Factor for the Whole y Direction

Assume that all the vehicles move in the same speed, v . At dt time interval, the vehicles will move by dy distance in the object plane

$$dy = vdt \quad (\text{III.A.1})$$

With no perspective, the calibration factor will be same for the whole y direction. Assume this constant calibration factor is γ . Then the pixel shift in the image plane will be dP

$$dP = \frac{dy}{\gamma} = \frac{vdt}{\gamma} \quad (\text{III.A.2})$$

Thus, $g(P)$ becomes $G(P)$,

$$\begin{aligned} G(P) &= \sum_{i=0}^{N-1} \{u[P - (P_{i1} + dP)] - u[P - (P_{i2} + dP)]\} \\ &= \sum_{i=0}^{N-1} \{u[(P - dP) - P_{i1}] - u[(P - dP) - P_{i2}]\} \\ Y_1 &\leq P \leq Y_2 \end{aligned} \quad (\text{III.A.3a})$$

$$\xrightarrow{\text{Eq.(III.1)}} G(P) = g(P - dP) \quad Y_1 \leq P \leq Y_2 \quad (\text{III.A.3b})$$

For Eqs.(III.A.3a) and (III.A.3b) to be true, we have assumed that no vehicle has moved into or out of the ROI region, as shown in FIGURE 7. That is,

$$\text{and} \quad g(P) = 0 \quad \text{for } Y_1 - dP \leq P < Y_1 \quad (\text{III.A.4a})$$

$$\text{or} \quad g(P) = 0 \quad \text{for } Y_2 - dP < P \leq Y_2 \quad (\text{III.A.4b})$$

$$\text{and} \quad G(P) = 0 \quad \text{for } Y_1 \leq P < Y_1 + dP \quad (\text{III.A.4c})$$

$$\text{and} \quad G(P) = 0 \quad \text{for } Y_2 < P \leq Y_2 + dP \quad (\text{III.A.4d})$$

In reality, this is not true. However, as long as $dP \ll Y_2 - Y_1$, the result will be similar for the real case.

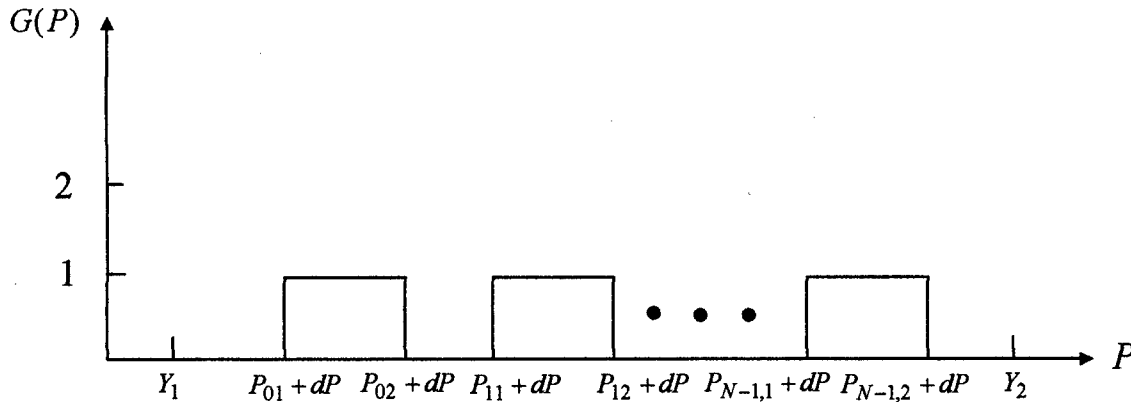


FIGURE 7 1-D Collapsed Waveform $G(P) = g(P - dP)$ of a Traffic Lane

From Eq.(III.A.3b), we see that $G(P)$ is a shifted version of $g(P)$, as expected. Now we want to compute the auto-correlation function $r_{gg}(P)$ of $g(P)$ and cross-correlation function $r_{Gg}(P)$ of $G(P)$ and $g(P)$. As defined,

$$r_{gg}(P) = \sum_{P1=Y_1}^{Y_2} g(P1)g(P1 - P)$$

$$-(Y_2 - Y_1) \leq P \leq (Y_2 - Y_1) \quad (\text{III.A.5a})$$

and

$$\begin{aligned}
 r_{Gg}(P) &= \sum_{P1=Y_1}^{Y_2} G(P1)g(P1-P) \\
 &\xrightarrow{\text{Eq.(III.5b)}} = \sum_{P1=Y_1}^{Y_2} g(P1-dP)g(P1-P) \\
 &\quad -(Y_2 - Y_1) \leq P \leq (Y_2 - Y_1) \tag{III.A.5b}
 \end{aligned}$$

We have dropped the complex conjugate on the second g function on the right-hand side of both Eqs.(III.A.5a) and (III.A.5b) since we deal with real functions here. The limits on P are derived on the fact that function $g(P1)$ is only defined in the range $[Y_1, Y_2]$.

Substitute $P1 - dP$ by $P1$ in Eq.(III.A.5b), we have

$$\begin{aligned}
 r_{Gg}(P) &= \sum_{P1=Y_1-dP}^{Y_2-dP} g(P1)g(P1+dP-P) \\
 &\xrightarrow{\text{Eq.(III.A.4a,b)}} = \sum_{P1=Y_1}^{Y_2} g(P1)g[P1-(P-dP)] \\
 \Rightarrow \quad r_{Gg}(P) &= r_{gg}(P-dP) \tag{III.A.6}
 \end{aligned}$$

We see that $r_{Gg}(P)$ is a shifted version of $r_{gg}(P)$. Now we will prove that $r_{gg}(P)$ achieves maximum at $P = 0$, thus $r_{Gg}(P)$ at $P = dP$, according to Eq.(III.A.6). For that purpose, we set up the following inequality

$$\begin{aligned}
 &\sum_{P1=Y_1}^{Y_2} [ag(P1) + g(P1-P)]^2 \geq 0 \tag{III.A.7a} \\
 \Rightarrow \quad &a^2 \sum_{P1=Y_1}^{Y_2} g^2(P1) + 2a \sum_{P1=Y_1}^{Y_2} g(P1)g(P1-P) + \sum_{P1=Y_1}^{Y_2} g^2(P1-P) \geq 0 \\
 \Rightarrow \quad &a^2 r_{gg}(0) + 2a r_{gg}(P) + r_{gg}(0) \geq 0
 \end{aligned}$$

We view the above inequality as a quadratic function of a . Because it is nonnegative, its discriminant has to be nonpositive. Thus,

$$4r_{gg}^2(P) - 4r_{gg}(0)r_{gg}(0) \leq 0$$

or

$$|r_{gg}(P)| \leq |r_{gg}(0)| = r_{gg}(0) \quad (\text{III.A.7b})$$

The last equality comes from the fact that

$$r_{gg}(0) = \sum_{P1=Y_1}^{Y_2} g^2(P1) \geq 0 \quad (\text{III.A.7c})$$

Thus we see from Eq.(III.9b) that $r_{gg}(P)$ achieves maximum at $P = 0$. Thus, from Eq.(III.A.6), $r_{Gg}(P)$ achieves its maximum at $P = dP$. Thus, by determining the peak position of the cross-correlation function of two waveforms obtained from two video frames, we can determine the pixel shift dP . Thus, from Eq.(III.A.2) we can get the flow speed since we know the calibration factor and the time between the two correlated frames. To better illustrate the above concept, we show the waveform and correlation function for only one car in FIGURE 8 (a) – (d).

B. Effect of Camera Perspective on the Flow Speed Computation

In Subsection A, we demonstrate the idea of correlation algorithm for flow speed computation with a uniform calibration factor along the y direction. For a realistic situation, the camera perspective will cause the calibration factor to vary along the y direction. Thus, we need to derive a formula for this case.

For the same distance dy in Eq.(III.A.1) in the object plane, the corresponding pixel shifts in the image plane will be different for the vehicles in different pixel positions. Assume that all vehicles have the same length, L . Thus,

$$P_{i2} = P_{i1} + \frac{L}{\gamma_{i1}} \quad 0 \leq i < N \quad (\text{III.B.1a})$$

Also assume that the calibration factors for the top and bottom edges of the i th vehicle are γ_{i1} and γ_{i2} and the corresponding pixel shifts are dP_{i1} and dP_{i2} , respectively. Thus,

$$dP_{ij} = \frac{dy}{\gamma_{ij}} = \frac{vdt}{\gamma_{ij}} \quad 0 \leq i < N \text{ and } j = 1, 2 \quad (\text{III.B.1b})$$

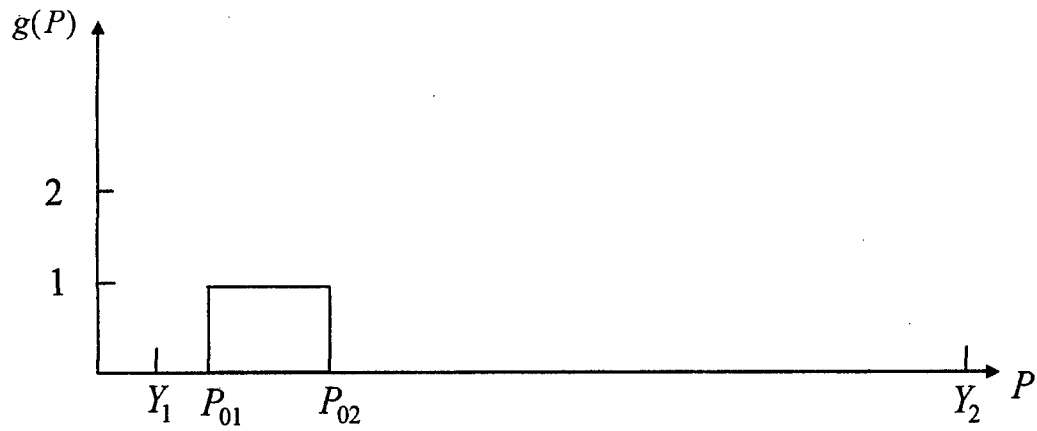


FIGURE 8 (a) 1-D Collapsed Waveform for One Vehicle

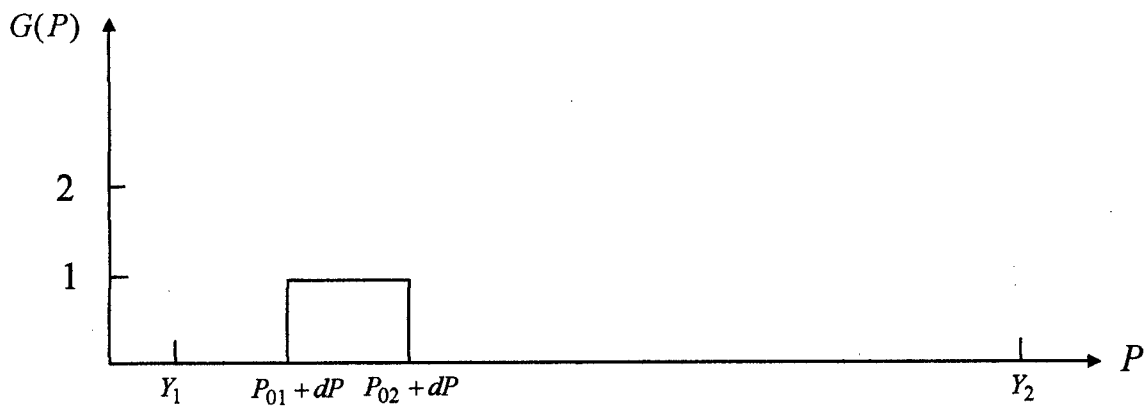


FIGURE 8 (b) 1-D Collapsed Waveform for One Vehicle with Pixel Shift dP

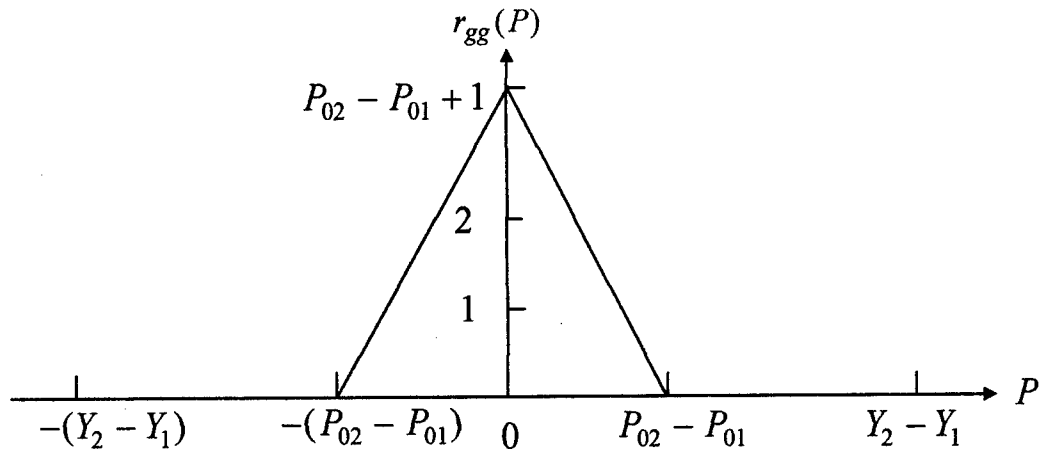


FIGURE 8 (c) Auto-Correlation of the Waveform in (a)

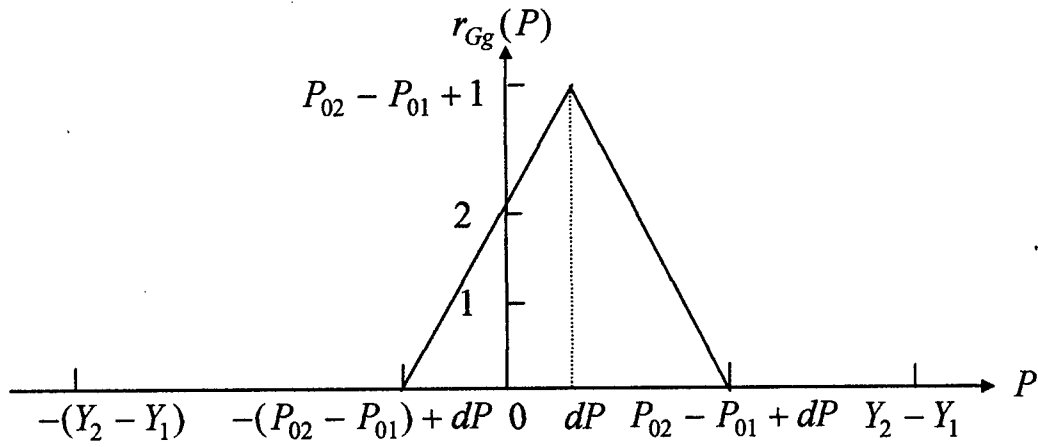


FIGURE 8 (d) Cross-Correlation of the Waveforms in (a) and (b)

The pixel positions and pixel shifts observe the following inequalities:

$$P_{i1} \leq P_{i2} < P_{j1} \leq P_{j2} \quad 0 \leq i < j < N \quad (\text{III.B.2a})$$

and

$$dP_{i1} \leq dP_{i2} < dP_{j1} \leq dP_{j2} \quad 0 \leq i < j < N \quad (\text{III.B.2b})$$

as shown in FIGURE 9.

For simplicity, we will assume that the pixel shifts are so small and the distances between vehicles are so large that

$$P_{i1} + dP_{i1} \leq P_{i2} + dP_{01} \quad 0 \leq i < N \quad (\text{III.B.2c})$$

$$P_{i1} + dP_{N-1,2} \leq P_{i2} + dP_{i2} \quad 0 \leq i < N \quad (\text{III.B.2d})$$

$$P_{i2} + dP_{i2} \leq P_{j1} \quad 0 \leq i < j < N \quad (\text{III.B.2e})$$

and

$$P_{i2} + dP_{N-1,2} \leq P_{j1} + dP_{j1} \quad 0 \leq i < j < N \quad (\text{III.B.2f})$$

Eq.(III.B.2c) describes that the pixel shift is so small that the shifted bottom edge of a vehicle in the current frame will not pass the top edge of the same vehicle with the smallest shift, dP_{01} . Eq.(III.B.2d) shows that the bottom edge of a vehicle shifted with the largest pixel shift, $dP_{N-1,2}$, can not exceed its shifted top edge. Eq.(III.B.2e) says that the distance between two vehicles is so large that the shifted top edge of a vehicle in the current frame can not exceed the bottom edge of the vehicle in front of it in the previous frame, while Eq.(III.B.2f) depicts that even with the largest pixel shift, $dP_{N-1,2}$, the top edge of any vehicle can not pass the shifted bottom edge of the vehicle in front of it in the previous frame.

The inequalities in Eqs.(III.B.2c)-(f) can be combined into the following two inequalities

$$P_{i1} + \max(dP_{i1} - dP_{01}, dP_{N-1,2} - dP_{i2}) \leq P_{i2} \quad 0 \leq i < N \quad (\text{III.B.3a})$$

and

$$P_{i2} + \max(dP_{i2}, dP_{N-1,2} - dP_{j1}) \leq P_{j1} \quad 0 \leq i < j < N \quad (\text{III.B.3b})$$

With the above assumptions, Eq.(III.A.3a) becomes

$$\begin{aligned} G(P) &= \sum_{i=0}^{N-1} \{u[P - (P_{i1} + dP_{i1})] - u[P - (P_{i2} + dP_{i2})]\} \\ &= \sum_{i=0}^{N-1} [u(P - P_{i1} - dP_{i1}) - u(P - P_{i2} - dP_{i2})] \\ Y_1 &\leq P \leq Y_2 \end{aligned} \quad (\text{III.B.4})$$

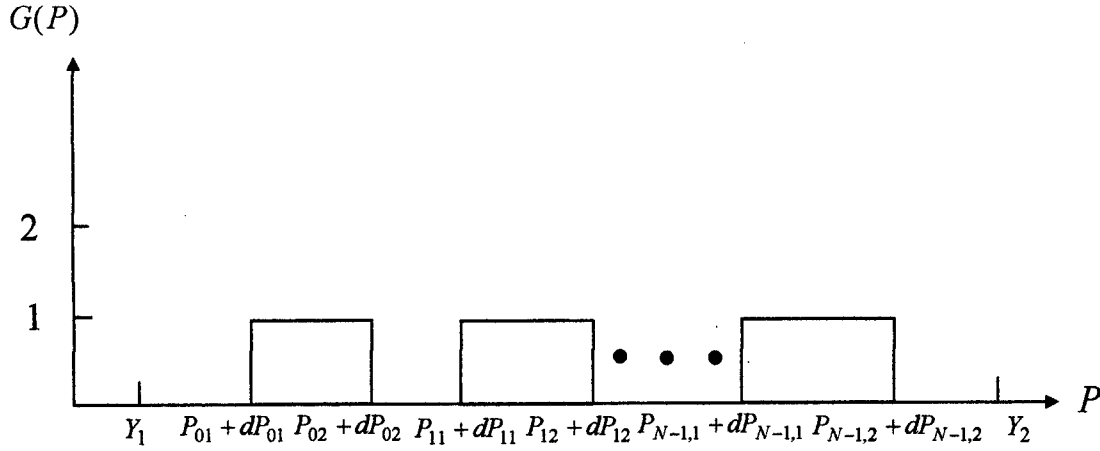


FIGURE 9 The Shifted 1-D Waveform with Varied Calibration Factor

Note that since the pixel shifts are different for different pixel position, $G(P)$ is no longer a shifted version of $g(P)$. However, since $G(P)$ is obtained from the vehicles shifting right in $g(P)$, the correlation peak should still be in the positive P position. Thus, we will concentrate on $P \geq 0$ region in the following analysis. Plug Eqs.(III.1) and (III.B.4) into Eq.(III.A.5b), we get

$$r_{Gg}(P) = \sum_{P1=Y_1}^{Y_2} \left\{ \sum_{i=0}^{N-1} [u(P1 - P_{i1} - dP_{i1}) - u(P1 - P_{i2} - dP_{i2})] \bullet \right. \\ \left. \sum_{i=0}^{N-1} [u(P1 - P_{i1} - P) - u(P1 - P_{i2} - P)] \right\}$$

$$0 \leq P \leq (Y_2 - Y_1)$$

or

$$r_{Gg}(P) = \sum_{P1=Y_1}^{Y_2} \sum_{i,j=0}^{N-1} [u(P1 - P_{i1} - dP_{i1})u(P1 - P_{j1} - P) \\ - u(P1 - P_{i2} - dP_{i2})u(P1 - P_{j1} - P) \\ - u(P1 - P_{i1} - dP_{i1})u(P1 - P_{j2} - P) \\ + u(P1 - P_{i2} - dP_{i2})u(P1 - P_{j2} - P)]$$

$$0 \leq P \leq (Y_2 - Y_1) \quad (\text{III.B.5})$$

From the definition of step function $u(P)$, we have

$$u(P_1 - a)u(P_1 - b) = u[P_1 - \max(a, b)] \quad (\text{III.B.6})$$

Thus Eq.(III.B.5) becomes

$$\begin{aligned} r_{Gg}(P) = & \sum_{P_1=Y_1}^{Y_2} \sum_{i,j=0}^{N-1} \{u[P_1 - \max(P_{i1} + dP_{i1}, P_{j1} + P)] \\ & - u[P_1 - \max(P_{i2} + dP_{i2}, P_{j1} + P)] \\ & - u[P_1 - \max(P_{i1} + dP_{i1}, P_{j2} + P)] \\ & + u[P_1 - \max(P_{i2} + dP_{i2}, P_{j2} + P)]\} \\ & 0 \leq P \leq (Y_2 - Y_1) \end{aligned} \quad (\text{III.B.7})$$

Exchange the order of summations in Eq.(III.B.7) and move the second summation into the bracket, we have

$$\begin{aligned} r_{Gg}(P) = & \sum_{i,j=0}^{N-1} \{ \sum_{P_1=Y_1}^{Y_2} u[P_1 - \max(P_{i1} + dP_{i1}, P_{j1} + P)] \\ & - \sum_{P_1=Y_1}^{Y_2} u[P_1 - \max(P_{i2} + dP_{i2}, P_{j1} + P)] \\ & - \sum_{P_1=Y_1}^{Y_2} u[P_1 - \max(P_{i1} + dP_{i1}, P_{j2} + P)] \\ & + \sum_{P_1=Y_1}^{Y_2} u[P_1 - \max(P_{i2} + dP_{i2}, P_{j2} + P)] \} \\ & 0 \leq P \leq (Y_2 - Y_1) \end{aligned} \quad (\text{III.B.8})$$

Note

$$\sum_{P_1=Y_1}^{Y_2} u(P_1 - a) = \begin{cases} Y_2 - a + 1 & Y_1 \leq a \leq Y_2 \\ Y_2 - Y_1 + 1 & a < Y_1 \\ 0 & a > Y_2 \end{cases} \quad (\text{III.B.9})$$

and since

$$Y_1 \leq P_{i1} \leq P_{i2} + dP_{i2} \leq Y_2 \quad 0 \leq i < N \quad (\text{III.B.10})$$

$$\Rightarrow \max(P_{ik} + dP_{ik}, P_{jl} + P) \geq Y_1 \quad 0 \leq i, j < N \text{ and } k, l = 1, 2 \quad (\text{III.B.11})$$

we have from Eq.(III.B.8)

$$\begin{aligned} r_{Gg}(P) = & \sum_{i,j=0}^{N-1} \{ \max[Y_2 - \max(P_{i1} + dP_{i1}, P_{j1} + P), 0] \\ & - \max[Y_2 - \max(P_{i2} + dP_{i2}, P_{j1} + P), 0] \\ & - \max[Y_2 - \max(P_{i1} + dP_{i1}, P_{j2} + P), 0] \\ & + \max[Y_2 - \max(P_{i2} + dP_{i2}, P_{j2} + P), 0] \} \\ & 0 \leq P \leq (Y_2 - Y_1) \end{aligned} \quad (\text{III.B.12})$$

Divide summation over j into three regions, $j < i$, $j = i$, and $j > i$ as in the following.

$$\begin{aligned} r_{Gg}(P) = & \sum_{i=0}^{N-1} (\sum_{j>i} + \sum_{j=i} + \sum_{j<i}) \{ \max[Y_2 - \max(P_{i1} + dP_{i1}, P_{j1} + P), 0] \\ & - \max[Y_2 - \max(P_{i2} + dP_{i2}, P_{j1} + P), 0] \\ & - \max[Y_2 - \max(P_{i1} + dP_{i1}, P_{j2} + P), 0] \\ & + \max[Y_2 - \max(P_{i2} + dP_{i2}, P_{j2} + P), 0] \} \\ & 0 \leq P \leq (Y_2 - Y_1) \end{aligned} \quad (\text{III.B.13})$$

For the first sum over $j > i$, due to the assumptions made in Eqs.(III.B.2a)-(f), we have for $0 \leq P \leq (Y_2 - Y_1)$,

$$P_{j2} + P \geq P_{j1} + P \geq P_{i2} + dP_{i2} \geq P_{i1} + dP_{i1}$$

$$0 \leq P \leq (Y_2 - Y_1), \quad 0 \leq i < j < N \quad (\text{III.B.14})$$

Thus,

$$\begin{aligned}
 r_2 &\equiv \sum_{i=0}^{N-1} \sum_{j>i} \{ \max[Y_2 - \max(P_{i1} + dP_{i1}, P_{j1} + P), 0] \\
 &\quad - \max[Y_2 - \max(P_{i2} + dP_{i2}, P_{j1} + P), 0] \\
 &\quad - \max[Y_2 - \max(P_{i1} + dP_{i1}, P_{j2} + P), 0] \\
 &\quad + \max[Y_2 - \max(P_{i2} + dP_{i2}, P_{j2} + P), 0] \} \\
 &= \sum_{i=0}^{N-1} \sum_{j>i} \{ \max[Y_2 - (P_{j1} + P), 0] - \max[Y_2 - (P_{j1} + P), 0] \\
 &\quad - \max[Y_2 - (P_{j2} + P), 0] + \max[Y_2 - (P_{j2} + P), 0] \} \\
 &= 0 \quad 0 \leq P \leq (Y_2 - Y_1) \quad (\text{III.B.15})
 \end{aligned}$$

For the second sum over $j = i$, it is actually only one term, Let

$$\begin{aligned}
 r_0 &\equiv \sum_{i=0}^{N-1} \{ \max[Y_2 - \max(P_{i1} + dP_{i1}, P_{i1} + P), 0] \\
 &\quad - \max[Y_2 - \max(P_{i2} + dP_{i2}, P_{i1} + P), 0] \\
 &\quad - \max[Y_2 - \max(P_{i1} + dP_{i1}, P_{i2} + P), 0] \\
 &\quad + \max[Y_2 - \max(P_{i2} + dP_{i2}, P_{i2} + P), 0] \} \\
 &\quad 0 \leq P \leq (Y_2 - Y_1) \quad (\text{III.B.16a})
 \end{aligned}$$

And for the third sum over $j < i$, Let

$$\begin{aligned}
 r_1 &\equiv \sum_{i=0}^{N-1} \sum_{j<i} \{ \max[Y_2 - \max(P_{i1} + dP_{i1}, P_{j1} + P), 0] \\
 &\quad - \max[Y_2 - \max(P_{i2} + dP_{i2}, P_{j1} + P), 0]
 \end{aligned}$$

$$\begin{aligned}
& -\max[Y_2 - \max(P_{i1} + dP_{i1}, P_{j2} + P), 0] \\
& + \max[Y_2 - \max(P_{i2} + dP_{i2}, P_{j2} + P), 0] \} \\
& 0 \leq P \leq (Y_2 - Y_1) \tag{III.B.16b}
\end{aligned}$$

To solve the Eqs.(III.B.16a) and (b), we will assume that the pixel shifts are infinitesimal so that the new waveform does not deform too much from its original shape. Thus, the maximum occurs when each vehicle waveform tries to match its own waveform in the previous frame, that is, the maximum position P satisfies

$$dP_{01} \leq P \leq dP_{N-1,2} \tag{III.B.17}$$

This means that only the summation term over $j = i$, that is, r_0 , is nonzero. To show that r_1 is indeed zero under the condition in Eq.(III.B.14) and assumptions in Eqs.(III.B.2a)-(f), we use Eq.(III.B.16b). With assumptions in Eqs.(III.B.2a)-(f) and Eq.(III.B.17), we have

$$\begin{aligned}
P_{i2} + dP_{i2} & \geq P_{i1} + dP_{i1} \geq P_{j2} + dP_{N-1,2} \geq P_{j2} + P \geq P_{j1} + P \\
dP_{01} & \leq P \leq dP_{N-1,2}, \quad 0 \leq j < i < N \tag{III.B.18}
\end{aligned}$$

Thus,

$$\begin{aligned}
r_1 &= \sum_{i=0}^{N-1} \sum_{j < i} \{ \max[Y_2 - (P_{i1} + dP_{i1}), 0] - \max[Y_2 - (P_{i2} + dP_{i2}), 0] \\
& \quad - \max[Y_2 - (P_{i1} + dP_{i1}), 0] + \max[Y_2 - (P_{i2} + dP_{i2}), 0] \} \\
&= 0 \tag{III.B.19}
\end{aligned}$$

So,

$$r_{Gg}(P) = r_0 \tag{III.B.20}$$

Also, with the condition in Eq.(III.B.17), we have

$$\max(P_{ik} + dP_{ik}, P_{jl} + P) \leq Y_2 \tag{III.B.21}$$

Therefore, Eq.(III.B.16a) becomes

$$r_0 = \sum_{i=0}^{N-1} \{ [Y_2 - \max(P_{i1} + dP_{i1}, P_{i1} + P)]$$

$$\begin{aligned}
& -[Y_2 - \max(P_{i2} + dP_{i2}, P_{i1} + P)] \\
& -[Y_2 - \max(P_{i1} + dP_{i1}, P_{i2} + P)] \\
& +[Y_2 - \max(P_{i2} + dP_{i2}, P_{i2} + P)]\} \\
& = \sum_{i=0}^{N-1} [\max(P_{i2} + dP_{i2}, P_{i1} + P) - \max(P_{i1} + dP_{i1}, P_{i1} + P) \\
& \quad + \max(P_{i1} + dP_{i1}, P_{i2} + P) - \max(P_{i2} + dP_{i2}, P_{i2} + P)] \\
& \quad dP_{01} \leq P \leq dP_{N-1,2} \quad (\text{III.B.22})
\end{aligned}$$

To determine at which pixel position P the maximum is, we divide $[dP_{01}, dP_{N-1,2}]$ into regions $[dP_{j1}, dP_{j2}]$, $0 \leq j < N$, and $[dP_{j2}, dP_{j+1,1}]$, $0 \leq j < N-1$. The first region is within vehicles and the second region is in between two adjacent vehicles. We want to obtain the expression of the cross-coorelation in both type of regions.

First, assume that P is in the second region, thus,

$$dP_{j2} \leq P \leq dP_{j+1,1} \quad 0 \leq j < N-1 \quad (\text{III.B.23})$$

therefore,

$$\begin{aligned}
P_{i2} + P & \geq P_{i2} + dP_{j2} \geq P_{i2} + dP_{i2} \geq P_{i1} + dP_{N-1,2} \\
& \geq P_{i1} + dP_{j+1,1} \geq P_{i1} + P \geq P_{i1} + dP_{j2} \geq P_{i1} + dP_{i1} \\
& dP_{j2} \leq P \leq dP_{j+1,1}, \quad 0 \leq i \leq j < N-1 \quad (\text{III.B.24a})
\end{aligned}$$

and

$$\begin{aligned}
P_{i2} + dP_{i2} & \geq P_{i2} + dP_{j+1,1} \geq P_{i2} + P \geq P_{i2} + dP_{j2} \\
& \geq P_{i1} + dP_{i1} \geq P_{i1} + dP_{j+1,1} \geq P_{i1} + P \\
& dP_{j2} \leq P \leq dP_{j+1,1}, \quad 0 \leq j < i < N \quad (\text{III.B.24b})
\end{aligned}$$

So

$$\begin{aligned}
r_{Gg}(P) & = \left(\sum_{i=0}^j + \sum_{i=j+1}^{N-1} \right) [\max(P_{i2} + dP_{i2}, P_{i1} + P) - \max(P_{i1} + dP_{i1}, P_{i1} + P) \\
& \quad + \max(P_{i1} + dP_{i1}, P_{i2} + P) - \max(P_{i2} + dP_{i2}, P_{i2} + P)]
\end{aligned}$$

$$\begin{aligned}
&= \sum_{i=0}^j [(P_{i2} + dP_{i2}) - (P_{i1} + P) + (P_{i2} + P) - (P_{i2} + P)] \\
&\quad + \sum_{i=j+1}^{N-1} [(P_{i2} + dP_{i2}) - (P_{i1} + dP_{i1}) + (P_{i2} + P) - (P_{i2} + dP_{i2})] \\
&= \sum_{i=0}^j [(P_{i2} + dP_{i2}) - (P_{i1} + P)] + \sum_{i=j+1}^{N-1} [(P_{i2} + P) - (P_{i1} + dP_{i1})] \\
&= \sum_{i=0}^{N-1} (P_{i2} - P_{i1}) - [\sum_{i=0}^j (P - dP_{i2}) + \sum_{i=j+1}^{N-1} (dP_{i1} - P)] \\
&\quad dP_{j2} \leq P \leq dP_{j+1,1} \quad 0 \leq j < N - 1 \quad (\text{III.B.25})
\end{aligned}$$

Second, assume that P is in the first region, thus,

$$dP_{j1} \leq P \leq dP_{j2} \quad 0 \leq j < N \quad (\text{III.B.26})$$

therefore,

$$\begin{aligned}
P_{i2} + P &\geq P_{i2} + dP_{j1} \geq P_{i2} + dP_{i2} \geq P_{i1} + dP_{N-1,2} \\
&\geq P_{i1} + dP_{j2} \geq P_{i1} + P \geq P_{i1} + dP_{j1} \geq P_{i1} + dP_{i1} \\
&\quad dP_{j1} \leq P \leq dP_{j2}, \quad 0 \leq i < j < N \quad (\text{III.B.27a})
\end{aligned}$$

$$\begin{aligned}
P_{j2} + dP_{j2} &\geq P_{j2} + P \geq P_{j1} + P \geq P_{j1} + dP_{j1} \\
&\quad dP_{j1} \leq P \leq dP_{j2}, \quad 0 \leq i = j < N \quad (\text{III.B.27b})
\end{aligned}$$

and

$$\begin{aligned}
P_{i2} + dP_{i2} &\geq P_{i2} + dP_{j2} \geq P_{i2} + P \geq P_{i2} + dP_{j1} \\
&\geq P_{i1} + dP_{i1} \geq P_{i1} + dP_{j2} \geq P_{i1} + P \\
&\quad dP_{j1} \leq P \leq dP_{j2}, \quad 0 \leq j < i < N \quad (\text{III.B.27c})
\end{aligned}$$

The only difference between P in this region and in first region is in $i = j$ term. So

$$\begin{aligned}
r_{Gg}(P) &= \left(\sum_{i=0}^{j-1} + \sum_{i=j} + \sum_{i=j+1}^{N-1} \right) [\max(P_{i2} + dP_{i2}, P_{i1} + P) - \max(P_{i1} + dP_{i1}, P_{i1} + P)] \\
&\quad + \max(P_{i1} + dP_{i1}, P_{i2} + P) - \max(P_{i2} + dP_{i2}, P_{i2} + P)] \\
&= \sum_{i=0}^{j-1} [(P_{i2} + dP_{i2}) - (P_{i1} + P) + (P_{i2} + P) - (P_{i2} + P)] \\
&\quad + [(P_{j2} + dP_{j2}) - (P_{j1} + P) + (P_{j2} + P) - (P_{j2} + dP_{j2})] \\
&\quad + \sum_{i=j+1}^{N-1} [(P_{i2} + dP_{i2}) - (P_{i1} + dP_{i1}) + (P_{i2} + P) - (P_{i2} + dP_{i2})] \\
&= (P_{j2} - P_{j1}) + \sum_{i=0}^{j-1} [(P_{i2} + dP_{i2}) - (P_{i1} + P)] \\
&\quad + \sum_{i=j+1}^{N-1} [(P_{i2} + P) - (P_{i1} + dP_{i1})] \\
&= \sum_{i=0}^{N-1} (P_{i2} - P_{i1}) - \left[\sum_{i=0}^{j-1} (P - dP_{i2}) + \sum_{i=j+1}^{N-1} (dP_{i1} - P) \right]
\end{aligned}$$

$$dP_{j1} \leq P \leq dP_{j2} \quad 0 \leq j < N \quad (\text{III.B.28})$$

Thus,

$$r_{Gg}(P) = \begin{cases} \sum_{i=0}^{N-1} (P_{i2} - P_{i1}) - \left[\sum_{i=0}^{j-1} (P - dP_{i2}) + \sum_{i=j+1}^{N-1} (dP_{i1} - P) \right] \\ \quad dP_{j1} \leq P \leq dP_{j2}, 0 \leq j < N \\ \sum_{i=0}^{N-1} (P_{i2} - P_{i1}) - \left[\sum_{i=0}^j (P - dP_{i2}) + \sum_{i=j+1}^{N-1} (dP_{i1} - P) \right] \\ \quad dP_{j2} \leq P \leq dP_{j+1,1}, 0 \leq j < N-1 \end{cases} \quad (\text{III.B.29})$$

We will prove that $r_{Gg}(P)$ achieves maximum at

$$j = N / 2 - 1 \quad (\text{III.B.30a})$$

and

$$P = P_{\max}, \quad dP_{N/2-1,2} \leq P_{\max} \leq dP_{N/2,1} \quad (\text{III.B.30b})$$

when N is even and

$$j = (N - 1) / 2 \quad (\text{III.B.30c})$$

and

$$P = P_{\max}, \quad dP_{(N-1)/2,1} \leq P_{\max} \leq dP_{(N-1)/2,2} \quad (\text{III.B.30d})$$

when N is odd. We will prove the above conclusions in the following steps.

(i) N is even

(a) Prove that

$$r_{Gg}(P') - r_{Gg}(P) \begin{cases} > 0 & 0 \leq j < N/2 - 1 \\ = 0 & j = N/2 - 1 \\ < 0 & N/2 - 1 < j < N - 1 \end{cases}$$

$$dP_{j2} \leq P < P' \leq dP_{j+1,1} \quad 0 \leq j < N - 1 \quad (\text{III.B.31})$$

that is, for $dP_{j2} \leq P \leq dP_{j+1,1}$, $r_{Gg}(P)$ increases as P increases in the region where $0 \leq j < N/2 - 1$, stays constant as P increases in the region where $j = N/2 - 1$, and decreases as P increases in the region $N/2 - 1 < j < N - 1$.

$$\begin{aligned} r_{Gg}(P') - r_{Gg}(P) &= \left[\sum_{i=0}^j (P - dP_{i2}) + \sum_{i=j+1}^{N-1} (dP_{i1} - P) \right] \\ &\quad - \left[\sum_{i=0}^j (P' - dP_{i2}) + \sum_{i=j+1}^{N-1} (dP_{i1} - P') \right] \\ &= \sum_{i=j+1}^{N-1} (P' - P) - \sum_{i=0}^j (P' - P) \\ &= [N - 2(j + 1)](P' - P) \end{aligned}$$

$$\xrightarrow{N \text{ even}} \begin{cases} > 0 & 0 \leq j < N/2 - 1 \\ = 0 & j = N/2 - 1 \\ < 0 & N/2 - 1 < j < N - 1 \end{cases} \quad (\text{III.B.32})$$

(b) Prove that

$$r_{Gg}(P') - r_{Gg}(P) \begin{cases} > 0 & 0 \leq j \leq N/2 - 1 \\ < 0 & N/2 - 1 < j < N \end{cases}$$

$$dP_{j1} \leq P < P' \leq dP_{j2} \quad 0 \leq j < N \quad (\text{III.B.33})$$

that is, for $dP_{j1} \leq P \leq dP_{j2}$, $r_{Gg}(P)$ increases as P increases in the region where $0 \leq j \leq N/2 - 1$ and decreases as P increases in the region $N/2 - 1 < j < N$.

$$\begin{aligned} r_{Gg}(P') - r_{Gg}(P) &= \left[\sum_{i=0}^{j-1} (P - dP_{i2}) + \sum_{i=j+1}^{N-1} (dP_{i1} - P) \right] \\ &\quad - \left[\sum_{i=0}^{j-1} (P' - dP_{i2}) + \sum_{i=j+1}^{N-1} (dP_{i1} - P') \right] \\ &= \sum_{i=j+1}^{N-1} (P' - P) - \sum_{i=0}^{j-1} (P' - P) \\ &= [N - 2j - 1](P' - P) \end{aligned}$$

$$\xrightarrow{N \text{ even}} \begin{cases} > 0 & 0 \leq j \leq N/2 - 1 \\ < 0 & N/2 - 1 < j < N \end{cases} \quad (\text{III.B.34})$$

(c) Prove that

$$r_{Gg}(P') - r_{Gg}(P) \begin{cases} > 0 & 0 \leq j \leq N/2 - 1 \\ < 0 & N/2 - 1 < j < N - 1 \end{cases}$$

$$dP_{j1} \leq P \leq dP_{j2}, dP_{j2} \leq P' \leq dP_{j+1,1}, 0 \leq j < N - 1 \quad (\text{III.B.35})$$

that is, for P increases from one region $[dP_{j1}, dP_{j2}]$ to the next region $[dP_{j2}, dP_{j+1,1}]$, $r_{Gg}(P)$ increases where $0 \leq j \leq N/2 - 1$ and decreases in the region $N/2 - 1 < j < N - 1$.

$$\begin{aligned} r_{Gg}(P') - r_{Gg}(P) &= \left[\sum_{i=0}^{j-1} (P - dP_{i2}) + \sum_{i=j+1}^{N-1} (dP_{i1} - P) \right] \\ &\quad - \left[\sum_{i=0}^j (P' - dP_{i2}) + \sum_{i=j+1}^{N-1} (dP_{i1} - P') \right] \end{aligned}$$

$$= \sum_{i=j+1}^{N-1} (P' - P) - \sum_{i=0}^j (P' - P) - (P - dP_{j2})$$

$$= [N - 2(j + 1)](P' - P) + (dP_{j2} - P)$$

$$\xrightarrow{N \text{ even, } dP_{j2} - P \geq 0, \text{ and } dP_{j2} - P' \leq 0} \begin{cases} > 0 & 0 \leq j \leq N/2 - 1 \\ < 0 & N/2 - 1 < j < N - 1 \end{cases} \quad (\text{III.B.36})$$

(d) Prove that

$$r_{Gg}(P') - r_{Gg}(P) \begin{cases} > 0 & 0 \leq j < N/2 - 1 \\ < 0 & N/2 - 1 \leq j < N - 1 \end{cases}$$

$$dP_{j2} \leq P \leq dP_{j+1,1}, dP_{j+1,1} \leq P' \leq dP_{j+1,2}, 0 \leq j < N - 1 \quad (\text{III.B.37})$$

that is, for P increases from one region $[dP_{j2}, dP_{j+1,1}]$ to the next region $[dP_{j+1,1}, dP_{j+1,2}]$, $r_{Gg}(P)$ increases where $0 \leq j \leq N/2 - 1$ and decreases in the region $N/2 - 1 < j < N - 1$.

$$r_{Gg}(P') - r_{Gg}(P) = \left[\sum_{i=0}^j (P - dP_{i2}) + \sum_{i=j+1}^{N-1} (dP_{i1} - P) \right]$$

$$- \left[\sum_{i=0}^j (P' - dP_{i2}) + \sum_{i=j+2}^{N-1} (dP_{i1} - P') \right]$$

$$= \sum_{i=j+1}^{N-1} (P' - P) - \sum_{i=0}^j (P' - P) + (dP_{j+1,1} - P')$$

$$= [N - 2(j + 1)](P' - P) + (dP_{j+1,1} - P')$$

$$\xrightarrow{N \text{ even, } dP_{j+1,1} - P \geq 0 \text{ and } dP_{j+1,1} - P' \leq 0} \begin{cases} > 0 & j < N/2 - 1 \\ < 0 & j \geq N/2 - 1 \end{cases} \quad (\text{III.B.38})$$

Combine the above (a) to (d) proofs, we conclude that $r_{Gg}(P)$ achieves its maximum at $j = N/2 - 1$, and $dP_{N/2-1,2} \leq P \leq dP_{N/2,1}$, when N is even. Now we prove the result for N odd.

(ii) N is odd

(a) Prove that

$$r_{Gg}(P') - r_{Gg}(P) \begin{cases} > 0 & 0 \leq j < (N-1)/2 \\ < 0 & (N-1)/2 \leq j < N-1 \end{cases}$$

$$dP_{j2} \leq P < P' \leq dP_{j+1,1} \quad 0 \leq j < N-1 \quad (\text{III.B.39})$$

that is, for $dP_{j2} \leq P \leq dP_{j+1,1}$, $r_{Gg}(P)$ increases as P increases in the region where $0 \leq j < (N-1)/2$ and decreases as P increases in the region $(N-1)/2 \leq j < N-1$.

$$\begin{aligned} r_{Gg}(P') - r_{Gg}(P) &= \left[\sum_{i=0}^j (P - dP_{i2}) + \sum_{i=j+1}^{N-1} (dP_{i1} - P) \right] \\ &\quad - \left[\sum_{i=0}^j (P' - dP_{i2}) + \sum_{i=j+1}^{N-1} (dP_{i1} - P') \right] \\ &= \sum_{i=j+1}^{N-1} (P' - P) - \sum_{i=0}^j (P' - P) \\ &= [N - 2(j+1)](P' - P) \end{aligned}$$

$$\xrightarrow{N \text{ odd}} \begin{cases} > 0 & 0 \leq j < (N-1)/2 \\ < 0 & (N-1)/2 \leq j < N \end{cases} \quad (\text{III.B.40})$$

(b) Prove that

$$r_{Gg}(P') - r_{Gg}(P) \begin{cases} > 0 & 0 \leq j < (N-1)/2 \\ = 0 & j = (N-1)/2 \\ < 0 & (N-1)/2 < j < N \end{cases}$$

$$dP_{j1} \leq P < P' \leq dP_{j2} \quad 0 \leq j < N \quad (\text{III.B.41})$$

that is, for $dP_{j1} \leq P \leq dP_{j2}$, $r_{Gg}(P)$ increases as P increases in the region where $0 \leq j < (N-1)/2$, stays constant as P increases in the region where $j = (N-1)/2$, and decreases as P increases in the region $(N-1)/2 < j < N-1$.

$$r_{Gg}(P') - r_{Gg}(P) = \left[\sum_{i=0}^{j-1} (P - dP_{i2}) + \sum_{i=j+1}^{N-1} (dP_{i1} - P) \right]$$

$$\begin{aligned}
& -\left[\sum_{i=0}^{j-1}(P'-dP_{i2}) + \sum_{i=j+1}^{N-1}(dP_{i1} - P')\right] \\
& = \sum_{i=j+1}^{N-1}(P'-P) - \sum_{i=0}^{j-1}(P'-P) \\
& = [N - 2j - 1](P' - P)
\end{aligned}$$

$$\begin{array}{c} \xrightarrow{N \text{ odd}} \end{array} \left\{ \begin{array}{ll} > 0 & 0 \leq j < (N-1)/2 \\ = 0 & j = (N-1)/2 \\ < 0 & (N-1)/2 < j < N \end{array} \right. \quad (\text{III.B.42})$$

(c) Prove that

$$r_{Gg}(P') - r_{Gg}(P) \begin{cases} > 0 & 0 \leq j < (N-1)/2 \\ < 0 & (N-1)/2 \leq j < N-1 \end{cases}$$

$$dP_{j1} \leq P \leq dP_{j2}, \quad dP_{j2} \leq P' \leq dP_{j+1,1}, \quad 0 \leq j < N-1 \quad (\text{III.B.43})$$

that is, for P increases from one region $[dP_{j1}, dP_{j2}]$ to the next region $[dP_{j2}, dP_{j+1,1}]$, $r_{Gg}(P)$ increases where $0 \leq j < (N-1)/2$ and decreases in the region $(N-1)/2 \leq j < N-1$.

$$\begin{aligned}
r_{Gg}(P') - r_{Gg}(P) & = \left[\sum_{i=0}^{j-1}(P - dP_{i2}) + \sum_{i=j+1}^{N-1}(dP_{i1} - P)\right] \\
& \quad - \left[\sum_{i=0}^j(P' - dP_{i2}) + \sum_{i=j+1}^{N-1}(dP_{i1} - P')\right] \\
& = \sum_{i=j+1}^{N-1}(P' - P) - \sum_{i=0}^j(P' - P) - (P - dP_{j2}) \\
& = [N - 2(j+1)](P' - P) + (dP_{j2} - P)
\end{aligned}$$

$$\begin{array}{c} \xrightarrow{N \text{ odd, } dP_{j2} - P \geq 0, \text{ and } dP_{j2} - P' \leq 0} \end{array} \left\{ \begin{array}{ll} > 0 & 0 \leq j < (N-1)/2 \\ < 0 & (N-1)/2 \leq j < N-1 \end{array} \right. \quad (\text{III.B.44})$$

(d) Prove that

$$r_{Gg}(P') - r_{Gg}(P) \begin{cases} > 0 & 0 \leq j < (N-1)/2 \\ < 0 & (N-1)/2 \leq j < N-1 \end{cases}$$

$$dP_{j2} \leq P \leq dP_{j+1,1}, dP_{j+1,1} \leq P' \leq dP_{j+1,2}, 0 \leq j < N-1 \quad (\text{III.B.45})$$

that is, for P increases from one region $[dP_{j2}, dP_{j+1,1}]$ to the next region $[dP_{j+1,1}, dP_{j+1,2}]$, $r_{Gg}(P)$ increases where $0 \leq j < (N-1)/2$ and decreases in the region $(N-1)/2 \leq j < N-1$.

$$\begin{aligned} r_{Gg}(P') - r_{Gg}(P) &= \left[\sum_{i=0}^j (P - dP_{i2}) + \sum_{i=j+1}^{N-1} (dP_{i1} - P) \right] \\ &\quad - \left[\sum_{i=0}^j (P' - dP_{i2}) + \sum_{i=j+2}^{N-1} (dP_{i1} - P') \right] \\ &= \sum_{i=j+1}^{N-1} (P' - P) - \sum_{i=0}^j (P' - P) + (dP_{j+1,1} - P') \\ &= [N - 2(j+1)](P' - P) + (dP_{j+1,1} - P') \end{aligned}$$

$$\xrightarrow{N \text{ odd, } dP_{j+1,1} - P \geq 0, \text{ and } dP_{j+1,1} - P' \leq 0} \begin{cases} > 0 & 0 \leq j < (N-1)/2 \\ < 0 & (N-1)/2 \leq j < N-1 \end{cases} \quad (\text{III.B.46})$$

Combine the above (a) to (d) proofs, we conclude that $r_{Gg}(P)$ achieves its maximum at $j = (N-1)/2$, and $dP_{(N-1)/2,1} \leq P_{\max} \leq dP_{(N-1)/2,2}$, when N is odd. Combine (i) and (ii), we conclude our proof. From the above result, we can see that the maximum of the cross-correlation is at the median of the pixel shifts.

In the above, we assume that the intensity for all vehicles are uniform. In reality, the intensities will be different for both the same vehicle and different vehicles. Thus we will most probably not get a range of maximum points. Typically it will have only one maximum point. This point should be at

$$P_{\max} = \begin{cases} \frac{dP_{N/2-1,2} + dP_{N/2,1}}{2} & N \text{ even} \\ \frac{dP_{(N-1)/2,1} + dP_{(N-1)/2,2}}{2} & N \text{ odd} \end{cases} \quad (\text{III.B.47})$$

To demonstrate the idea, we show a two-vehicle, $N=2$, example. With $N=2$, j can only take 0 value, then, Eq.(III.B.29) becomes (N even)

$$r_{Gg}(P) = \sum_{i=0}^1 (P_{i2} - P_{i1}) - [(P - dP_{02}) + (dP_{11} - P)]$$

$$= \sum_{i=0}^1 (P_{i2} - P_{i1}) + dP_{02} - dP_{11}$$

$$dP_{02} \leq P \leq dP_{11} \quad (\text{III.B.48})$$

We see that $r_{Gg}(P)$ is a constant. Thus it achieves maximum at $dP_{02} \leq P \leq dP_{11}$. This can be seen in FIGURE 10 (a)-(c).

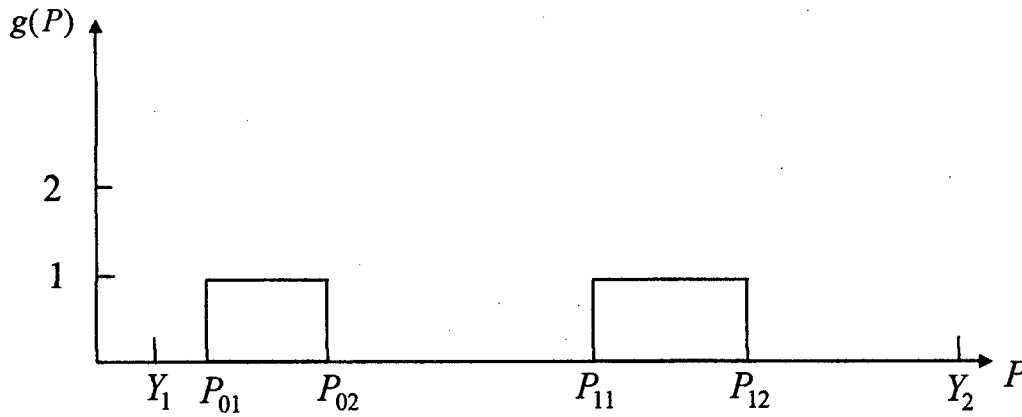


FIGURE 10 (a) 1-D Collapsed Waveform for Two Vehicles

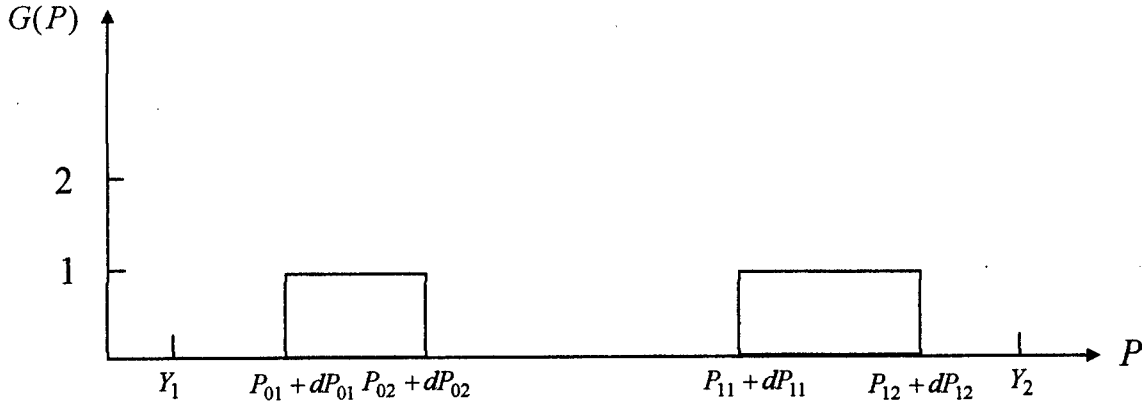


FIGURE 10 (b) 1-D Shifted Collapsed Waveform for Two Vehicles

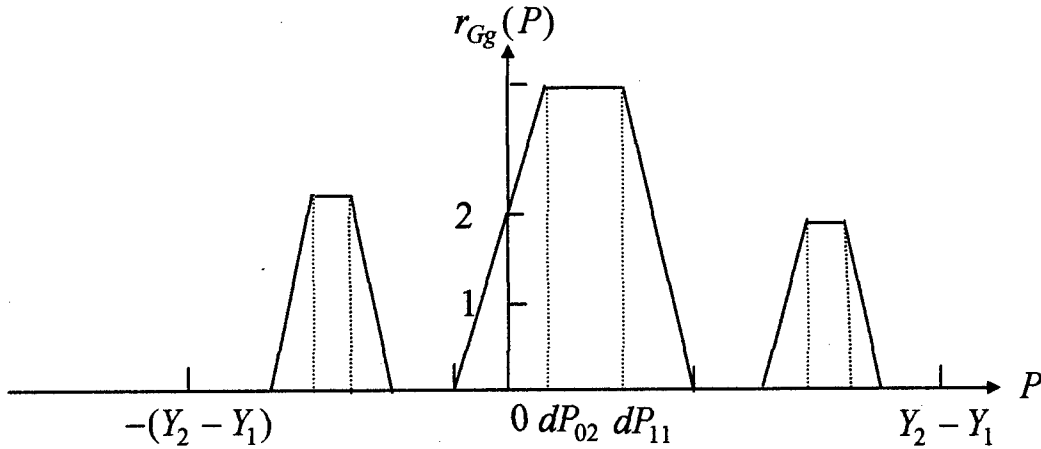


FIGURE 10 (c) Cross-Correlation of the Waveforms in (a) and (b)

5.4 Real Application

In the above discussion, we correlated two waveforms coming from two frames. We assume that the waveform has moved dP pixels from the first frame to the second frame. The value of dP depends on the distance between these two frames. We will call these two frames as correlated frames. Due to the discrete nature of the pixel grid, the value of dP will be zero for certain correlated frames and vehicle speed. The bigger dP is, the higher resolution, or accuracy, the flow speed has. However, because of the finite length of the ROI and the dispersive nature of the waveform due to the perspective, the higher the dP is, the less accurate the flow speed is. Thus, there is a tradeoff between the above two factors. In the real application, we pick the dP

value to be about 1/10th of the ROI length. We will assume in the following discussion that this dP value corresponds to two correlated frames which are N_f frames apart.

In the previous sections, we assumed that the background is uniformly zero. In reality, however, the background image will not be zero. Thus, in order to be able to extract the waveform of the actual moving vehicles, we need to subtract the background waveform. There are two ways of subtracting the background waveform. One is by obtaining an actual background image and its waveform, the other is by using a frame image and its waveform. We will discuss both methods below.

A. Obtaining an Actual Background Waveform

Assume that $g_i(P)$, $0 \leq i < M$, are waveforms for M consecutive frames. There are two ways of computing the background waveform, $g_b(P)$: one is by doing a M frame windowing average, or finite impulse response (FIR) filtering, and the other is by doing a running average, or infinite impulse response (IIR) filtering.

(a) FIR Filtering

In this method, we average the M consecutive frames to obtain the background waveform,

$$g_b(P) = \frac{g_0(P) + g_1(P) + \dots + g_{M-1}(P)}{M} = \frac{1}{M} \sum_{i=0}^{M-1} g_i(P) \quad (\text{IV.A.1})$$

This is a moving window averaging. After we have obtained the background waveform, we can then subtract it from the correlated waveforms to obtain no-background correlated waveforms.

$$g_i'(P) = g_i(P) - g_b(P) \quad (\text{IV.A.2})$$

We can then apply the correlation algorithm to obtain the pixel shift.

$$\begin{aligned} r(P) &= \sum_{P1=Y_1}^{Y_2} g_{i+N_f}'(P1) g_i'(P1 - P) \\ &= \sum_{P1=Y_1}^{Y_2} [g_{i+N_f}(P1) - g_b(P1)][g_i(P1 - P) - g_b(P1 - P)] \end{aligned} \quad (\text{IV.A.3})$$

For simplicity, we have dropped the subscript in the correlation symbol r . From now on, we will use r to represent the cross-correlation function.

(b) IIR Filtering

In this method, we do a running average, or a IIR filtering. The background waveform is updated by a certain percentage of its previous value and the new frame waveform. The mathematical forms are as follows.

$$g_{b,j}(P) = \beta g_{b,j-1}(P) + (1 - \beta) g_i(P) \quad 1 \leq i < \infty \quad 0 \leq \beta \leq 1 \quad (\text{IV.A.4a})$$

$$g_{b,0}(P) = g_0(P) \quad (\text{IV.A.4b})$$

where the coefficient β controls the percentage of the new frame waveform to be averaged into the background. When $\beta = 1$, the background waveform will be same as its initial value $g_{b,0}(P)$ all the time, which is not desirable. When $\beta = 0$, the background waveform will be equal to the new frame all the time. This results in the frame subtraction algorithm which we will discuss later. Methodologically, this method is in between the windowing averaging algorithm and the frame subtraction algorithm.

After we have obtained the background waveform, we can then subtract it from the correlated waveforms to obtain no-background correlated waveforms.

$$g_i'(P) = g_i(P) - g_{b,j}(P) \quad (\text{IV.A.5})$$

We can then apply the correlation algorithm to obtain the pixel shift.

$$\begin{aligned} r(P) &= \sum_{P1=Y_1}^{Y_2} g_{i+N_f}'(P1) g_i'(P1 - P) \\ &= \sum_{P1=Y_1}^{Y_2} [g_{i+N_f}(P1) - g_{b,j}(P1)] [g_i(P1 - P) - g_{b,j}(P1 - P)] \end{aligned} \quad (\text{IV.A.6})$$

The above two methods show two ways of obtain background waveform. In order to obtain a good background waveform with the above two methods, the number of times a vehicle is at a particular pixel position has to be far less than the number of averaging frames. In other words, most of the frames don't have any vehicles in a particular pixel position. In this situation, the vehicles that are present in that particular pixel position in certain frames are averaged out, and thus leave only very small intensities in the final background waveform. This requires that the traffic be light. In the case that the traffic is heavy, most of the frames will have a vehicle in a

particular pixel position, in other words, that particular pixel position will be heavily covered by vehicles during the time period of the background averaging, thus the intensities of the vehicles that are in that particular pixel position will not get averaged out over all the frames. In stead, it will have a high intensity left over in the background waveform. In the extreme case that there is a vehicle in a particular pixel position in every frame, the resulting background waveform will be the actual background waveform plus the average waveform of vehicles. If we subtract this background waveform from the correlated waveforms, we will reduce the contrast of the actual vehicle intensities, thus increase the error of the flow speed computation. Since in a heavy used highway, this will happen quite often, we will not use the background waveform obtained by the above two methods for background subtraction. In the following, we will discuss the frame subtraction algorithm for background subtraction.

B. Frame Subtraction Algorithm

Frame Subtraction algorithm, as it stands, subtracts two frames to remove the background waveform. For this purpose, we can subtract both correlated waveforms by a common frame, as follows.

$$g_i'(P) = g_i(P) - g_j(P) \quad j \neq i \quad (\text{IV.B.1})$$

We can then apply the correlation algorithm to obtain the pixel shift.

$$\begin{aligned} r(P) &= \sum_{P1=Y_1}^{Y_2} g_{i+N_f}'(P1) g_i'(P1 - P) \\ &= \sum_{P1=Y_1}^{Y_2} [g_{i+N_f}(P1) - g_j(P1)] [g_i(P1 - P) - g_j(P1 - P)] \\ &\quad j \neq i \text{ and } j \neq i + N_f \quad (\text{IV.B.2a}) \end{aligned}$$

However, there is a pitfall with this method. In order to show this, we expand the multiplication in Eq.(IV.B.2a).

$$\begin{aligned} r(P) &= \sum_{P1=Y_1}^{Y_2} [g_{i+N_f}(P1) g_i(P1 - P) - g_j(P1) g_i(P1 - P) \\ &\quad - g_{i+N_f}(P1) g_j(P1 - P) + g_j(P1) g_j(P1 - P)] \\ &\quad j \neq i \text{ and } j \neq i + N_f \quad (\text{IV.B.2b}) \end{aligned}$$

Unlike the background subtraction, where the background waveform is obtained by doing the averaging over many to infinite frames, which also averages the random noise out, the frame waveform $g_j(P1)$, which is used for subtraction in this method, contains random noise. Thus, the average of the random noise in the first three terms in Eq.(IV.B.2b) will be zero while that of the last term will not be since it correlates by itself. Since the peak of the last term resides at zero shift, if the random noise happens to be big in certain cases, the last term will dominate, and thus will provide the overall peak at zero shift, which causes the error in the flow speed computation. Therefore, we will not use this method.

In order to reduce the influence of the random noise, we propose the use of two frames for background subtraction. In other words, each correlated frame subtracts a different frame,

$$g_i'(P) = g_i(P) - g_j(P) \quad j \neq i \quad (\text{IV.B.3a})$$

and

$$g_{i+N_f}'(P) = g_{i+N_f}(P) - g_l(P) \quad l \neq i + N_f, j \neq l \quad (\text{IV.B.3b})$$

We can then apply the correlation algorithm to obtain the pixel shift.

$$\begin{aligned} r(P) &= \sum_{P1=Y_1}^{Y_2} g_{i+N_f}'(P1) g_i'(P1 - P) \\ &= \sum_{P1=Y_1}^{Y_2} [g_{i+N_f}(P1) - g_j(P1)] [g_i(P1 - P) - g_j(P1 - P)] \\ &\quad j \neq i, l \neq i + N_f, \text{ and } j \neq l \quad (\text{IV.B.4a}) \end{aligned}$$

Expand the multiplication in Eq.(IV.B.4a).

$$\begin{aligned} r(P) &= \sum_{P1=Y_1}^{Y_2} [g_{i+N_f}(P1) g_i(P1 - P) - g_l(P1) g_i(P1 - P) \\ &\quad - g_{i+N_f}(P1) g_j(P1 - P) + g_l(P1) g_j(P1 - P)] \\ &\quad j \neq i, l \neq i + N_f, \text{ and } j \neq l \quad (\text{IV.B.4b}) \end{aligned}$$

From Eq.(IV.B.4b), we see that none of the subtracted frames correlates with itself, thus the influence of the random noise is reduced.

In the actual computation, in order not to subtract most of a vehicle out in the frame subtraction, we have to require that each subtracted frame be separated certain number of frames from its corresponding correlated frame. Since the distance between two correlated frames are N_f frames apart, we can set the number of frames between the subtracted frame and its corresponding correlated frame to $N_f + 1$. Thus,

$$g_i'(P) = g_i(P) - g_{i+N_f+1}(P) \quad (\text{IV.B.5a})$$

and

$$g_{i+N_f}'(P) = g_{i+N_f}(P) - g_{i+2N_f+1}(P) \quad (\text{IV.B.5b})$$

and the correlation function is

$$\begin{aligned} r(P) &= \sum_{P1=Y_1}^{Y_2} g_{i+N_f}'(P1) g_i'(P1 - P) \\ &= \sum_{P1=Y_1}^{Y_2} [g_{i+N_f}(P1) - g_{i+2N_f+1}(P1)] [g_i(P1 - P) - g_{i+N_f+1}(P1 - P)] \end{aligned} \quad (\text{IV.B.6})$$

5.5 Conclusions

From the previous sections, we conclude that

- (a) The collapsed waveform algorithm reduces the complexity of a 2-D image while preserving sufficient information needed, which increases our computation efficiency. The only drawback is that the width information is lost. However, since the correlation algorithm does not require the knowledge of the vehicle width, this loss of information does not affect our result.
- (b) In the case that the perspective is ignored, or the calibration factor is assumed to be constant in the whole y direction, the correlation algorithm is perfect for computing the waveform shift.
- (c) In the case that the camera perspective is included in our computation, or the calibration factor is varied along the whole y direction, the pixel shift computed by the correlation algorithm is the median of the pixel shifts of all the vehicles in the ROI. This provides a way for perspective compensation. It also proves that the correlation algorithm is also applicable for flow speed computation in the varied calibration factor case.

(d) For background subtraction, using an averaged background waveform reduces the contrast of the interested object intensity, that is, the vehicle intensity. The use of a common frame in frame subtraction preserves the contrast of the vehicle intensity, but enhances random noise, thus reduces the accuracy of the flow speed computation. In order to both preserve the contrast of the vehicle intensity and reduce the random noise, we introduce the four-frame correlation algorithm. Two of the frames are used as the correlated frames and the other two are used for background subtraction purpose.

6.0 Camera Perspective

6.1 Introduction

With a traffic surveillance system using cameras, large region of traffic can be monitored simultaneously. However, for monitoring and control of the traffic, the region of interest is important. To our system, the TFVC system, some algorithms impose some requirements on the camera perspective. Thus, we will derive the relationship between camera orientation and flow speed calculation and discuss its significance.

6.2 Relation between Camera Perspective and Flow Speed Computation

In the following, we will use optical principle to derive relations between the camera pole height, the angle between the camera main optical axis and horizontal axis, and the calibration factor. In the following derivation, all units are in foot.

Let

f = focal length (feet)

h' = camera height (feet)

d = distance of the pole to the lane (feet)

β = angle between camera main optical axis and ground (degree)

α = angle between camera main optical axis and traffic lane (degree)

ω = CCD size, or pixel size = $10 \mu\text{m}/\text{pixel} = 10 / (12 * 2.54 * 10^4)$
= 1/30480 (feet/pixel)

p_m = maximum number of pixels in the image plane in vertical direction
= 480 (pixels) (This corresponds to the vertical field of view).

In FIGURE 11, the coordinate systems for the traffic and the image planes are $O_1 - Y_1$ and $O_2 - Y_2$, respectively. The origin O_1 for the image plane is at the top of the image plane. Thus, if we assume that C_1 is the center point of the image plane, then distance $O_1C_1 = \omega * (p_m / 2 - 1)$ (feet). The origin O_2 for the traffic plane is at the bottom of the pole. C_2 is the point where the camera main optical axis and the traffic lane intersect. The variables are defined as follows:

$h = OO_2$ (feet) = effective camera pole height = $\sqrt{h'^2 + d^2}$

$L_1 = O_1C_1$ (feet) = $\omega * (p_m / 2 - 1)$ (feet)

$L_2 = O_2C_2$ (feet) = $h \cot \alpha = \sqrt{h'^2 + d^2} \cot \alpha$ (feet)

p = image position on the focal plane of the camera (pixels)
= O_1A_1 (pixels) ($0 \leq p \leq p_m - 1$)

y_1 = image position on the focal plane of the camera (feet)
= O_1A_1 (feet) ($0 \leq y_1 \leq \omega * (p_m - 1)$)

y_2 = vehicle position on the highway = O_2A_2 (feet)

$z = A_2C'_2$ (feet)

$$h_1 = OC'_2 \text{ (feet)}$$

$$h_2 = C'_2 C_2 \text{ (feet)}$$

From the above definition, we have

$$y_1 = p\omega \quad (\text{II.1a})$$

and

$$\sin \alpha = \frac{h}{h'} \sin \beta \quad (\text{II.1b})$$

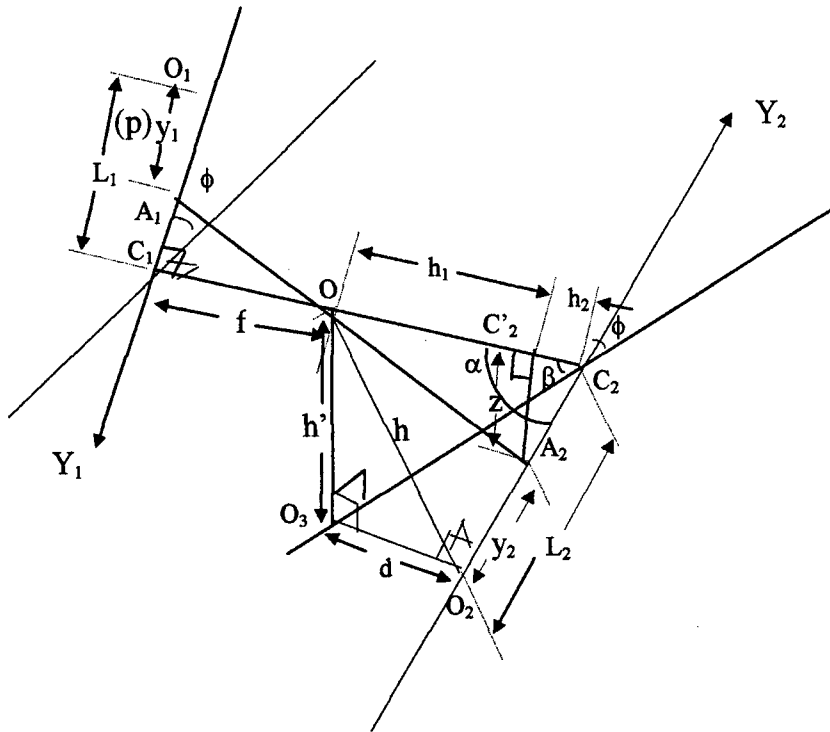


FIGURE 11 Schematic Drawing of the Camera Perspective

From triangle $\Delta C_2 O_2 O \sim$ triangle $\Delta C'_2 A_2 O$ in FIGURE 11,
 From Fig. FIGURE 11, triangle $\Delta C_1 A_1 O \sim$ triangle $\Delta C'_2 A_2 O$, this gives

$$\frac{L_1 - y_1}{z} = \frac{f}{h_1}$$

$$\Rightarrow y_1 = L_1 - \frac{fz}{h_1} \quad (\text{II.2})$$

From ΔC_2O_2O , we have

$$C_2O = h_1 + h_2 = \frac{h}{\sin \alpha}$$

$$\Rightarrow h_1 = \frac{h}{\sin \alpha} - h_2 \quad (\text{II.3})$$

From $\Delta A_2C'_2C_2$, we have

$$h_2 = (L_2 - y_2) \cos \alpha \quad (\text{II.4})$$

and

$$z = (L_2 - y_2) \sin \alpha \quad (\text{II.5})$$

Plug Eq.(II.4) into Eq.(II.3), we have

$$h_1 = \frac{h}{\sin \alpha} - (L_2 - y_2) \cos \alpha \quad (\text{II.6})$$

Plug Eqs. (II.5) and (II.6) into Eq.(II.2), we have

$$\begin{aligned} y_1 &= L_1 - \frac{f(L_2 - y_2) \sin \alpha}{\frac{h}{\sin \alpha} - (L_2 - y_2) \cos \alpha} \\ &= L_1 - \frac{f(L_2 - y_2) \sin^2 \alpha}{h - (L_2 - y_2) \sin \alpha \cos \alpha} \\ &= L_1 - \frac{2f(L_2 - y_2) \sin^2 \alpha}{2h - (L_2 - y_2) \sin 2\alpha} \end{aligned} \quad (\text{II.7})$$

With Eqs.(II.1a) and (II.7), we have

$$p = \frac{1}{\omega} \left(L_1 - \frac{2f(L_2 - y_2) \sin^2 \alpha}{2h - (L_2 - y_2) \sin 2\alpha} \right) \quad (\text{II.8})$$

From definitions of L_1 and L_2 , we have

$$p = \left(\frac{p_m}{2} - 1\right) - \frac{f(h \cos \alpha - y_2 \sin \alpha)}{\omega(h \sin \alpha + y_2 \cos \alpha)} \quad (\text{II.9a})$$

Because we have the access to the image picture, it is better to express y_2 as a function of p . From Eq.(II.9a), we have

$$y_2 = h \frac{f \cos \alpha - \omega\left(\frac{p_m}{2} - 1 - p\right) \sin \alpha}{f \sin \alpha + \omega\left(\frac{p_m}{2} - 1 - p\right) \cos \alpha} \quad (\text{II.9b})$$

We can simplify Eqs.(II.9a) and (b). Let

$$\tan \xi(y_2) \equiv \frac{y_2}{h} \quad (\text{II.10a})$$

and

$$\tan \zeta(p) \equiv \frac{\omega\left(\frac{p_m}{2} - 1 - p\right)}{f} \quad (\text{II.10b})$$

where the indices y_2 and p indicate the dependence of ξ and ζ on y_2 and p , respectively, we can then rewrite Eq.(II.9a) and (b) as

$$p = \left(\frac{p_m}{2} - 1\right) - \frac{f}{\omega} \cot(\alpha + \xi(y_2)) \quad (\text{II.11a})$$

and

$$y_2 = h \cot(\alpha + \zeta(p)) \quad (\text{II.11b})$$

Because $0 \leq p \leq p_m - 1$, from Eqs.(II.10b) and (II.11b), we have

$$h \cot(\alpha + \zeta(0)) \leq y_2 \leq h \cot(\alpha + \zeta(p_m - 1)) \quad (\text{II.12a})$$

where

$$\tan \zeta(0) \equiv \frac{\omega\left(\frac{p_m}{2} - 1\right)}{f} \quad (\text{II.12b})$$

and

$$\tan \zeta(p_m - 1) \equiv -\frac{\omega p_m}{2f} \quad (\text{II.12c})$$

So, the minimum, maximum values, and range of y_2 corresponding to the whole camera field of view are:

$$y_{2\min} = h \cot(\alpha + \zeta(0)) \quad (\text{II.13a})$$

$$y_{2\max} = h \cot(\alpha + \zeta(p_m - 1)) \quad (\text{II.13b})$$

$$\begin{aligned} \Delta y_2 &= y_{2\max} - y_{2\min} \\ &= h[\cot(\alpha + \zeta(p_m - 1)) - \cot(\alpha + \zeta(0))] \end{aligned} \quad (\text{II.13c})$$

For an ROI centering at p_0 with range P in the image plane,

$$p_0 - P/2 \leq p \leq p_0 + P/2 - 1 \quad (\text{II.14a})$$

thus from Eqs.(II.10b) and (II.11b), we have

$$h \cot(\alpha + \zeta(p_0 - P/2)) \leq y_2 \leq h \cot(\alpha + \zeta(p_0 + P/2 - 1)) \quad (\text{II.14b})$$

where

$$\tan \zeta(p_0 - P/2) \equiv \frac{\omega(\frac{p_m + P}{2} - 1 - p_0)}{f} \quad (\text{II.14c})$$

and

$$\tan \zeta(p_0 + P/2 - 1) \equiv \frac{\omega(\frac{p_m - P}{2} - p_0)}{f} \quad (\text{II.14d})$$

So the center, minimum, maximum, and range of y_2 are

$$y'_{2\text{center}} = h \cot(\alpha + \zeta(p_0)) \quad (\text{II.15a})$$

$$y'_{2\min} = h \cot(\alpha + \zeta(p_0 - P/2)) \quad (\text{II.15b})$$

$$y'_{2\max} = h \cot(\alpha + \zeta(p_0 + P/2 - 1)) \quad (\text{II.15c})$$

and

$$\Delta y'_2 = y'_{2\max} - y'_{2\min}$$

$$= h[\cot(\alpha + \zeta(p_0 + P/2 - 1)) - \cot(\alpha + \zeta(p_0 - P/2))] \quad (\text{II.15d})$$

Now, we will derive the relationship between the calibration factor γ (feet/pixel) and the vehicle position p . The calibration factor γ is defined as follows.

$$\gamma \equiv \frac{dy_2}{dp} \quad (\text{II.16a})$$

Differentiating Eq.(II.9b) gives

$$\gamma = \frac{f\omega h}{[f \sin \alpha + \omega(\frac{P_m}{2} - 1 - p) \cos \alpha]^2} \quad (\text{II.16b})$$

or

$$\gamma = \frac{f\omega h}{[f^2 + \omega^2(\frac{P_m}{2} - 1 - p)^2] \sin^2(\alpha + \zeta(p))} \quad (\text{II.16c})$$

In our code, we use MPH which is defined as

$$MPH \equiv \frac{\text{miles / hour}}{\text{pixels / sec}} \quad (\text{II.17a})$$

The relationship between MPH and γ is

$$MPH = \frac{15}{22} \gamma \quad (\text{II.17b})$$

From Eq.(II.16b), we get

$$\frac{1}{\sqrt{\gamma}} = \frac{f \sin \alpha + \omega(\frac{P_m}{2} - 1 - p) \cos \alpha}{\sqrt{f\omega h}}$$

$$\Rightarrow \frac{1}{\sqrt{\gamma}} = \frac{f \sin \alpha + \omega(\frac{P_m}{2} - 1) \cos \alpha}{\sqrt{f\omega h}} - \frac{\sqrt{\omega} \cos \alpha}{\sqrt{fh}} p \quad (\text{II.18a})$$

$$\Rightarrow \frac{1}{\sqrt{\gamma}} = a + bp \quad (\text{II.18b})$$

where

$$a \equiv \frac{f \sin \alpha + \omega \left(\frac{p_m}{2} - 1 \right) \cos \alpha}{\sqrt{f \omega h}}$$

$$b \equiv -\frac{\sqrt{\omega} \cos \alpha}{\sqrt{f h}} \quad (\text{II.18c})$$

From Eq.(II.18a), we see that inverse of square root of calibration factor, $1/\sqrt{\gamma}$, is a linear function of the image position p . We will use this relation to calibrate the flow speed according to vehicle position in next section.

Now we will derive some limits on the camera pole height and camera angle. Assume that vehicle speed is v_r and the time difference between two correlated frames is dt , then the distance that the vehicle in position y_2 moves in time dt is

$$dy_2 = v_r dt \quad (\text{II.19a})$$

which gives the pixel movement dp_0 in image position p_0

$$dp_0 = \frac{dy_2}{\gamma} = \frac{v_r dt}{\gamma} \quad (\text{II.19b})$$

or

$$\frac{dp_0}{v_r dt} = \frac{[f^2 + \omega^2 \left(\frac{p_m}{2} - 1 - p_0 \right)^2] \sin^2(\alpha + \zeta(p_0))}{f \omega h} \quad (\text{II.19c})$$

As expected, if f , h , and α are fixed, the calibration factor at the right-hand side of Eq.(II.19c) is a constant at each specific point p_0 in the image plane. Thus, for a fixed dt , as v_r increases, dp_0 increases. When v_r achieves the maximum value $v_{r \max}$, dp_0 achieves its maximum value $dp_{0, \max}^{dt}$, where the superscript dt indicates the dependence of $dp_{0, \max}^{dt}$ on dt . Hence Eq.(II.19c) becomes

$$\frac{dp_{0,\max}^{dt}}{v_{r,\max} dt} = \frac{[f^2 + \omega^2 (\frac{P_m}{2} - 1 - p_0)^2] \sin^2(\alpha + \zeta(p_0))}{f\omega h} \quad (\text{II.20})$$

For flow speed computation to be reliable and accurate, we require that a vehicle stay in the region of interest (ROI) at least N_{\min} times. Assume that the height of the ROI is P , thus

$$dp_{0,\max}^{dt} \leq \frac{P}{N_{\min}} \quad (\text{II.21})$$

Eqs.(II.20) and (II.21) yield

$$\frac{v_{r,\max} dt [f^2 + \omega^2 (\frac{P_m}{2} - 1 - p_0)^2] \sin^2(\alpha + \zeta(p_0))}{f\omega h} \leq \frac{P}{N_{\min}} \quad (\text{II.22})$$

In the following, we will derive limits on camera angle α and pole height h .

A. Derivation of Maximum Camera Angle α

Rearrange Eq.(II.22), we get

$$[f^2 + \omega^2 (\frac{P_m}{2} - 1 - p_0)^2] \sin^2(\alpha + \zeta(p_0)) \leq \frac{f\omega h}{v_{r,\max} dt} \frac{P}{N_{\min}} \quad (\text{II.A.1})$$

or

$$\sin(\alpha + \zeta(p_0)) \leq \sqrt{\frac{1}{f^2 + \omega^2 (\frac{P_m}{2} - 1 - p_0)^2} \frac{f\omega h}{v_{r,\max} dt} \frac{P}{N_{\min}}} \quad 0 \leq \alpha \leq 90^\circ \quad (\text{II.A.2})$$

So, α_{\max} satisfies the following condition

$$\alpha_{\max} = \arcsin \sqrt{\frac{1}{f^2 + \omega^2 (\frac{P_m}{2} - 1 - p_0)^2} \frac{f\omega h}{v_{r,\max} dt} \frac{P}{N_{\min}}} - \zeta(p_0) \quad 0 \leq \alpha_{\max} \leq 90^\circ \quad (\text{II.A.3})$$

From Eq.(II.A.3), we can see that α_{\max} is a monatomic increasing function of h and a monatomic decreasing function of dt and f .

For fixed h and f , as dt decreases, α_{\max} increases. However, in order to be able to compute flow speed, dt has a minimum dt_{\min} which is the time between two closest correlated frames. In our case,

$$dt_{\min} = \frac{1}{15}(\text{sec}) \quad (\text{II.A.4})$$

because of our 4-frame correlation scheme. Use dt_{\min} and Eq.(II.A.3), we get

$$\alpha_{\max} = \arcsin \sqrt{\frac{1}{f^2 + \omega^2 \left(\frac{P_m}{2} - 1 - p_0\right)^2} \frac{f\omega h}{v_{r\max} dt_{\min}} \frac{P}{N_{\min}}} - \zeta(p_0) \quad 0 \leq \alpha_{\max} \leq 90^\circ \quad (\text{II.A.5})$$

Now we can calculate the maximum camera angle α_{\max} . Assume that

$$P = 100(\text{pixels}) \quad (\text{II.A.6a})$$

$$p_0 = 120(\text{pixels}) \quad (\text{II.A.6b})$$

$$v_{\max} = 80(\text{miles / hour}) = 352 / 3(\text{feet / s}) \quad (\text{II.A.6c})$$

$$N_{\min} = 5 \quad (\text{II.A.6d})$$

$$h = 40(\text{feet}) \quad (\text{II.A.6e})$$

$$f = 6 \sim 60(\text{mm}) = 5 / 254 \sim 50 / 254(\text{feet}) \quad (\text{II.A.6f})$$

(i) Case 1, $f = 5 / 254(\text{feet})$, that is, camera is zoomed all the way out:

$$\zeta(p_0) = \arctan \frac{(1 / 30480) * \left(\frac{480}{2} - 1 - 120\right)}{5 / 254} = 11.2^\circ \quad (\text{II.A.7})$$

$$\alpha_{\max} = \arcsin \sqrt{\frac{1}{\left(\frac{5}{254}\right)^2 + \left(\frac{1}{30480}\right)^2 (119)^2} \frac{\frac{5}{254} * \frac{1}{30480} * 40}{\frac{352}{3} * \frac{1}{15}} \frac{100}{5}} - 11.2$$

$$\alpha_{\max} = 12.7^\circ \quad (\text{II.A.8a})$$

With this angle, we can calculate the center, minimum, maximum distances, the range the camera can see, and the calibration factor. From Eqs.(II.13a)-(c), (II.15b), and (II.16b), we have

$$y_{2\min} = 40 \frac{(5/254)\cos 24.4^\circ - (1/30480)(\frac{480}{2} - 1)\sin 24.4^\circ}{(5/254)\sin 24.4^\circ + (1/30480)(\frac{480}{2} - 1)\cos 24.4^\circ}$$

$$y_{2\min} = 39(\text{feet}) \quad (\text{II.A.8b})$$

$$y_{2\max} = 40 \frac{(5/254)\cos 24.4^\circ + (1/30480)\frac{480}{2}\sin 24.4^\circ}{(5/254)\sin 24.4^\circ - (1/30480)\frac{480}{2}\cos 24.4^\circ}$$

$$y_{2\max} = 881(\text{feet}) \quad (\text{II.A.8c})$$

$$\Delta y_2 = y_{2\max} - y_{2\min} = 881 - 39 = 842(\text{feet}) \quad (\text{II.A.8d})$$

$$\gamma_{p_0} = \frac{(1/30480) * 40}{(5/254) * \sin^2 24.4^\circ} \quad (\text{II.A.8e})$$

$$MPH = \frac{15}{22} \gamma = 0.266 \quad (\text{II.A.8f})$$

We see that the distance of our ROI to the pole for case (i) is only 88 feet for the maximum angle. And the range that camera can see is from 39 feet to about 881 feet, or 842 feet (~1/6 mile) range.

(ii) Case 2, $f = 50/254(\text{feet})$, that is, camera is zoomed all the way in:

$$\alpha_{\max} = \arcsin \sqrt{\frac{(1/30480) * 40}{(352/3) * (1/15) * (50/254)} \frac{100}{5}}$$

$$\alpha_{\max} = 7.5^\circ \quad (\text{II.A.9a})$$

With this angle, we can calculate the center, minimum, maximum distances, the range the camera can see, and the calibration factor . From Eqs.(II.11a)-(c), (II.13), and (II.14b), we have

$$y_{2\text{center}} = 40 \cot 7.5^\circ = 303(\text{feet}) \quad (\text{II.A.9b})$$

$$y_{2\text{min}} = 40 \frac{(50 / 254) \cos 7.5^\circ - (1 / 30480) \left(\frac{480}{2} - 1 \right) \sin 7.5^\circ}{(50 / 254) \sin 7.5^\circ + (1 / 30480) \left(\frac{480}{2} - 1 \right) \cos 7.5^\circ}$$

$$y_{2\text{min}} = 232(\text{feet}) \quad (\text{II.A.9c})$$

$$y_{2\text{max}} = 40 \frac{(50 / 254) \cos 7.5^\circ + (1 / 30480) \frac{480}{2} \sin 7.5^\circ}{(50 / 254) \sin 7.5^\circ - (1 / 30480) \frac{480}{2} \cos 7.5^\circ}$$

$$y_{2\text{max}} = 439(\text{feet}) \quad (\text{II.A.9d})$$

$$\Delta y_2 = y_{2\text{max}} - y_{2\text{min}} = 439 - 232 = 207(\text{feet}) \quad (\text{II.A.9e})$$

$$\gamma_{\text{center}} = \frac{(1 / 30480) * 40}{(50 / 254) * \sin^2 7.5^\circ}$$

$$\gamma_{\text{center}} = 0.391 \quad (\text{II.A.9f})$$

$$MPH = \frac{15}{22} \gamma = 0.266 \quad (\text{II.A.9g})$$

We see that the distance of our ROI to the pole for case (ii) is about 303 feet for the maximum angle. And the range that camera can see is from 232 feet to about 439 feet, or 207 feet (~1/25 mile) range.

In the above, we obtain the maximum camera angle corresponding to zoom-out and zoom-in focal lengths and the minimum dt_{min} , and its related quantities, such as the center distance, the minimum and maximum distances, and the range that the camera can see. In the following, we will derive similar set of equations base on our commonly used dt value. Currently, we use $dt = 1 / 3(\text{sec})$, or 10 frames between two correlated frames. With this value

and the set of parameters in Eqs.(II.7a)-(e), we recalculate the maximum angle α_{\max} as follows.

(iii) Case 3, $f = 5 / 254(\text{feet})$, that is, camera is zoomed all the way out:

$$\alpha_{\max} = \arcsin \sqrt{\frac{(1 / 30480) * 40}{(352 / 3) * (1 / 3) * (5 / 254)} \frac{100}{5}}$$

$$\alpha_{\max} = 11^{\circ} \quad (\text{II.A.10a})$$

With this angle, we can calculate the center, minimum, maximum distances, the range the camera can see, and the calibration factor . From Eqs.(11a), (11b), (11c), (12b), and (14), we have

$$y_{2\text{center}} = 40 \cot 11^{\circ} = 206(\text{feet}) \quad (\text{II.A.10b})$$

$$y_{2\min} = 40 \frac{(5 / 254) \cos 11^{\circ} - (1 / 30480) (\frac{480}{2} - 1) \sin 11^{\circ}}{(5 / 254) \sin 11^{\circ} + (1 / 30480) (\frac{480}{2} - 1) \cos 11^{\circ}}$$

$$y_{2\min} = 62(\text{feet}) \quad (\text{II.A.10c})$$

$$y_{2\max} = \infty(\text{feet}) \quad (\text{II.A.10d})$$

$$\Delta y_2 = y_{2\max} - y_{2\min} = \infty(\text{feet}) \quad (\text{II.A.10e})$$

$$\gamma_{\text{center}} = \frac{(1 / 30480) * 40}{(5 / 254) * \sin^2 11^{\circ}}$$

$$\gamma_{\text{center}} = 1.83 \quad (\text{II.A.10f})$$

$$MPH = \frac{15}{22} \gamma = 1.25 \quad (\text{II.A.10g})$$

We see that the distance of our ROI to the pole for case (iii) is about 206 feet for the maximum angle. And the range that camera can see is from 62 feet to infinity.

(iv) Case 4, $f = 50 / 254(\text{feet})$, that is, camera is zoomed all the way in:

$$\alpha_{\max} = \arcsin \sqrt{\frac{(1/30480) * 40}{(352/3) * (1/3) * (50/254)} \frac{100}{5}}$$

$$\alpha_{\max} = 3.4^{\circ} \quad (\text{II.A.11a})$$

With this angle, we can calculate the center, minimum, maximum distances, the range the camera can see, and the calibration factor . From Eqs.(11a), (11b), (11c), (12b), and (14), we have

$$y_{2\text{center}} = 40 \cot 3.4^{\circ} = 673(\text{feet}) \quad (\text{II.A.11b})$$

$$y_{2\min} = 40 \frac{(50/254) \cos 3.4^{\circ} - (1/30480) \left(\frac{480}{2} - 1 \right) \sin 3.4^{\circ}}{(50/254) \sin 3.4^{\circ} + (1/30480) \left(\frac{480}{2} - 1 \right) \cos 3.4^{\circ}}$$

$$y_{2\min} = 402(\text{feet}) \quad (\text{II.A.11c})$$

$$y_{2\max} = 40 \frac{(50/254) \cos 3.4^{\circ} + (1/30480) * \frac{480}{2} \sin 3.4^{\circ}}{(50/254) \sin 3.4^{\circ} - (1/30480) * \frac{480}{2} \cos 3.4^{\circ}}$$

$$y_{2\max} = 2066(\text{feet}) \quad (\text{II.A.11d})$$

$$\Delta y_2 = y_{2\max} - y_{2\min} = 2066 - 402 = 1664(\text{feet}) \quad (\text{II.A.11e})$$

$$\gamma_{\text{center}} = \frac{(1/30480) * 40}{(50/254) * \sin^2 3.4^{\circ}}$$

$$\gamma_{\text{center}} = 1.90 \quad (\text{II.A.11f})$$

$$MPH = \frac{15}{22} \gamma = 1.29 \quad (\text{II.A.11g})$$

We see that the distance of our ROI to the pole for case (iv) is 673 feet for the maximum angle. And the range that camera can see is from 402 feet to about 2066 feet ($\sim 2/5$ mile), or 1664 feet ($\sim 1/3$ mile) range.

From the above results, we can see that in order to satisfy our requirements on vehicles being in the ROI for at least $N_{\min} = 5$ times with $dt_{\min} = 1/3(\text{sec})$, the maximum camera angle is 11° for $f = 5/254(\text{feet})$ (camera is zoomed all the way out), while the maximum camera angle is 3.4° for $f = 50/254(\text{feet})$ (camera is zoomed all the way in). Even though the calibration factors for center position in both cases are similar, the distances of the center position to the pole are quite different. The distance of the center position to the pole in case (iii) is far smaller than that in case (iv) (206 feet in case (iii) to 673 feet in case (iv)). That is, we can see closer distance in case (iii) than in case (iv). Thus, it is beneficial to use $f = 5/254(\text{feet})$ (camera is zoomed all the way out) for our flow speed calculation. Another advantage on using $f = 5/254(\text{feet})$ is for camera preset. If camera is zoomed all the way out, the preset will find its zoom position easier and quicker. There is, however, a disadvantage on using $f = 5/254(\text{feet})$. Because of the different geometry's in different areas, the traffic lanes may have a big angle from vertical direction in some areas for camera zooming all the way out, which presents some problem to our lane definition algorithm due to the way it was designed.

B. Derivation of Minimum Pole Height h

In the above section, we derived various quantities related to maximum camera angle α_{\max} . In this section, we will derive minimum pole height h_{\min} and its related quantities.

Rearranging Eq.(II.22) gives

$$\frac{v_{r\max} dt [f \sin \alpha + \omega(\frac{ysize}{2} - 1 - p) \cos \alpha]^2}{f \omega h} \leq \frac{Y}{N_{\min}} \quad (\text{II.B.1})$$

$$h \geq \frac{v_{r\max} dt [f \sin \alpha + \omega(\frac{ysize}{2} - 1 - p) \cos \alpha]^2 N_{\min}}{f \omega Y} \quad (\text{II.B.2})$$

Thus, the minimum pole height h_{\min} is

$$h_{\min} = \frac{v_{r\max} dt [f \sin \alpha + \omega(\frac{ysize}{2} - 1 - p) \cos \alpha]^2 N_{\min}}{f \omega Y} \quad (\text{II.B.3})$$

Assume that dt takes on its minimum dt_{\min} as discussed in Section A, then

$$h_{\min} = \frac{v_{r\max} dt_{\min} [f \sin \alpha + \omega(\frac{ysize}{2} - 1 - p) \cos \alpha]^2 N_{\min}}{f \omega Y} \quad (\text{II.B.4})$$

As in Section A, we will use the center portion of the image for computation. Therefore,

$$h_{\min} = \frac{v_{r\max} dt_{\min} f N_{\min} \sin^2 \alpha}{\omega Y} \quad (\text{II.B.5})$$

Eq.(II.B.5) shows that h_{\min} is a monotonic increasing function of α . Thus, in order for the camera to be able to have a bigger maximum angle, the pole height has to be higher. Although a higher pole means a bigger maximum camera angle, it does not mean that its center distance $y_{2\text{center}}$ is closer. Plug Eq.(II.B.5) into Eq.(II.11a), we get

$$y_{2\text{center}} = \frac{v_{r\max} dt_{\min} f N_{\min} \sin 2\alpha}{2\omega Y} \quad (\text{II.B.6})$$

From Eq.(II.B.6), we see that when $\alpha = 45^\circ$, $y_{2\text{center}}$ reaches its maximum. $y_{2\text{center}}$ is a monotonic increasing function of α for $0^\circ \leq \alpha \leq 45^\circ$ and a monotonic decreasing function of α for $45^\circ \leq \alpha \leq 90^\circ$. Thus, when α increases from 0° to 45° , the minimum pole height increases, and the center distance $y_{2\text{center}}$ that camera can see increases. when α increases from 45° to 90° , the minimum pole height increases, but the center distance $y_{2\text{center}}$ that camera can see decreases.

From the above discussion, we can see that increaseing pole height can increase the maximum camera angle allowed, but it does not necessarily mean that the distance it can see is closer. For the maximum camera angle that is less than 45° , the higher the pole, the farther the center distance the camera can see. For the maximum camera angle that is larger than 45° , the higher the pole, the closer the center distance the camera can see. Therefore, higher pole does not mean better. Certainly, if there are objects along the highway, then higher pole will give us better view of the highway.

With $\alpha = 45^\circ$, the minimum pole height and the center distance $y_{2\text{center}}$ are

$$h_{\min} = y_{2\text{center}} = \frac{v_{r\max} dt_{\min} f N_{\min}}{2\omega Y} \quad (\text{II.B.7})$$

Use the set of parameters in Eqs.(II.A.7a)-(c) and (II.A.7e), we can compute the minimum pole height h_{\min} for camera zooming all the way out and in as follows:

(i) Case 1, $f = 5 / 254(\text{feet})$, that is, camera is zoomed all the way out

From Eq.(II.A.8a), we know that $h_{\min} = 40(\text{feet})$ corresponds to $\alpha_{\max} = 24.4^\circ$. In order to increase maximum camera angle α_{\max} , h_{\min} has to be increased. In the following, we will compute several values of h_{\min} with respect to different values of maximum camera angle α_{\max} .

(a) $\alpha_{\max} = 30^\circ$

$$h_{\min} = \frac{(352 / 3) * (1 / 15) * (5 / 254) * 5 * \sin^2 30^\circ}{(1 / 30480) * 100}$$

$$h_{\min} = 59(\text{feet}) \quad (\text{II.B.8a})$$

With this height, we can calculate the center, minimum, maximum distances, the range the camera can see, and the calibration factor. From Eqs.(II.11a)-(c), (II.13), and (II.14b), we have

$$y_{2\text{center}} = 59 \cot 30^\circ = 102(\text{feet}) \quad (\text{II.B.8b})$$

$$y_{2\min} = 59 \frac{(5 / 254) \cos 30^\circ - (1 / 30480) \left(\frac{480}{2} - 1 \right) \sin 30^\circ}{(5 / 254) \sin 30^\circ + (1 / 30480) \left(\frac{480}{2} - 1 \right) \cos 30^\circ}$$

$$y_{2\min} = 47(\text{feet}) \quad (\text{II.B.8c})$$

$$y_{2\max} = 59 \frac{(5/254) \cos 30^\circ + (1/30480) * \frac{480}{2} \sin 30^\circ}{(5/254) \sin 30^\circ - (1/30480) * \frac{480}{2} \cos 30^\circ}$$

$$y_{2\max} = 410(\text{feet}) \quad (\text{II.B.8d})$$

$$\Delta y_2 = y_{2\max} - y_{2\min} = 410 - 47 = 363(\text{feet}) \quad (\text{II.B.8e})$$

$$\gamma_{\text{center}} = \frac{(1/30480) * 59}{(5/254) * \sin^2 30^\circ}$$

$$\gamma_{\text{center}} = 0.393 \quad (\text{II.B.8f})$$

$$MPH = \frac{15}{22} \gamma = 0.268 \quad (\text{II.B.8g})$$

$$(b) \alpha_{\max} = 45^\circ$$

$$h_{\min} = \frac{(352/3) * (1/15) * (5/254) * 5 * \sin^2 45^\circ}{(1/30480) * 100}$$

$$h_{\min} = 117(\text{feet}) \quad (\text{II.B.9a})$$

With this height, we can calculate the center, minimum, maximum distances, the range the camera can see, and the calibration factor . From Eqs.(II.11a)-(c), (II.13), and (II.14b), we have

$$y_{2\text{center}} = 117 \cot 45^\circ = 117(\text{feet}) \quad (\text{II.B.9b})$$

$$y_{2\min} = 117 \frac{(5/254) \cos 45^\circ - (1/30480) (\frac{480}{2} - 1) \sin 45^\circ}{(5/254) \sin 45^\circ + (1/30480) (\frac{480}{2} - 1) \cos 45^\circ}$$

$$y_{2\min} = 50(\text{feet}) \quad (\text{II.B.9c})$$

$$y_{2\max} = 117 \frac{(5/254)\cos 45^\circ + (1/30480) * \frac{480}{2} \sin 45^\circ}{(5/254)\sin 45^\circ - (1/30480) * \frac{480}{2} \cos 45^\circ}$$

$$y_{2\max} = 273(\text{feet}) \quad (\text{II.B.9d})$$

$$\Delta y_2 = y_{2\max} - y_{2\min} = 273 - 50 = 223(\text{feet}) \quad (\text{II.B.9e})$$

$$\gamma_{\text{center}} = \frac{(1/30480) * 117}{(5/254) * \sin^2 45^\circ}$$

$$\gamma_{\text{center}} = 0.390 \quad (\text{II.B.9f})$$

$$MPH = \frac{15}{22} \gamma = 0.267 \quad (\text{II.B.9g})$$

(c) $\alpha_{\max} = 90^\circ$, that is, camera looks straight down,

$$h_{\min} = \frac{(352/3) * (1/15) * (5/254) * 5 * \sin^2 90^\circ}{(1/30480) * 100}$$

$$h_{\min} = 234(\text{feet}) \quad (\text{II.B.10a})$$

With this height, we can calculate the center, minimum, maximum distances, the range the camera can see, and the calibration factor. From Eqs.(II.11a)-(c), (II.13), and (II.14b), we have

$$y_{2\text{center}} = 234 \cot 90^\circ = 0(\text{feet}) \quad (\text{II.B.10b})$$

$$y_{2\min} = 234 \frac{(5/254)\cos 90^\circ - (1/30480)(\frac{480}{2} - 1)\sin 90^\circ}{(5/254)\sin 90^\circ + (1/30480)(\frac{480}{2} - 1)\cos 90^\circ}$$

$$y_{2\min} = -93(\text{feet}) \quad (\text{II.B.10c})$$

$$y_{2\max} = 234 \frac{(5/254)\cos 90^\circ + (1/30480) * \frac{480}{2} \sin 90^\circ}{(5/254)\sin 90^\circ - (1/30480) * \frac{480}{2} \cos 90^\circ}$$

$$y_{2\max} = 94(\text{feet}) \quad (\text{II.B.10d})$$

$$\Delta y_2 = y_{2\max} - y_{2\min} = 94 + 93 = 187(\text{feet}) \quad (\text{II.B.10e})$$

$$\gamma_{\text{center}} = \frac{(1/30480) * 234}{(5/254) * \sin^2 90^\circ}$$

$$\gamma_{\text{center}} = 0.390 \quad (\text{II.B.10f})$$

$$MPH = \frac{15}{22} \gamma = 0.267 \quad (\text{II.B.10g})$$

(ii) Case 2, $f = 50/254(\text{feet})$, that is, camera is zoomed all the way in

From Eq.(II.A.9), we know that $h_{\min} = 40(\text{feet})$ corresponds to $\alpha_{\max} = 7.5^\circ$. As in the above case, we will compute several values of h_{\min} with respect to different values of maximum camera angle α_{\max} below.

(a) $\alpha_{\max} = 15^\circ$

$$h_{\min} = \frac{(352/3) * (1/15) * (50/254) * 5 * \sin^2 15^\circ}{(1/30480) * 100}$$

$$h_{\min} = 157(\text{feet}) \quad (\text{II.B.11a})$$

With this height, we can calculate the center, minimum, maximum distances, the range the camera can see, and the calibration factor. From Eqs.(II.11a)-(c), (II.13), and (II.14b), we have

$$y_{2\text{center}} = 157 \cot 15^\circ = 586(\text{feet}) \quad (\text{II.B.11b})$$

$$y_{2\min} = 157 \frac{(50 / 254) \cos 15^\circ - (1 / 30480) \left(\frac{480}{2} - 1 \right) \sin 15^\circ}{(50 / 254) \sin 15^\circ + (1 / 30480) \left(\frac{480}{2} - 1 \right) \cos 15^\circ}$$

$$y_{2\min} = 505(\text{feet}) \quad (\text{II.B.11c})$$

$$y_{2\max} = 157 \frac{(50 / 254) \cos 15^\circ + (1 / 30480) * \frac{480}{2} \sin 15^\circ}{(50 / 254) \sin 15^\circ - (1 / 30480) * \frac{480}{2} \cos 15^\circ}$$

$$y_{2\max} = 696(\text{feet}) \quad (\text{II.B.11d})$$

$$\Delta y_2 = y_{2\max} - y_{2\min} = 696 - 505 = 191(\text{feet}) \quad (\text{II.B.11e})$$

$$\gamma_{\text{center}} = \frac{(1 / 30480) * 157}{(50 / 254) * \sin^2 15^\circ}$$

$$\gamma_{\text{center}} = 0.391 \quad (\text{II.B.11f})$$

$$MPH = \frac{15}{22} \gamma = 0.266 \quad (\text{II.B.11g})$$

$$(b) \alpha_{\max} = 30^\circ$$

$$h_{\min} = \frac{(352 / 3) * (1 / 15) * (50 / 254) * 5 * \sin^2 30^\circ}{(1 / 30480) * 100}$$

$$h_{\min} = 586(\text{feet}) \quad (\text{II.B.12a})$$

With this height, we can calculate the center, minimum, maximum distances, the range the camera can see, and the calibration factor . From Eqs.(II.11a)-(c), (II.13), and (II.14b), we have

$$y_{2\text{center}} = 586 \cot 30^\circ = 1015(\text{feet}) \quad (\text{II.B.12b})$$

$$y_{2\min} = 586 \frac{(50/254)\cos 30^\circ - (1/30480)(\frac{480}{2} - 1)\sin 30^\circ}{(50/254)\sin 30^\circ + (1/30480)(\frac{480}{2} - 1)\cos 30^\circ}$$

$$y_{2\min} = 928(\text{feet}) \quad (\text{II.B.12c})$$

$$y_{2\max} = 586 \frac{(50/254)\cos 30^\circ + (1/30480) * \frac{480}{2} \sin 30^\circ}{(50/254)\sin 30^\circ - (1/30480) * \frac{480}{2} \cos 30^\circ}$$

$$y_{2\max} = 1116(\text{feet}) \quad (\text{II.B.12d})$$

$$\Delta y_2 = y_{2\max} - y_{2\min} = 1116 - 928 = 188(\text{feet}) \quad (\text{II.B.12e})$$

$$\gamma_{\text{center}} = \frac{(1/30480) * 586}{(50/254) * \sin^2 30^\circ}$$

$$\gamma_{\text{center}} = 0.390 \quad (\text{II.B.12f})$$

$$MPH = \frac{15}{22} \gamma = 0.266 \quad (\text{II.B.12g})$$

From Eqs.(II.B.12a)-(g), we see that with camera zooms all the way in and camera angle at 30° , the camera pole has to be 590 feet. As camera angle increases, the pole height would need to be higher, which is unrealistic. Thus, we will not compute the higher camera angle situation for this case.

As in Section A, we will also derive all quantities for $dt = 1/3(\text{sec})$, our usual separation between two correlated frames.

(iii) Case 3, $f = 5/254(\text{feet})$, that is, camera is zoomed all the way out

From Eq.(II.A.10a), we know that $h_{\min} = 40(\text{feet})$ corresponds to $\alpha_{\max} = 11^\circ$. In the following, we will compute several values of h_{\min} with respect to different values of maximum camera angle α_{\max} .

$$(a) \alpha_{\max} = 15^\circ$$

$$h_{\min} = \frac{(352/3) * (1/3) * (5/254) * 5 * \sin^2 15^\circ}{(1/30480) * 100}$$

$$h_{\min} = 79(\text{feet}) \quad (\text{II.B.13a})$$

With this height, we can calculate the center, minimum, maximum distances, the range the camera can see, and the calibration factor . From Eqs.(II.11a)-(c), (II.13), and (II.14b), we have

$$y_{2\text{center}} = 79 \cot 15^\circ = 295(\text{feet}) \quad (\text{II.B.13b})$$

$$y_{2\min} = 79 \frac{(5/254) \cos 15^\circ - (1/30480) \left(\frac{480}{2} - 1 \right) \sin 15^\circ}{(5/254) \sin 15^\circ + (1/30480) \left(\frac{480}{2} - 1 \right) \cos 15^\circ}$$

$$y_{2\min} = 106(\text{feet}) \quad (\text{II.B.13c})$$

$$y_{2\max} = \infty(\text{feet}) \quad (\text{II.B.13d})$$

$$\Delta y_2 = y_{2\max} - y_{2\min} = \infty(\text{feet}) \quad (\text{II.B.13e})$$

$$\gamma_{\text{center}} = \frac{(1/30480) * 79}{(5/254) * \sin^2 15^\circ}$$

$$\gamma_{\text{center}} = 1.965 \quad (\text{II.B.13f})$$

$$MPH = \frac{15}{22} \gamma = 1.340 \quad (\text{II.B.13g})$$

$$(b) \alpha_{\max} = 30^\circ$$

$$h_{\min} = \frac{(352/3) * (1/3) * (5/254) * 5 * \sin^2 30^\circ}{(1/30480) * 100}$$

$$h_{\min} = 293(\text{feet}) \quad (\text{II.B.14a})$$

With this height, we can calculate the center, minimum, maximum distances, the range the camera can see, and the calibration factor. From Eqs.(11a)-(c), (II.13), and (II.14b), we have

$$y_{2\text{center}} = 293 \cot 30^\circ = 507(\text{feet}) \quad (\text{II.B.14b})$$

$$y_{2\min} = 293 \frac{(5/254) \cos 30^\circ - (1/30480) \left(\frac{480}{2} - 1 \right) \sin 30^\circ}{(5/254) \sin 30^\circ + (1/30480) \left(\frac{480}{2} - 1 \right) \cos 30^\circ}$$

$$y_{2\min} = 231(\text{feet}) \quad (\text{II.B.14c})$$

$$y_{2\max} = 293 \frac{(5/254) \cos 30^\circ + (1/30480) * \frac{480}{2} \sin 30^\circ}{(5/254) \sin 30^\circ - (1/30480) * \frac{480}{2} \cos 30^\circ}$$

$$y_{2\max} = 2034(\text{feet}) \quad (\text{II.B.14d})$$

$$\Delta y_2 = y_{2\max} - y_{2\min} = 2034 - 231 = 1803(\text{feet}) \quad (\text{II.B.14e})$$

$$\gamma_{\text{center}} = \frac{(1/30480) * 293}{(5/254) * \sin^2 30^\circ}$$

$$\gamma_{\text{center}} = 1.953 \quad (\text{II.B.14f})$$

$$MPH = \frac{15}{22} \gamma = 1.332 \quad (\text{II.B.14g})$$

From the above results, we see that when the maximum camera angle is 30° , the minimum pole height required is already about 293 feet. For bigger maximum camera angle, the minimum pole height will be even higher, which is unrealistic. Thus, we will not compute the minimum pole height for cases where the maximum camera angle is above 30° . Also, we will not compute the minimum pole height for cases where the camera zooms all the way in.

In the above, we compute the relationship between pole height, camera angle, and the center distance. In the following, we will discuss how the error in camera angle affects the calibration factor.

C. Effect of the Error in Camera Angle on the Calibration Factor

Differentiate Eq.(II.12a) with respect to α , we obtain the absolute change of the calibration factor related to error in α

$$d\gamma = -\frac{2f\omega h(f \cos \alpha - \omega(\frac{ysize}{2} - 1 - p) \sin \alpha)}{[f \sin \alpha + \omega(\frac{ysize}{2} - 1 - p) \cos \alpha]^3} d\alpha \quad (\text{II.C.1a})$$

We can also compute the relative change of the calibration factor

$$\frac{d\gamma}{\gamma} = -\frac{2(f \cos \alpha - \omega(\frac{ysize}{2} - 1 - p) \sin \alpha)}{[f \sin \alpha + \omega(\frac{ysize}{2} - 1 - p) \cos \alpha]} d\alpha \quad (\text{II.C.1b})$$

For the center,

$$d\gamma_{\text{center}} = -\frac{2\omega h \cos \alpha}{f \sin^3 \alpha} d\alpha \quad (\text{II.C.2a})$$

and

$$\frac{d\gamma_{\text{center}}}{\gamma_{\text{center}}} = -2 \cot \alpha d\alpha \quad (\text{II.C.2b})$$

Eq.(II.C.2a) shows that if the camera angle becomes bigger, or $d\alpha$ is positive, then $d\gamma_{\text{center}}$ is negative, or the calibration factor becomes smaller. Also from Eq.(II.C.2a), we can see that the absolute change of the calibration factor for bigger f value is smaller, assuming that α and $d\alpha$ are the same for all values of f . However, according to Eq.(II.C.2b), the relative change of the calibration factor depends only on angle α , and thus is the same for all values of f .

The above shows the effect of $d\alpha$ on the change of the calibration factor for different values of f when α and $d\alpha$ are the same. We will show in the following the effect of $d\alpha$ on the change of the calibration factor for different values of f when the calibration factors for different f values are the same before camera shifts. Denote the calibration factor as γ_c . Thus, from Eq.(II.13),

$$\gamma_c = \frac{\omega h}{f \sin^2 \alpha} \quad (\text{II.C.3})$$

From Eq.(II.C.3), we see that f is a monotonic decreasing function of α , or α is a monotonic decreasing function of f . Thus the bigger the value of f is, the smaller the angle α is. Substitute Eq.(II.C.3) into Eq.(II.C.2b), we have

$$d\gamma_{\text{center}} = -2\gamma_c \cot \alpha d\alpha \quad (\text{II.C.4})$$

From Eq.(II.C.4), we see that for the same $d\alpha$, absolute $d\gamma_{\text{center}}$ is a monotonic decreasing function of α . From Eq.(II.C.3), we know that α is a monotonic decreasing function of f . Therefore, absolute $d\gamma_{\text{center}}$ is a monotonic increasing function of f . Thus, for the same error in camera angle, the higher the value of f is, the more effect it has on the change of the calibration factor. In this case, the relative change in the calibration factor also increases with the value of f .

In the following, we are going to derive a formula on the effect of specific number of pixel shift, Δp , due to the error in camera angle, $\Delta\alpha$, on the calibration factor. Because the number is finite, we can not use differential form any more. Assume that the preset angle is α_i . After moving the camera away from the preset position, we want to put it back into the preset position. Due to whatever source of error, the camera comes back to the preset position with an error in camera angle, $\Delta\alpha$. So the final angle is

$$\alpha_f = \alpha_i + \Delta\alpha \quad (\text{II.C.5})$$

From Eq.(II.9a), we have the initial and the final image position p_i and p_f for the same point y_2 on highway

$$p_i = \left(\frac{ysize}{2} - 1 \right) - \frac{f h \cos \alpha_i - y_2 \sin \alpha_i}{\omega h \sin \alpha_i + y_2 \cos \alpha_i} \quad (\text{II.C.6a})$$

and

$$p_f = \left(\frac{ysize}{2} - 1\right) - \frac{f h \cos \alpha_f - y_2 \sin \alpha_f}{\omega h \sin \alpha_f + y_2 \cos \alpha_f} \quad (\text{II.C.6b})$$

Thus,

$$\Delta p = \frac{f}{\omega} \left(\frac{h \cos \alpha_i - y_2 \sin \alpha_i}{h \sin \alpha_i + y_2 \cos \alpha_i} - \frac{h \cos \alpha_f - y_2 \sin \alpha_f}{h \sin \alpha_f + y_2 \cos \alpha_f} \right) \quad (\text{II.C.6c})$$

As in the previous sections, we will discuss only the center position. Assume y_2 takes on the center value $y_{2\text{center}}$ initially, then

$$y_{2\text{center}} = h \cot \alpha_i \quad (\text{II.C.7})$$

Plug Eq.(II.C.7) into Eq.(II.C.6c), we have

$$\begin{aligned} \Delta p_{\text{center}} &= -\frac{f \cos \alpha_f - \cot \alpha_i \sin \alpha_f}{\omega \sin \alpha_f + \cot \alpha_i \cos \alpha_f} \\ &= \frac{f \sin \alpha_f \cos \alpha_i - \sin \alpha_i \cos \alpha_f}{\omega \cos \alpha_i \cos \alpha_f + \sin \alpha_f \sin \alpha_i} \\ \Delta p_{\text{center}} &= \frac{f}{\omega} \tan \Delta \alpha \end{aligned} \quad (\text{II.C.8})$$

It is interesting to know that Δp_{center} only depends on the error in camera angle, but not the camera angle itself. Thus for the same error in the camera angle, the pixel shift for the same point on the highway will be the same, no matter what camera angle is. Express $\Delta \alpha$ as a function of Δp_{center} , we have

$$\Delta \alpha = \arctan\left(\Delta p_{\text{center}} \frac{\omega}{f}\right) \quad (\text{II.C.9})$$

Eq.(II.C.9) says that for a same point $y_{2\text{center}}$ on the highway, in order for it to shift Δp_{center} on the image plane, the camera angle has to shift $\Delta \alpha$. Now we want to derive a formula for the Δy_2 shift on the highway for the same pixel point p on the image plane with respect to the camera angle shift $\Delta \alpha$. From Eq.(II.9b), we have

$$y_{2i} = h \frac{f \cos \alpha_i - \omega(\frac{ysize}{2} - 1 - p) \sin \alpha_i}{f \sin \alpha_i + \omega(\frac{ysize}{2} - 1 - p) \cos \alpha_i} \quad (\text{II.C.10a})$$

and

$$y_{2f} = h \frac{f \cos \alpha_f - \omega(\frac{ysize}{2} - 1 - p) \sin \alpha_f}{f \sin \alpha_f + \omega(\frac{ysize}{2} - 1 - p) \cos \alpha_f} \quad (\text{II.C.10b})$$

Thus,

$$\begin{aligned} \Delta y_2 &= y_{2f} - y_{2i} \\ &= h \left(\frac{f \cos \alpha_f - \omega(\frac{ysize}{2} - 1 - p) \sin \alpha_f}{f \sin \alpha_f + \omega(\frac{ysize}{2} - 1 - p) \cos \alpha_f} \right. \\ &\quad \left. - \frac{f \cos \alpha_i - \omega(\frac{ysize}{2} - 1 - p) \sin \alpha_i}{f \sin \alpha_i + \omega(\frac{ysize}{2} - 1 - p) \cos \alpha_i} \right) \end{aligned} \quad (\text{II.C.10c})$$

For the center pixel

$$p_{\text{center}} = ysize / 2 - 1 \quad (\text{II.C.11})$$

on the image plane, we have

$$\Delta y_{2\text{center}} = h(\cot \alpha_f - \cot \alpha_i) = h[\cot(\alpha_i + \Delta \alpha) - \cot \alpha_i] \quad (\text{II.C.12})$$

Plug Eq.(II.C.9) into Eq.(II.C.12), we can express $\Delta x_{2\text{center}}$ in terms of Δp_{center} as follows:

$$\Delta y_{2\text{center}} = -h \frac{\tan \Delta \alpha}{\sin^2 \alpha_i + \frac{1}{2} \sin 2\alpha_i \tan \Delta \alpha}$$

$$\Delta y_{2\text{center}} = -h \frac{\Delta p_{\text{center}} \frac{\omega}{f}}{\sin^2 \alpha_i + \Delta p_{\text{center}} \frac{\omega}{2f} \sin 2\alpha_i} \quad (\text{II.C.13})$$

Now, we can calculate the change in the calibration factor. From Eq.(II.12a), we have

$$\gamma_i = \frac{f\omega h}{[f \sin \alpha_i + \omega(\frac{ysize}{2} - 1 - p) \cos \alpha_i]^2} \quad (\text{II.C.14a})$$

and

$$\gamma_f = \frac{f\omega h}{[f \sin \alpha_f + \omega(\frac{ysize}{2} - 1 - p) \cos \alpha_f]^2} \quad (\text{II.C.14b})$$

Thus,

$$\Delta \gamma = \frac{f\omega h}{[f \sin \alpha_f + \omega(\frac{ysize}{2} - 1 - p) \cos \alpha_f]^2} - \frac{f\omega h}{[f \sin \alpha_i + \omega(\frac{ysize}{2} - 1 - p) \cos \alpha_i]^2} \quad (\text{II.C.14c})$$

For the center point in Eq.(II.C.11), we have

$$\Delta \gamma_{\text{center}} = \frac{\omega h}{f} \left(\frac{1}{\sin^2 \alpha_f} - \frac{1}{\sin^2 \alpha_i} \right)$$

$$\Delta \gamma_{\text{center}} = \frac{\omega h}{f} \left[\frac{1}{\sin^2 (\alpha_i + \Delta \alpha)} - \frac{1}{\sin^2 \alpha_i} \right] \quad (\text{II.C.15a})$$

and

$$\gamma_{\text{center}} = \frac{\omega h}{f} \frac{1}{\sin^2 \alpha_i} \quad (\text{II.C.15b})$$

So the relative change is

$$\frac{\Delta\gamma_{\text{center}}}{\gamma_{\text{center}}} = \frac{\sin^2 \alpha_i}{\sin^2(\alpha_i + \Delta\alpha)} - 1 \quad (\text{II.C.15c})$$

Now we want to express $\Delta\gamma_{\text{center}}$ in terms of Δp_{center} . Plug Eq.(II.C.9) into Eqs.(II.C.15a) and (II.C.15c), we have

$$\begin{aligned} \Delta\gamma_{\text{center}} &= \frac{\omega h \sin^2 \alpha_i - \sin^2(\alpha_i + \Delta\alpha)}{f \sin^2(\alpha_i + \Delta\alpha) \sin^2 \alpha_i} \\ &= -\frac{\omega h (\sin 2\alpha_i + \cos 2\alpha_i \tan \Delta\alpha) \tan \Delta\alpha}{f (\sin^2 \alpha_i + \frac{1}{2} \sin 2\alpha_i \tan \Delta\alpha)^2} \end{aligned}$$

$$\Delta\gamma_{\text{center}} = -\Delta p_{\text{center}} \frac{\omega^2 h}{f^2} \frac{\sin 2\alpha_i + \Delta p_{\text{center}} \frac{\omega}{f} \cos 2\alpha_i}{(\sin^2 \alpha_i + \Delta p_{\text{center}} \frac{\omega}{2f} \sin 2\alpha_i)^2} \quad (\text{II.C.16a})$$

and

$$\frac{\Delta\gamma_{\text{center}}}{\gamma_{\text{center}}} = -\Delta p_{\text{center}} \frac{\omega}{f} \frac{\sin 2\alpha_i + \Delta p_{\text{center}} \frac{\omega}{f} \cos 2\alpha_i}{(\sin \alpha_i + \Delta p_{\text{center}} \frac{\omega}{f} \cos \alpha_i)^2} \quad (\text{II.C.16b})$$

With Eqs.(II.C.9), (II.C.13), and (II.C.16), we can calculate some specific numbers. For this calculation, we will use the set of parameters in Case 4 in Section A. Also, in order to satisfy our requirement that vehicles stay in the ROI for at least N_{\min} times for both camera zooming all the way out and in, we assume that $\alpha_i = 3^\circ$. We will consider several different Δp_{center} .

(i) Case 1, $f = 5 / 254(\text{feet})$, that is, camera is zoomed all the way out.

(a) $\Delta p_{\text{center}} = 10$

From Eqs.(II.C.7), (II.C.9), (II.C.13), and (II.C.16), we have

$$y_{2\text{center}} = 40 \cot 3^\circ = 763(\text{feet}) \quad (\text{II.C.17a})$$

$$\Delta\alpha = \arctan(10 \frac{1/30480}{5/254}) = 0.96^\circ \quad (\text{II.C.17b})$$

$$\Delta y_{2\text{center}} = -40 \frac{10 \frac{1/30480}{5/254}}{\sin^2 3^\circ + 10 \frac{1/30480}{2 * 5/254} \sin 6^\circ}$$

$$\Delta y_{2\text{center}} = -184(\text{feet}) \quad (\text{II.C.17c})$$

$$\Delta \gamma_{\text{center}} = -10 \frac{(1/30480)^2 * 40}{(5/254)^2} \frac{\sin 6^\circ + 10 \frac{1/30480}{5/254} \cos 6^\circ}{(\sin^2 3^\circ + 10 \frac{1/30480}{2 * 5/254} \sin 6^\circ)^2}$$

$$\Delta \gamma_{\text{center}} = -10.3 \quad (\text{II.C.17d})$$

$$\gamma_{\text{center}} = 40 \frac{1/30480}{5/254} \frac{1}{\sin^2 3^\circ}$$

$$\gamma_{\text{center}} = 24.3 \quad (\text{II.C.17e})$$

$$\frac{\Delta \gamma_{\text{center}}}{\gamma_{\text{center}}} = -\frac{10.3}{24.3} = -42\% \quad (\text{II.C.17f})$$

This is a big change in the calibration factor. The reason for this big change is in the fact that camera angle is small and it is zoomed all the way in. Also, the error in camera angle is about 1 degree, which is about 33% error. For bigger Δp_{center} , it will be even worse, so we will not calculate those values.

(ii) Case 2, $f = 50/254(\text{feet})$, that is, camera is zoomed all the way in:

$$(a) \Delta p_{\text{center}} = 10$$

From Eqs.(II.C.7), (II.C.9), (II.C.13), and (II.C.16), we have

$$\Delta\alpha = \arctan\left(10 \frac{1/30480}{50/254}\right) = 0.096^\circ \quad (\text{II.C.18a})$$

$$\Delta y_{2\text{center}} = -40 \frac{10 \frac{1/30480}{50/254}}{\sin^2 3^\circ + 10 \frac{1/30480}{2 * 50/254} \sin 6^\circ}$$

$$\Delta y_{2\text{center}} = -24(\text{feet}) \quad (\text{II.C.18b})$$

$$\Delta \gamma_{\text{center}} = -10 \frac{(1/30480)^2 * 40}{(50/254)^2} \frac{\sin 6^\circ + 10 \frac{1/30480}{50/254} \cos 6^\circ}{(\sin^2 3^\circ + 10 \frac{1/30480}{2 * 50/254} \sin 6^\circ)^2}$$

$$\Delta \gamma_{\text{center}} = -0.148 \quad (\text{II.C.18c})$$

$$\gamma_{\text{center}} = 40 \frac{1/30480}{50/254} \frac{1}{\sin^2 3^\circ}$$

$$\gamma_{\text{center}} = 2.43 \quad (\text{II.C.18d})$$

$$\frac{\Delta \gamma_{\text{center}}}{\gamma_{\text{center}}} = -\frac{0.148}{2.43} = -6.1\% \quad (\text{II.C.18e})$$

We can see from the above results that for the same number of pixel shift, the error in the camera angle allowed for case 2 is far smaller. Correspondingly, The error in the calibration factor is substantially smaller. Even though the change in the calibration factor is within the tolerance for our purpose, it is not realistic because the error in the camera angle is normally more than 0.5° . For that reason and for comparison purpose, we will assume that the error in camera angle for case 2 is also 0.96° . Thus, from Eqs.(II.C.7), (II.C.8), (II.C.13), and (II.C.16), we have

$$(b) \Delta\alpha = 0.96^\circ$$

$$\Delta p_{\text{center}} = \frac{50/254}{1/30480} \tan 0.96^\circ = 100 \quad (\text{II.C.19a})$$

$$\Delta y_{2\text{center}} = -40 \frac{100 \frac{1/30480}{50/254}}{\sin^2 3^\circ + 100 \frac{1/30480}{2 * 50/254} \sin 6^\circ}$$

$$\Delta y_{2\text{center}} = -185(\text{feet}) \quad (\text{II.C.19b})$$

$$\Delta \gamma_{\text{center}} = -100 \frac{(1/30480)^2 * 40}{(50/254)^2} \frac{\sin 6^\circ + 100 \frac{1/30480}{50/254} \cos 6^\circ}{(\sin^2 3^\circ + 100 \frac{1/30480}{2 * 50/254} \sin 6^\circ)^2}$$

$$\Delta \gamma_{\text{center}} = -1.03 \quad (\text{II.C.19c})$$

$$\gamma_{\text{center}} = 40 \frac{1/30480}{50/254} \frac{1}{\sin^2 3^\circ}$$

$$\gamma_{\text{center}} = 2.43 \quad (\text{II.C.19d})$$

$$\frac{\Delta \gamma_{\text{center}}}{\gamma_{\text{center}}} = -\frac{1.03}{2.43} = -42\% \quad (\text{II.C.19e})$$

We can see that the number of pixel shift in this case is about 100, 10 times of that in the previous case, but the change in the calibration factor is smaller for camera zooming all the way in than for camera zooming all the way out with the same camera angle and error in the camera angle, as discussed earlier. Also, we can see that the relative change in calibration factor is about the same. However, the error in the calibration factor is still substantial.

From the above results, we can see that $\alpha_i = 3^\circ$ is too small for camera zooming all the way out ($f = 5/254(\text{feet})$). In order to get comparable results for this case, we will compute several camera angle values.

$$(a) \alpha_i = 10^\circ, \Delta p_{\text{center}} = 10$$

From Eqs. (II.C.7), (II.C.9), (II.C.13), and (II.C.16), we have

$$y_{2\text{center}} = 40 \cot 10^\circ = 227(\text{feet}) \quad (\text{II.C.20a})$$

$$\Delta\alpha = \arctan\left(10 \frac{1/30480}{5/254}\right) = 0.96^\circ \quad (\text{II.C.20b})$$

$$\Delta y_{2\text{center}} = -40 \frac{10 \frac{1/30480}{5/254}}{\sin^2 10^\circ + 10 \frac{1/30480}{2 * 5/254} \sin 20^\circ}$$

$$\Delta y_{2\text{center}} = -20(\text{feet}) \quad (\text{II.C.20c})$$

$$\Delta \gamma_{\text{center}} = -10 \frac{(1/30480)^2 * 40 \frac{\sin 20^\circ + 10 \frac{1/30480}{5/254} \cos 20^\circ}{(\sin^2 10^\circ + 10 \frac{1/30480}{2 * 5/254} \sin 20^\circ)^2}}$$

$$\Delta \gamma_{\text{center}} = -0.365 \quad (\text{II.C.20d})$$

$$\gamma_{\text{center}} = 40 \frac{1/30480}{5/254} \frac{1}{\sin^2 10^\circ}$$

$$\gamma_{\text{center}} = 2.21 \quad (\text{II.C.20e})$$

$$\frac{\Delta \gamma_{\text{center}}}{\gamma_{\text{center}}} = -\frac{0.365}{2.21} = -16\% \quad (\text{II.C.20f})$$

Thus, the calibration factor is about 16% off for 10 pixel shift on the image plane at angle $\alpha_i = 10^\circ$, which is big.

$$(b) \alpha_i = 20^\circ, \Delta p_{\text{center}} = 10$$

From Eqs.(II.C.7), (II.C.9), (II.C.13), and (II.C.16), we have

$$y_{2\text{center}} = 40 \cot 20^\circ = 110(\text{feet}) \quad (\text{II.C.21a})$$

$$\Delta\alpha = \arctan\left(10 \frac{1/30480}{5/254}\right) = 0.96^\circ \quad (\text{II.C.21b})$$

$$\Delta y_{2\text{center}} = -40 \frac{10 \frac{1/30480}{5/254}}{\sin^2 20^\circ + 10 \frac{1/30480}{2 * 5/254} \sin 40^\circ}$$

$$\Delta y_{2\text{center}} = -5.5(\text{feet}) \quad (\text{II.C.21c})$$

$$\Delta \gamma_{\text{center}} = -10 \frac{(1/30480)^2 * 40}{(5/254)^2} \frac{\sin 40^\circ + 10 \frac{1/30480}{5/254} \cos 40^\circ}{(\sin^2 20^\circ + 10 \frac{1/30480}{2 * 5/254} \sin 40^\circ)^2}$$

$$\Delta \gamma_{\text{center}} = -0.049 \quad (\text{II.C.21d})$$

$$\gamma_{\text{center}} = 40 \frac{1/30480}{5/254} \frac{1}{\sin^2 20^\circ}$$

$$\gamma_{\text{center}} = 0.57 \quad (\text{II.C.21e})$$

$$\frac{\Delta \gamma_{\text{center}}}{\gamma_{\text{center}}} = -\frac{0.049}{0.57} = -8.5\% \quad (\text{II.C.21f})$$

The relative change in calibration factor is smaller in this case. For $dt = 1/15(\text{sec})$, this angle is still within the maximum camera angle allowed as computed in Eq.(II.C.8a). However, this angle is bigger than the maximum angle allowed as computed in Eq.(II.C.10a) for $dt = 1/3(\text{sec})$.

D. Compensation of Calibration Factor with regard to the Camera Perspective

From Eq.(II.12b), we see that the calibration factor γ is a nonlinear function of the pixel position p . Because the ROI which the algorithm uses to compute flow speed is large, we need to compensate for the difference in calibration factors in different pixel positions. From Eq.(II.16a), we can see that if we can know coefficients a and b , we will know precisely the calibration factor for each pixel position. Coefficients a and b can be obtained using Eq.(II.16b) if we know the camera angle. However, it is very hard, if possible, in practice to measure the camera angle accurately. Therefore, we have to compute a and b empirically.

There are four methods of obtaining a and b this way. The first method sets up two rulers at two places on the roadway for the calibration. The second and fourth methods assume that the average and the median of the pixel shifts of all the vehicles in the ROI in one frame to be the

pixel shift computed with the correlation algorithm, respectively, then use Eqs.(II.12a), (II.16a), and (II.16b) to obtain a and b. The third method assumes that the average of all the vehicle positions in the ROI in one frame is the place where the pixel shift computed by correlation algorithm occurs, then uses Eqs.(II.12a), (II.16a), and (II.16b) to obtain a and b. The first method is based on the fact that the calibration factor depends only on the geometry of the roadway, the camera position, and camera angle. The second, third, and fourth methods use the vehicle speed for the calibration. We will discuss the four methods in detail in the following. For simplicity, we will call the pixel shift computed by correlation algorithm as the overall pixel shift.

(a) Set up two calibration points in an ROI

Because the calibration factor depends only on the geometry of the roadway and the camera position and not the vehicle speed, we can just set up rulers at two places on the roadway to compute the calibration factor. Assume that we set up two calibration rulers, with equal distance, c feet, at two calibration points, p_1^0 and p_2^0 , and the corresponding pixel difference are dp_1^0 and dp_2^0 , respectively. Thus we can obtain two calibration factors γ_1^0 and γ_2^0 as follows:

$$\gamma_1^0 = \frac{c}{dp_1^0} \quad (\text{II.D.1a})$$

and

$$\gamma_2^0 = \frac{c}{dp_2^0} \quad (\text{II.D.1b})$$

With the two calibration factors, we can get from Eq.(II.16a)

$$a + bp_1^0 = \frac{1}{\sqrt{\gamma_1^0}} = \sqrt{\frac{dp_1^0}{c}} \quad (\text{II.D.2a})$$

and

$$a + bp_2^0 = \frac{1}{\sqrt{\gamma_2^0}} = \sqrt{\frac{dp_2^0}{c}} \quad (\text{II.D.2b})$$

Thus,

$$a = \frac{\sqrt{dp_1^0} p_2^0 - \sqrt{dp_2^0} p_1^0}{(p_2^0 - p_1^0)\sqrt{c}} \quad (\text{II.D.3a})$$

and

$$b = \frac{\sqrt{dp_2^0} - \sqrt{dp_1^0}}{(p_2^0 - p_1^0)\sqrt{c}} \quad (\text{II.D.3b})$$

Eqs.(II.D.3a) and (II.D.3b) are based on the two manually setup calibration points.

The above method uses two calibration points for obtaining a and b. It does not need to know if vehicles are present at the scene since calibration factor depends only on the roadway geometry, the camera position, and its angle. However, since we can determine the pixel displacement of a vehicle in a ROI in two correlated frames with the correlation method, we will know the calibration factor if we know the corresponding vehicle displacement on the roadway. Because the vehicle displacement is equal to the vehicle speed times the time it takes to travel that distance and that time is the same as the timing between two correlated frames, which we already know, we will know the vehicle displacement if we know the vehicle speed. This gives us the possibility of using flow speed to do the calibration. In the following three methods, we will use flow speed for the calibration.

Assume that there are M vehicles in the ROI in one frame with pixel positions p_i , $i = 0, \dots, M-1$. The corresponding calibration factors are γ_i , $i = 0, \dots, M-1$. The overall pixel shift is dp . Also, all the vehicles travel at the same speed v and the time between two correlated frames is dt . We have three ways of compensating for the perspective. They are as follows.

(b) The average of the pixel shifts of all vehicles in the ROI in one frame is the overall pixel shift

The first method averages over the pixel shifts of all vehicles in the ROI in one frame and regards it as the overall pixel shift. With this method, we have

$$dp = \frac{vdt / \gamma_0 + vdt / \gamma_2 + \dots + vdt / \gamma_{M-1}}{M}$$

or

$$dp = \frac{vdt}{M} \sum_{i=0}^{M-1} \frac{1}{\gamma_i} \quad (\text{II.D.4})$$

From Eq.(II.D.4), We have

$$v = \frac{M}{\sum_{i=0}^{M-1} \frac{1}{\gamma_i}} \frac{dp}{dt} \equiv \gamma \frac{dp}{dt} \quad (\text{II.D.5})$$

where

$$\gamma \equiv \frac{M}{\sum_{i=0}^{M-1} \frac{1}{\gamma_i}} \quad (\text{II.D.6a})$$

is the equivalent calibration factor for the whole ROI with M vehicles in the ROI.

Or, with Eq.(II.16a),

$$\gamma \equiv \frac{M}{\sum_{i=0}^{M-1} (a + bp_i)^2} \quad (\text{II.D.6b})$$

Plug Eq.(II.D.7a) into Eq.(II.14b), we get

$$MPH = \frac{15}{22} \frac{M}{\sum_{i=0}^{M-1} (a + bp_i)^2} \quad (\text{II.D.6c})$$

From Eq.(II.D.6c), we see that the MPH varies according to the number of vehicles present and their positions on the image plane, which is in contrast to our current constant MPH method. Our constant MPH method is a limit case of Eq.(II.D.6c) when there is only a vehicle and its position is in the center of the ROI in one frame or when the vehicles are evenly distributed across the ROI in one frame.

We see from the above that the calibration factor γ as defined in Eq.(II.D.6a) is the average calibration factor for the whole ROI. It is not the ordinary average, but in the same form as in the parallel resistors case. From Eq.(II.D.6b), we see that as long as we know the coefficients a and b and the vehicle positions, we know the average calibration factor for the ROI, thus the accurate flow speed.

We can use the method described in (I) to obtain coefficients a and b . We can also use Eqs.(II.D.5) and (II.D.6b) to obtain a and b . For that purpose, we will express Eqs.(II.D.5) and (II.D.6b) as an equation for a and b . Plug Eq.(II.D.6b) into Eq.(II.D.5), We have

$$v = \frac{M}{\sum_{i=0}^{M-1} (a + bp_i)^2} \frac{dp}{dt} \quad (\text{II.D.7})$$

Express Eq.(II.D.7) as a quadratic function on a and b , we get

$$a^2 + ab \frac{\sum_{i=0}^{M-1} p_i}{M} + b^2 \frac{\sum_{i=0}^{M-1} p_i^2}{M} = \frac{dp}{v dt} \quad (\text{II.D.8})$$

Eq.(II.D.8) is a 2-variable order 2 nonlinear equation on a and b . To solve for a and b , we need two equations. For that purpose, we set up two adjacent ROI's, ROI 0 and ROI 1. Assume that there are M_0 and M_1 vehicles in ROI 0 and ROI 1 in one frame and their pixel positions are

p_{0i} and p_{1j} , $i = 0, \dots, M_0 - 1$, $j = 0, \dots, M_1 - 1$, respectively. Also, the corresponding pixel shifts computed by the correlation algorithm are dp_0 , and dp_1 , respectively, and the flow speed is v . Thus,

$$a^2 + ab \frac{\sum_{i=0}^{M_0-1} p_{0i}}{M_0} + b^2 \frac{\sum_{i=0}^{M_0-1} p_{0i}^2}{M_0} = \frac{dp_0}{vdt} \quad (\text{II.D.9a})$$

and

$$a^2 + ab \frac{\sum_{i=0}^{M_1-1} p_{1i}}{M_1} + b^2 \frac{\sum_{i=0}^{M_1-1} p_{1i}^2}{M_1} = \frac{dp_1}{vdt} \quad (\text{II.D.9b})$$

From Eqs.(II.D.9a) and (II.D.9b), we can solve for a and b . However, it is difficult to solve for a and b using the above equations when M_0 and M_1 are all greater than 1. This is especially true when we use multi-measurements to solve for a and b as will be discussed later. Nonetheless, when either M_0 or M_1 or both equal 1, it is easy to solve for a and b . Assume they are both 1 (for either one of them is 1, the derivation is straightforward), then from Eqs.(II.D.9a) and (II.D.9b), we get

$$a^2 + abp_{00} + b^2 p_{00}^2 = \frac{dp_0}{vdt}$$

(II.D.10a)

and

$$a^2 + abp_{10} + b^2 p_{10}^2 = \frac{dp_1}{vdt}$$

(II.D.10b)

or

$$a + bp_{00} = \sqrt{\frac{dp_0}{vdt}} \quad (\text{II.D.11a})$$

and

$$a + bp_{10} = \sqrt{\frac{dp_1}{vdt}} \quad (\text{II.D.11b})$$

It is straightforward to solve the above equations for a and b . Solving Eqs.(II.D.11a) and (II.D.11b) yields

$$a = \frac{p_{10}\sqrt{dp_0} - p_{00}\sqrt{dp_1}}{(p_{10} - p_{00})\sqrt{vdt}} \quad (\text{II.D.12a})$$

and

$$b = \frac{\sqrt{dp_1} - \sqrt{dp_0}}{(p_{10} - p_{00})\sqrt{vdt}} \quad (\text{II.D.12b})$$

The derivation of Eqs.(II.D.12a) and (II.D.12b) requires that there be only one vehicle in each ROI in one frame. In order to satisfy this requirement, the ROI's have to be small enough to contain one vehicle at a time. This can be done by defining the ROI to be a little bit larger than a vehicle. However, this is a serious drawback since if the ROI is too small, the waveform will be distorted significantly due to the leakage and influx of vehicles unless the timing between two correlated frames is small, in which case the pixel shift will be small, but the accuracy of our flow speed computation will be reduced.

In the above, we use only one measurement for the computation of a and b. In reality, the measurement will be corrupted by noise and other errors, so we need to take many measurements and do some type of processing to obtain a and b. We will describe two ways of doing it in the following:

(i) Averaging

Since each ROI is small enough to allow only one vehicle in it, the multiple measurements of the positions should be very close. Thus, we could just simply average the measurements to obtain only one value for each quantity. Assume that we take N measurements and the readings of the vehicle positions and the overall pixel shifts for ROI 0 and 1 are p_{0i} , p_{1i} , dp_{0i} , and dp_{1i} , $i = 0, \dots, N-1$, and the corresponding average positions and overall pixel shifts are $\overline{p_0}$, $\overline{p_1}$, $\overline{dp_0}$, and $\overline{dp_1}$, respectively. Also, the N measurements of the flow speeds are v_i , $i = 0, \dots, N-1$, and its average value is \overline{v} . Then,

$$\overline{v} = \frac{1}{N} \sum_{i=0}^{N-1} v_i \quad (\text{II.D.13a})$$

$$\overline{p_0} = \frac{1}{N} \sum_{i=0}^{N-1} p_{0i} \quad (\text{II.D.13b})$$

$$\overline{p_1} = \frac{1}{N} \sum_{i=0}^{N-1} p_{1i} \quad (\text{II.D.13c})$$

$$\overline{dp_0} = \frac{1}{N} \sum_{i=0}^{N-1} dp_{0i} \quad (\text{II.D.13d})$$

and

$$\overline{dp_1} = \frac{1}{N} \sum_{i=0}^{N-1} dp_{1i} \quad (\text{II.D.13e})$$

Thus, using Eqs.(II.D.12a) and (II.D.12b) and Eqs.(13a)-(e), we have

$$a = \frac{\overline{p_1} \sqrt{\overline{dp_0}} - \overline{p_0} \sqrt{\overline{dp_1}}}{(\overline{p_1} - \overline{p_0}) \sqrt{v dt}} \quad (\text{II.D.14a})$$

and

$$b = \frac{\sqrt{\overline{dp_1}} - \sqrt{\overline{dp_0}}}{(\overline{p_1} - \overline{p_0}) \sqrt{v dt}} \quad (\text{II.D.14b})$$

(ii) Least Square Fitting

We can also use least square fitting to obtain a and b. In this case, only one ROI is needed. Assume the same measurements for ROI 0 as in (i). The sum of the squared error of each individual measurement is

$$e = \sum_{i=0}^{N-1} \left| \sqrt{\frac{dp_{0i}}{v_i dt}} - (a + bp_{0i}) \right|^2 \quad (\text{II.D.15})$$

Differentiate over a and b, we have

$$\frac{\partial e}{\partial a} = -2 \sum_{i=0}^{N-1} \left(\sqrt{\frac{dp_{0i}}{v_i dt}} - a - bp_{0i} \right) \quad (\text{II.D.16a})$$

and

$$\frac{\partial e}{\partial b} = -2 \sum_{i=0}^{N-1} \left(\sqrt{\frac{dp_{0i}}{v_i dt}} - a - bp_{0i} \right) p_{0i} \quad (\text{II.D.16b})$$

For e to be minimum, we require

$$\frac{\partial \mathcal{E}}{\partial a} = 0 \quad (\text{II.D.17a})$$

and

$$\frac{\partial \mathcal{E}}{\partial b} = 0 \quad (\text{II.D.17b})$$

Thus, from Eqs.(II.D.16a), (II.D.16b), (II.D.17a), and (II.D.17b), we get

$$Na + b \sum_{i=0}^{N-1} p_{0i} = \sum_{i=0}^{N-1} \sqrt{\frac{dp_{0i}}{v_i dt}} \quad (\text{II.D.18a})$$

and

$$a \sum_{i=0}^{N-1} p_{0i} + b \sum_{i=0}^{N-1} p_{0i}^2 = \sum_{i=0}^{N-1} p_{0i} \sqrt{\frac{dp_{0i}}{v_i dt}} \quad (\text{II.D.18b})$$

Solve Eqs.(II.D.18a) and (II.D.18b) for a and b, we have

$$a = \frac{(\sum_{i=0}^{N-1} p_{0i}^2)(\sum_{i=0}^{N-1} \sqrt{\frac{dp_{0i}}{v_i dt}}) - (\sum_{i=0}^{N-1} p_{0i}) \sum_{i=0}^{N-1} (p_{0i} \sqrt{\frac{dp_{0i}}{v_i dt}})}{N \sum_{i=0}^{N-1} p_{0i}^2 - (\sum_{i=0}^{N-1} p_{0i})^2} \quad (\text{II.D.19a})$$

and

$$b = \frac{N \sum_{i=0}^{N-1} (p_{0i} \sqrt{\frac{dp_{0i}}{v_i dt}}) - (\sum_{i=0}^{N-1} p_{0i})(\sum_{i=0}^{N-1} \sqrt{\frac{dp_{0i}}{v_i dt}})}{N \sum_{i=0}^{N-1} p_{0i}^2 - (\sum_{i=0}^{N-1} p_{0i})^2} \quad (\text{II.D.19b})$$

In the above, we discussed the averaging over pixel shifts method. In this method, it is difficult to solve for coefficients a and b analytically with multiple vehicles in the ROI in one frame. It is especially difficult when we use multi-measurements with least square fitting to solve for a and b because it is a nonlinear 2-variable order 2 equation. To get around this problem, we make the ROI small enough for just one vehicle. The drawback with this is that it can not tolerate even a small camera angle error, which will totally shift the ROI when we come back to the original preset value. Also, this will not allow for close range ROI because the vehicle will be moving so fast that it will move out of the ROI even within two consecutive frames. The biggest problem with this is that due to the correlation method, the ROI has to be big enough to allow a vehicle to stay inside the ROI for several correlated frames. This means that the ROI has to be much larger than one vehicle for the vehicle to shift and still be in the ROI for several correlated frames. This will generally require that the ROI be several times larger than a vehicle length. Thus, it will cause error by using Eqs.(II.D.19a) and (II.D.19b) to compute a and b. Therefore, we will not use this method for calibration.

(c) The overall pixel shift occurs at the average of the pixel positions of all vehicles in the ROI in one frame

In the above method, we average over the pixel shifts of all the vehicles in the ROI in one frame and take it as the overall pixel shift. However, for obtaining a and b with multiple measurements, this method is awkward unless we use a ROI small enough for just one vehicle as described above. Even in this case, the region still has to be bigger than a vehicle in order for the correlation to work. Thus, we can not guarantee that only one car present at a time. There may be part of another vehicle present at the same time, which causes error in the perspective compensation. Hence, the above method is not a good method for calibration. In this subsection, we will discuss another method, averaging over the pixel positions of all the vehicles in the ROI in one frame. This method assumes that the average of the pixel positions of all the vehicles in the ROI in one frame to be the place where overall pixel shift occurs.

In this method, we need only one region. For each measurement, we average over all the vehicle positions in the ROI in one frame to get a single position value, then we assume that the overall pixel shift corresponds to that average position. The problem is then equivalent to a single vehicle in that average position in the ROI as in case (b)(ii). Thus, all the formulas there are applicable here, except that the vehicle position p_{0i} in the ROI for each measurement in case (b)(ii) is replaced by the average position of the multiple vehicles in the ROI for each measurement. Assume that we take N measurements and there are M_i vehicles at the ith measurement. Let p_{ij} , $i = 0, \dots, N - 1$ and $j = 0, \dots, M_i - 1$, be the jth vehicle position for the ith measurement and dp_i and v_i , $i = 0, \dots, N - 1$, be the overall pixel shift and vehicle speed for the ith measurement. In addition, let \bar{p}_i and γ_i , $i = 0, \dots, N - 1$, be the average pixel position and its corresponding calibration factor for measurement i, respectively. Then, the average pixel position for measurement i is

$$\bar{p}_i = \frac{1}{M_i} \sum_{j=0}^{M_i-1} p_{ij} \quad (\text{II.D.20})$$

Thus,

$$dp_i = \frac{v_i dt}{\gamma_i} = (a + b\bar{p}_i)^2 v_i dt \quad (\text{II.D.21})$$

or

$$v_i = \frac{1}{(a + b\bar{p}_i)^2} \frac{dp_i}{dt} \quad (\text{II.D.22})$$

We will use least square method to solve for a and b. The equations that we are going to derive are essentially the same as those in case (b)(ii). The sum of the squared error of each individual measurement is

$$e = \sum_{i=0}^{N-1} \left| \sqrt{\frac{dp_i}{v_i dt}} - (a + b \overline{p_i}) \right|^2 \quad (\text{II.D.23})$$

Differentiate over a and b, we have

$$\frac{\partial e}{\partial a} = -2 \sum_{i=0}^{N-1} \left(\sqrt{\frac{dp_i}{v_i dt}} - a - b \overline{p_i} \right) \quad (\text{II.D.24a})$$

and

$$\frac{\partial e}{\partial b} = -2 \sum_{i=0}^{N-1} \left(\sqrt{\frac{dp_i}{v_i dt}} - a - b \overline{p_i} \right) \overline{p_i} \quad (\text{II.D.24b})$$

For e to be minimum, we require

$$\frac{\partial e}{\partial a} = 0 \quad (\text{II.D.25a})$$

and

$$\frac{\partial e}{\partial b} = 0 \quad (\text{II.D.25b})$$

Thus, from Eqs. (II.D.24a), (II.D.24b), (II.D.25a), and (II.D.25b), we get

$$Na + b \sum_{i=0}^{N-1} \overline{p_i} = \sum_{i=0}^{N-1} \sqrt{\frac{dp_i}{v_i dt}} \quad (\text{II.D.26a})$$

and

$$a \sum_{i=0}^{N-1} \overline{p_i} + b \sum_{i=0}^{N-1} \overline{p_i}^2 = \sum_{i=0}^{N-1} \overline{p_i} \sqrt{\frac{dp_i}{v_i dt}} \quad (\text{II.D.26b})$$

Solve Eqs. (II.D.26a) and (II.D.26b) for a and b, we have

$$a = \frac{\left(\sum_{i=0}^{N-1} \overline{p_i}^2 \right) \left(\sum_{i=0}^{N-1} \sqrt{\frac{dp_i}{v_i dt}} \right) - \left(\sum_{i=0}^{N-1} \overline{p_i} \right) \sum_{i=0}^{N-1} \left(\overline{p_i} \sqrt{\frac{dp_i}{v_i dt}} \right)}{N \sum_{i=0}^{N-1} \overline{p_i}^2 - \left(\sum_{i=0}^{N-1} \overline{p_i} \right)^2} \quad (\text{II.D.27a})$$

and

$$b = \frac{N \sum_{i=0}^{N-1} (\overline{p_i} \sqrt{\frac{dp_i}{v_i dt}}) - (\sum_{i=0}^{N-1} \overline{p_i}) (\sum_{i=0}^{N-1} \sqrt{\frac{dp_i}{v_i dt}})}{N \sum_{i=0}^{N-1} \overline{p_i}^2 - (\sum_{i=0}^{N-1} \overline{p_i})^2} \quad (\text{II.D.27b})$$

With Eqs.(II.D.20), (II.D.27a), and (II.D.27b), we can solve for a and b. After we have known a and b, we could use Eqs.(II.D.20) and (II.D.22) to determine the flow speed.

(d) The median of the pixel shifts of all vehicles in the ROI in one frame is the overall pixel shift

In this subsection, we will discuss the fourth method, which assumes that the median of the pixel shifts of all vehicles in the ROI in one frame is the overall pixel shift. This method is a preferred method since it is based on a proof for the same result in the flow speed computation. However, because the proof is based on some ideal assumptions which include uniform intensity for all vehicles, small pixel shift, and large separation between vehicles, etc, the result may not hold for the actual situation. Therefore, we can not claim that this method is an accurate one.

Assume that we make N measurements and there are M_i vehicles at the i th measurement. Let p_{im} and γ_{im} , $i = 0, \dots, N-1$, be the position of the median of the pixel shifts of all vehicles in the ROI and its corresponding calibration factor in the i th measurement, and dp_i and v_i , $i = 0, \dots, N-1$, be the overall pixel shift and vehicle speed for the i th measurement, respectively. Thus, dp_i and p_{im} are related by the following relationship

$$dp_i = \frac{v_i dt}{\gamma_{im}} = (a + bp_{im})^2 v_i dt \quad (\text{II.D.28})$$

or

$$v_i = \frac{1}{(a + bp_{im})^2} \frac{dp_i}{dt} \quad (\text{II.D.29})$$

Comparing Eq.(II.D.21) with Eq.(II.D.28), we can that the difference between this method and the third method is in how we relate the overall pixel shift to the pixel position. In the third method, we assume that the overall pixel shift corresponds to the average pixel position of all vehicles in the ROI in one frame, while in this method, we relate the overall pixel shift to the median of the pixel shifts of all vehicle in the ROI in one frame. Therefore, if we replace $\overline{p_i}$ by p_{im} in all the equations in Subsection (c), we will get the formulas for this method. Thus with least square fitting, we can get the equations for obtaining a and b from Eqs.(II.D.27a) and (II.D.27b) as follows.

$$a = \frac{(\sum_{i=0}^{N-1} p_{im}^2)(\sum_{i=0}^{N-1} \sqrt{\frac{dp_i}{v_i dt}}) - (\sum_{i=0}^{N-1} p_{im}) \sum_{i=0}^{N-1} (p_{im} \sqrt{\frac{dp_i}{v_i dt}})}{N \sum_{i=0}^{N-1} p_{im}^2 - (\sum_{i=0}^{N-1} p_{im})^2} \quad (\text{II.D.30a})$$

and

$$b = \frac{N \sum_{i=0}^{N-1} (p_{im} \sqrt{\frac{dp_i}{v_i dt}}) - (\sum_{i=0}^{N-1} p_{im})(\sum_{i=0}^{N-1} \sqrt{\frac{dp_i}{v_i dt}})}{N \sum_{i=0}^{N-1} p_{im}^2 - (\sum_{i=0}^{N-1} p_{im})^2} \quad (\text{II.D.30b})$$

With Eqs.(II.D.30a) and (II.D.30b), we can compute the coefficients a and b. After we obtain a and b, we will know the calibration factor for each individual pixel position with Eq.(II.16a). The flow speed is then determined by determining the pixel position corresponding to the median of the pixel shifts of all vehicles in the ROI in one frame.

In the above, we discuss four methods for determining the coefficients a and b. The first method has a merit in that it straightforwardly determines a and b with rulers at two calibration points.

The second, third, and fourth methods use the flow speed for calibration. With the second method, the pixel shifts of all vehicles in the ROI in one frame is averaged and the average pixel shift is taken as the overall pixel shift. We then derived a set of equations for determining a and b. This method has a disadvantage in that it is very complex for solving a and b analytically, especially in the case of mutiple measurements.

The third method and the fourth method are very similar in the way they relate the overall pixel shift to the pixel position. The third method assumes that the pixel position corresponding to the overall pixel shift is the average pixel position of all vehicles in the ROI in one frame, while the fourth method relates the overall pixel shift to the pixel position where the median pixel shift of all vehicles in the ROI in one frame is at. These two methods are equivalent when the traffic is heavy since in that case the average pixel position of all vehicles in the ROI in one frame is the same or very close to pixel position corresponding to the median pixel shift. However, they may be quite different when the traffic is light, since in that case the pixel position corresponding to the median pixel shift may be quite far away from the average pixel position. Nonetheless, we expect these two methods to perform about the same in a long period of time due to the average nature of these methods. This is especially true if we use the same method for obtaining a and b and for computing flow speed.

Either method (c) or method (d) can be used for perspective compensation. However, due to the proof in the flow speed computation, we believe that method (d) is closer to the actual situation than method (d). Therefore, we will use method (d) for our perspective compensation.

6.3 Conclusions

In section 6 of this technical report, we discuss the camera perspective with respect to flow speed computation. From the various equations derived in the above, we can have several conclusions.

- (a) Even though the camera angle is limited by the requirement that the vehicles in the ROI have to stay in that ROI for specific number of times, the distance that it can see is still close enough. The closest distance that the camera can see while still satisfying the requirement is around 100 feet.
- (b) The pole high is not a big factor with respect to camera perspective. However, due to the obstructions along the highway, such as a sign, a light pole, or trees, the higher the pole, the better. The suitable pole height will be about 60 feet.
- (c) The error in the pixel position due to the error in camera angle is independent of the camera angle itself. The calibration factor is sensitive to the error in the camera angle. For the same angle and same error in camera angle, zooming in is less sensitive than zooming out. Also, the higher the camera angle, the less sensitive the calibration factor to the error in the camera angle.
- (d) The camera perspective in flow speed computation can be compensated by determining the number of vehicles and their positions in the ROI in each set of correlated frames. The best way to obtain the coefficients a and b for calibration factor is by determining the pixel position corresponding to the median pixel shift of all vehicles in the ROI in each set of correlated frames and then using least square fitting method.

***MISSION
OF
AFRL/INFORMATION DIRECTORATE (IF)***

The advancement and application of information systems science and technology for aerospace command and control and its transition to air, space, and ground systems to meet customer needs in the areas of Global Awareness, Dynamic Planning and Execution, and Global Information Exchange is the focus of this AFRL organization. The directorate's areas of investigation include a broad spectrum of information and fusion, communication, collaborative environment and modeling and simulation, defensive information warfare, and intelligent information systems technologies.